CAPITAL UNIVERSITY OF SCIENCE AND TECHNOLOGY, ISLAMABAD



In Silico Screening of *Helianthus tuberosus* L. Leaf Phytochemicals as Potential Angiotensin-Converting Enzyme Inhibitors for Chronic Kidney Disease

by

Attia Tul Shafi

A thesis submitted in partial fulfillment for the degree of Master of Science

in the

Faculty of Health and life sciences
Department of Bioinformatics and Biosciences

2026

Copyright © 2026 by Attia Tul Shafi

All rights reserved. No part of this thesis may be reproduced, distributed, or transmitted in any form or by any means, including photocopying, recording, or other electronic or mechanical methods, by any information storage and retrieval system without the prior written permission of the author.

CERTIFICATE OF APPROVAL

In Silico Screening of _Helianthus tuberosus_ L. Leaf Phytochemicals as Potential Angiotensin-Converting Enzyme Inhibitors for Chronic Kidney Disease

by

Attia Tul Shafi

(MBS241009)

THESIS EXAMINING COMMITTEE

S. No.	Examiner	Name	Organization
(a)	External Examiner	Dr. Sayed Afzal Shah	NUMS, Islamabad
(b)	Internal Examiner	Dr. M. Asad Anwar	CUST, Islamabad

Dr. Sami Ullah Jan
Thesis Supervisor
October, 2026

Dr. S. Marriam Bakhtiar
Head
Dept. of Bioinfo. and Biosciences
October, 2026

Dr. Sahar Fazal
Dean
Faculty of Health and Life Sciences
October, 2026

Author's Declaration

I, **Attia Tul Shafi** hereby state that my MS thesis titled "***In Silico* Screening of *Helianthus tuberosus* L. Leaf Phytochemicals as Potential Angiotensin-Converting Enzyme Inhibitors for Chronic Kidney Disease**" is my own work and has not been submitted previously by me for taking any degree from Capital University of Science and Technology, Islamabad or anywhere else in the country/abroad.

At any time, if my statement is found to be incorrect even after my graduation, the University has the right to withdraw my MS Degree.



(Attia Tul Shafi)

Registration No: MBS241009

Plagiarism Undertaking

I solemnly declare that research work titled "***In Silico* Screening of *Helianthus tuberosus* L. Leaf Phytochemicals as Potential Angiotensin-Converting Enzyme Inhibitors for Chronic Kidney Disease**" presented in this thesis is solely my research work with no significant contribution from any other person. Small contributions/help wherever taken have been duly acknowledged, and the complete thesis has been written by me.

I understand the zero-tolerance policy of the HEC and Capital University of Science and Technology towards plagiarism. Therefore, I, as an author of the above-titled thesis, declare that no portion of my thesis has been plagiarized, and any material used as a reference is properly referred/cited.

I undertake that if I am found guilty of any formal plagiarism in the above titled thesis even after award of the MS Degree, the University reserves the right to withdraw/revoke my MS degree, and that HEC and the University have the right to publish my name on the HEC/University website, on which names of students are placed who submitted plagiarized work.



(Attia Tul Shafi)

Registration No: MBS241009

Acknowledgement

First and foremost, I would like to thank Allah for granting me the knowledge, strength, and patience needed to complete this research. I am deeply grateful to my supervisor, Dr. Sami Ullah Jan, for his guidance, patience, and constructive feedback throughout the course of this thesis.

I would also like to thank the faculty and staff of the Department of Bioinformatics and Biosciences at Capital University of Science and Technology for their support throughout my degree.

Finally, my sincere thanks go to my family, whose encouragement and support sustained me through every stage of this work.

(Attia Tul Shafi)

Abstract

Chronic kidney disease (CKD) progression is driven substantially by overactivity of the renin-angiotensin-aldosterone system, in which angiotensin-converting enzyme (ACE) is the pivotal catalytic target. Synthetic ACE inhibitors such as lisinopril remain first-line therapy but are limited by class-wide tolerability issues, motivating interest in plant-derived alternatives. This thesis evaluated five Jerusalem artichoke (*Helianthus tuberosus* L.) leaf phytochemicals, chlorogenic acid, caffeic acid, 5-p-coumaroylquinic acid, astragalin and heliangine, as candidate ACE inhibitors for CKD, using structure-based virtual screening (drug-likeness filtering, ADMET profiling, molecular docking and interaction analysis) benchmarked against lisinopril on the human ACE structure (PDB 1O8A).

Four of the five compounds, all but caffeic acid, emerged as leads, each outscoring lisinopril's docking affinity (-7.3 kcal/mol) and, unlike lisinopril, returning a clean hepatotoxicity prediction (astragalin, -8.6, heliangine and chlorogenic acid, -7.9, 5-p-coumaroylquinic acid, -7.7 kcal/mol). Heliangine combined the best predicted absorption with the panel's only AMES-positive signal, while astragalin's glycosylated structure limited its absorption despite the strongest binding score.

These results indicate that Jerusalem artichoke leaf phytochemicals are computationally plausible, and on several measures preferable, alternatives to lisinopril for ACE inhibition in CKD, representing the first such virtual screening of this plant material for a CKD indication. As computational predictions, they motivate future in vitro ACE-inhibition assays, genotoxicity testing of heliangine, and molecular dynamics validation.

Keywords: *Helianthus tuberosus* L., Chronic kidney disease, ACE, Molecular docking, Jerusalem artichoke, Phytochemicals, ADMET, Virtual screening.

Contents

Author's Declaration iii

Plagiarism Undertaking iv

Acknowledgement v

Abstract vi

List of Figures x

List of Tables xi

Abbreviations xiii

1 Introduction 1
- 1.1 Problem Statement . . . 5
- 1.2 Hypothesis . . . 5
- 1.3 Aim . . . 6
- 1.4 Objectives . . . 6

2 Literature Review 7
- 2.1 Chronic Kidney Disease and the Renin-Angiotensin-Aldosterone System . . . 7
  - 2.1.1 Global Burden and Clinical Significance . . . 7
  - 2.1.2 RAAS Pathophysiology and the Central Role of ACE . . . 8
  - 2.1.3 Evidence and Limitations of ACE Inhibition as a Therapeutic Strategy in CKD . . . 9
- 2.2 Angiotensin-Converting Enzyme as a Structure Based Drug Design Target . . . 11
  - 2.2.1 Structural Biology of ACE . . . 11
  - 2.2.2 Synthetic ACE Inhibitors and Their Limitations . . . 12
- 2.3 Natural and Plant-Derived ACE Inhibitors . . . 12
  - 2.3.1 Rationale for Phytochemical ACE Inhibitors . . . 12
  - 2.3.2 Structure-Activity Relationships of Phenolic and Flavonoid ACE Inhibitors . . . 13

2.3.3 Recent *In Silico* and In Vitro Studies of Plant-Derived ACE Inhibitors . . . 14
2.4 Jerusalem Artichoke: Phytochemistry and Bioactivity . . . 16
2.4.1 Morphological Features . . . 17
2.4.2 Life Cycle and Growth Pattern . . . 18
2.4.3 Traditional and Medicinal Uses . . . 18
2.4.4 General Phytochemical Composition . . . 20
2.4.5 Leaf-Specific Phytochemical Profile . . . 21
2.4.6 Reported Pharmacological Properties . . . 21
2.4.6.1 Antioxidant Activity . . . 24
2.4.6.2 Anti-Inflammatory Activity . . . 24
2.4.6.3 Antimicrobial and Antifungal Activity . . . 25
2.4.6.4 Antihyperglycaemic and Metabolic Activity . . . 25
2.4.6.5 Antihypertensive and Cardiovascular Activity . . . 26
2.5 ACE-Relevant Evidence for the Five Compounds of Interest . . . 26
2.5.1 Chlorogenic Acid . . . 27
2.5.2 Caffeic Acid . . . 28
2.5.3 5-p-Coumaroylquinic Acid . . . 28
2.5.4 Astragalin (Kaempferol-3-O-glucoside) . . . 29
2.5.5 Heliangine . . . 29
2.6 Computational and Experimental Approache in the Literature . . . 30
2.6.1 Structured Virtual Screening and Docking Platforms . . . 30
2.6.2 ADMET and Drug-Likeness Prediction Tools . . . 31
2.6.3 Summary of Reviewed Literature . . . 31
2.7 Research Gap in the Literature . . . 36

3 Methodology **38**
3.1 Selection of the Disease . . . 38
3.2 Preparation of the Target Protein . . . 39
3.2.1 Selection of Target Protein . . . 39
3.2.2 Active Site Prediction . . . 40
3.2.3 Physicochemical Characterization . . . 40
3.2.4 Functional Domain Analysis . . . 40
3.2.5 Protein Structure Preparation . . . 41
3.3 Selection and Preparation of Ligands . . . 41
3.3.1 Selection of Ligands . . . 41
3.3.2 Ligand Refinement and Preparation . . . 42
3.4 Virtual Screening of Phytochemicals . . . 42
3.4.1 Drug-Likeness Assessment (Lipinski's Rule of Five) . . . 42
3.4.2 ADMET Profiling . . . 43
3.5 Molecular Docking . . . 43
3.6 Protein-Ligand Interaction Analysis . . . 43
3.7 Lead Compound Identification . . . 44
3.8 Reference Drug Selection and Screening . . . 44

3.8.1 Identification of Reference Drug . . . 44
3.8.2 Screening of Reference Drug . . . 45
3.9 Comparative Analysis of Lead Compounds with the Reference Drug 45

4 Results 46
4.1 Selection and Preparation of the Target Protein . . . 47
4.1.1 Selection of Target Protein . . . 47
4.1.2 Active Site Prediction . . . 47
4.1.3 Physicochemical Characterization . . . 48
4.1.4 Functional Domain Analysis . . . 49
4.1.5 Protein Structure Preparation . . . 50
4.2 Selection and Screening of Ligands (Phytochemicals) . . . 51
4.2.1 Molecular Identity . . . 51
4.2.2 Ligand Refinement and Preparation . . . 53
4.2.3 Drug-Likeness Assessment (Lipinski's Rule of Five) . . . 54
4.2.4 ADMET Profiling . . . 55
4.2.4.1 Absorption . . . 55
4.2.4.2 Distribution . . . 56
4.2.4.3 Metabolism . . . 56
4.2.4.4 Excretion . . . 57
4.2.4.5 Toxicity . . . 58
4.3 Molecular Docking . . . 59
4.4 Protein–Ligand Interaction Analysis . . . 61
4.5 Lead Compound Identification . . . 64
4.6 Reference Drug Selection and Screening . . . 64
4.6.1 Identity and Drug-Likeness . . . 65
4.6.2 ADMET Profile . . . 66
4.6.3 Molecular Docking and Interaction Analysis . . . 68
4.7 Comparative Analysis of Lead Compounds with the Reference Drug 69
4.7.1 Chlorogenic Acid versus Lisinopril . . . 70
4.7.1.1 Interaction Comparison . . . 75
4.7.2 5-p-Coumaroylquinic Acid versus Lisinopril . . . 75
4.7.2.1 Interaction Comparison . . . 79
4.7.3 Astragalin versus Lisinopril . . . 81
4.7.3.1 Interaction Comparison . . . 84
4.7.4 Heliangine versus Lisinopril . . . 86
4.7.4.1 Interaction Comparison . . . 89

5 Discussion 92

6 Conclusion and Future Work 99
6.1 Conclusion . . . 99
6.2 Future Work . . . 100

Bibliography 102

List of Figures

2.1 The renin–angiotensin–aldosterone system (RAAS), showing the role of angiotensin-converting enzyme (ACE) in the cascade and the effects of ACE inhibition in chronic kidney disease progression . . . 10
2.2 Principal organs of *Helianthus tuberosus* L. (Jerusalem artichoke), including the whole plant, leaves, flowers and tubers [13] 17
2.3 Structural classification of five Jerusalem artichoke leaf phytochemicals by chemical class. 27

3.1 Overall methodological workflow followed in this study, showing the parallel Disease Selection and Plant Selection tracks converging through Molecular Docking and Interaction Analysis into a final Comparison against the reference drug, lisinopril 39

4.1 3D structure of ACE 47
4.2 Cavities detected on the target protein 48
4.3 Domain and family organisation of the ACE protein sequence . . . 50
4.4 Prepared 3D structure of ACE 51
4.5 Molecular interaction analysis of Astragalin with ACE 61
4.6 Molecular interaction analysis of Chlorogenic acid with ACE 62
4.7 Molecular interaction analysis of 5-p-Coumaroylquinic acid with ACE 62
4.8 Molecular interaction analysis of Caffeic acid with ACE 63
4.9 Molecular interaction analysis of Heliangine with ACE 63
4.10 Molecular interaction analysis of lisinopril with ACE 69
4.11 Molecular interaction analysis of lisinopril (top) and chlorogenic acid (bottom) with ACE 74
4.12 Molecular interaction analysis, lisinopril vs 5-p-coumaroylquinic acid 80
4.13 Molecular interaction analysis of lisinopril (top) and astragalin (bottom) with ACE 85
4.14 Molecular interaction analysis of lisinopril (top) and heliangine (bottom) with ACE 90

List of Tables

2.1 Taxonomic Classification of *Helianthus tuberosus* L. [14] 16
2.2 Ethnomedicinal Applications of Jerusalem Artichoke Correlated with Modern Pharmacological Findings [13] 19
2.3 Compound-Level Evidence for the Bioactivity of Jerusalem Artichoke Constituents [13] 22
2.4 Summary of structure-activity and computational-screening studies 32

4.1 Physicochemical parameters of the ACE protein sequence 49
4.2 Ligand identity, CID, formula, and 2D structure 52
4.3 Lipinski's Rule of Five parameters of ligands 54
4.4 Absorption parameters of ligands 55
4.5 Distribution parameters of ligands 56
4.6 Metabolism parameters of ligands 56
4.7 Excretion parameters of ligands 57
4.8 Toxicity parameters of ligands 58
4.9 Docking scores and the volume of cavity C1, ordered from strongest to weakest predicted binder, together with the corresponding docked complex for each compound 59
4.10 Lisinopril identity, PubChem CID, molecular formula, and 2D structure 65
4.11 Lipinski parameters for lisinopril 65
4.12 Absorption parameters for lisinopril 66
4.13 Distribution parameters for lisinopril 66
4.14 Metabolism parameters for lisinopril 67
4.15 Excretion parameters for lisinopril 67
4.16 Toxicity parameters for lisinopril 67
4.17 Docking result for lisinopril 68
4.18 Identity of lisinopril and Chlorogenic acid, with PubChem CID, molecular formula, and 2D structure 70
4.19 Lipinski's Rule of Five parameters for lisinopril and Chlorogenic acid 70
4.20 Absorption parameters for lisinopril and Chlorogenic acid 71
4.21 Distribution parameters for lisinopril and Chlorogenic acid 71
4.22 Metabolism (CYP450) parameters for lisinopril and Chlorogenic acid 72
4.23 Excretion parameters for lisinopril and Chlorogenic acid 72
4.24 Toxicity parameters for lisinopril and Chlorogenic acid 72
4.25 Docking scores and cavity volume for lisinopril and Chlorogenic acid, both occupying cavity C1, with their docked complexes 73

4.26 Identity of lisinopril and 5-p-Coumaroylquinic acid, with PubChem CID, molecular formula, and 2D structure 75
4.27 Lipinski Rule of Five, lisinopril vs 5-p-coumaroylquinic acid 76
4.28 Absorption parameters for lisinopril and 5-p-Coumaroylquinic acid . 76
4.29 Distribution parameters for lisinopril and 5-p-Coumaroylquinic acid 77
4.30 Metabolism (CYP450), lisinopril vs 5-p-coumaroylquinic acid 77
4.31 Excretion parameters for lisinopril and 5-p-Coumaroylquinic acid . 77
4.32 Toxicity parameters for lisinopril and 5-p-Coumaroylquinic acid . . 78
4.33 Docking scores and cavity volume, lisinopril vs 5-p-coumaroylquinic acid 78
4.34 Identity of lisinopril and Astragalin, with PubChem CID, molecular formula, and 2D structure 81
4.35 Lipinski's Rule of Five parameters for lisinopril and Astragalin . . . 81
4.36 Absorption parameters for lisinopril and Astragalin 82
4.37 Distribution parameters for lisinopril and Astragalin 82
4.38 Metabolism (CYP450) parameters for lisinopril and Astragalin . . . 83
4.39 Excretion parameters for lisinopril and Astragalin 83
4.40 Toxicity parameters for lisinopril and Astragalin 83
4.41 Docking scores and cavity volume for lisinopril and Astragalin, both occupying cavity C1, with their docked complexes 84
4.42 Identity of lisinopril and Heliangine, with PubChem CID, molecular formula, and 2D structure 86
4.43 Lipinski's Rule of Five parameters for lisinopril and Heliangine . . . 87
4.44 Absorption parameters for lisinopril and Heliangine 87
4.45 Distribution parameters for lisinopril and Heliangine 87
4.46 Metabolism (CYP450) parameters for lisinopril and Heliangine . . . 88
4.47 Excretion parameters for lisinopril and Heliangine 88
4.48 Toxicity parameters for lisinopril and Heliangine 88
4.49 Docking scores and cavity volume for lisinopril and Heliangine, both occupying cavity C1, with their docked complexes 89

Abbreviations

ACE	Angiotensin-Converting Enzyme
ADMET	Absorption, Distribution, Metabolism, Excretion, and Toxicity
AMES	Ames Bacterial Reverse Mutation (Mutagenicity) Test
BBB	Blood–Brain Barrier
CB-Dock2	Cavity-detection-guided Blind Docking Server, version 2
CID	Compound Identifier (PubChem)
CKD	Chronic Kidney Disease
CNS	Central Nervous System
CYP450	Cytochrome P450
CYP1A2	Cytochrome P450 Family 1, Subfamily A, Polypeptide 2
CYP2C9	Cytochrome P450 Family 2, Subfamily C, Polypeptide 9
CYP2C19	Cytochrome P450 Family 2, Subfamily C, Polypeptide 19
CYP2D6	Cytochrome P450 Family 2, Subfamily D, Polypeptide 6
CYP3A4	Cytochrome P450 Family 3, Subfamily A, Polypeptide 4
ESI	Electrospray Ionisation
FASTA	FAST-All (biological sequence file format)
GBD	Global Burden of Disease
GBIF	Global Biodiversity Information Facility
GRAVY	Grand Average of Hydropathicity
hERG	Human Ether-à-go-go-Related Gene
HPLC	High-Performance Liquid Chromatography
IC_{50}	Half-Maximal Inhibitory Concentration
KDIGO	Kidney Disease: Improving Global Outcomes
LD_{50}	Median Lethal Dose
LOAEL	Lowest Observed Adverse Effect Level

LogP	Logarithm of the Octanol–Water Partition Coefficient
MS	Mass Spectrometry
MW	Molecular Weight
OCT2	Organic Cation Transporter 2
PDB	Protein Data Bank
pI	Isoelectric Point
QSAR	Quantitative Structure-Activity Relationship
RAAS	Renin-Angiotensin-Aldosterone System
SAR	Structure-Activity Relationship
SDF	Structure-Data File
SMILES	Simplified Molecular Input Line Entry System
TNF	Tumour Necrosis Factor
UHPLC/UPLC	Ultra-High-Performance Liquid Chromatography
VCAM	Vascular Cell Adhesion Molecule

Chapter 1

Introduction

Chronic kidney disease (CKD) is a progressive, largely irreversible loss of renal filtration capacity that, without effective management, ends in kidney failure and lifelong dependence on dialysis or transplantation. CKD now affects an estimated 788 million adults worldwide as of 2023, according to the most recent Global Burden of Disease modelling, a figure that has more than doubled since 1990 [1, 2]. The need for kidney replacement therapy has grown even faster over the same period, with recipient numbers approaching 4.6 million, roughly three times the 1990 total, while the disease is now linked to close to 1.5 million deaths worldwide each year, a toll equivalent to one life lost approximately every twenty seconds [1, 2]. The same modelling forecasts a further rise of over 30% in age-standardised CKD mortality by 2050 relative to 2022, a direction of travel that runs counter to the falling death rates seen for stroke and ischaemic heart disease over the same horizon, and one severe enough to push CKD into third place among causes of death in Western Europe by mid-century [2]. This burden also falls unevenly across the world, disproportionately affecting low- and middle-income countries where access to renal replacement therapy remains limited, a disparity that sharpens the case for therapeutic options that are not only effective but affordable and well tolerated [1]. A large part of this progression is attributable to a single physiological cascade, the renin-angiotensin-aldosterone system (RAAS), whose sustained overactivity is now recognised as one of the principal drivers of both the onset and the advancement of CKD

[3]. In brief, falling renal perfusion pressure triggers renin release, which cleaves circulating angiotensinogen to angiotensin I; angiotensin-converting enzyme (ACE) then converts this inactive peptide into angiotensin II, a potent vasoconstrictor that raises systemic blood pressure, stimulates aldosterone-driven sodium and water retention, and constricts the renal efferent arteriole to raise glomerular capillary pressure [3, 4]. Sustained activity along this pathway drives progressive kidney tissue damage, elevated pressure within the glomerulus, injury to podocytes, leakage of protein into the urine, and scarring of the tubulointerstitial tissue, the classic pathological signature of advancing CKD [3]. ACE's position at the convergence point of this cascade, together with its independent role in degrading the vasodilator peptide bradykinin, has made it one of the most extensively validated targets in cardiovascular and renal pharmacology for more than four decades [5].

Captopril reached clinical use in the early 1980s as the first orally active member of this drug class, opening the era of pharmacological ACE inhibition that continues today [6]. The 2024 KDIGO guidelines still place renin-angiotensin system blockade, whether through an ACE inhibitor or an angiotensin receptor blocker, at the front line of both blood-pressure control and kidney protection in CKD, a position reinforced by an extensive and steadily growing body of clinical trial evidence [7]. What this decades-long clinical record has not resolved, however, is the class-wide tolerability profile shared by captopril and its successors, enalapril, lisinopril and fosinopril among them, namely a persistent dry cough tied to bradykinin build-up, elevated potassium levels, a drop in blood pressure after the first dose, and, in a small subset of patients, angioedema severe enough to be life-threatening [7]. None of these limitations reflects a flaw in the underlying pharmacological strategy; rather, they are properties of the specific synthetic scaffolds used to achieve it, and they are what continues to motivate the search for structurally distinct inhibitors capable of acting on the same validated target through a gentler chemistry [7].

This search has increasingly turned toward phytochemicals. A 2023 review centred on CKD drew together evidence that several herbal sources,*Rosmarinus officinalis*, *Hibiscus sabdariffa*, *Curcuma long* and *Moringa oleifera* among them, inhibit ACE in preclinical testing to a degree on par with captopril or enalapril, and

made the case for natural ACE inhibitors as a worthwhile complement to existing hypertension and CKD management [8]. Structure-activity work on phenolic compounds has since pinned down part of the mechanism: potency tracks closely with how many hydroxyl groups sit on the aromatic ring, and inhibition proceeds mainly through coordination of ACE's catalytic zinc ion, an interaction reinforced by hydrogen bonding and hydrophobic contact with the surrounding active-site residues [9]. A more recent comparative assay of phenolic acids and flavonoids refined this picture further, placing chlorogenic acid at the top of a nine-acid potency ranking and caffeic acid at the bottom, while identifying kaempferol, the aglycone of the flavonol glucoside astragalin, as the third most potent of seven flavonoid aglycones examined [10]. These rankings matter directly to the present study, because they place two of its five candidate compounds at defined points along an established structure-activity spectrum rather than leaving them untested against any prior benchmark.

Parallel to this mechanistic work, a distinct and rapidly growing line of research has applied structure-based virtual screening, combining drug-likeness filtering, pharmacokinetic and toxicity prediction, and molecular docking against a crystallographic ACE receptor, to identify candidate natural inhibitors from specific plant sources. The closest precedent to the present study is a pair of 2026 investigations of Nypa fruticans (nipa palm) leaf phytochemicals, carried out explicitly in the context of hypertension and chronic kidney disease. The first identified quercetin, rosmarinic acid and caffeic acid as lead candidates through SwissADME, pkCSM and ACE docking, reporting binding affinities for quercetin and rosmarinic acid that exceeded the enalapril reference [11]. The second confirmed renoprotective activity for the same extract in a gentamicin-induced nephrotoxicity rat model, closing the loop between computational prediction and experimental outcome [12]. Together, these two studies confirm that this screening strategy is well established and genuinely capable of turning up plant compounds that outperform synthetic ACE inhibitors on paper, though the plant involved and the compounds identified are almost entirely different from those considered here, leaving the specific question posed by Jerusalem artichoke leaf phytochemistry unanswered. *Helianthus*

tuberosus L. (Jerusalem artichoke) is a hardy, rhizomatous perennial belonging to the genus Helianthus within the family Asteraceae, a genus of approximately fifty species of which only the common sunflower and Jerusalem artichoke are cultivated at any scale for medicinal and nutritional value, and whose taxonomic classification for this species is confirmed against the GBIF Backbone Taxonomy [13, 14].

Few crops ask as little of the land as this one: it copes with poor and variable soils without needing added fertiliser or pesticide, shrugs off frost and most common pests, and keeps growing even under semi-arid conditions, across annual precipitation of 31 to 282 cm, mean temperatures of 6.3 to 26.6°C, and soil pH values of 4.5 to 8.2 [13]. This resilience, together with minimal agronomic maintenance requirements, has sustained cultivation of the species across temperate regions worldwide for well over a century, historically for its edible, inulin-rich tubers, and more recently as a source of animal fodder and biofuel feedstock [13]. Although the tuber has historically attracted the greater share of agronomic and nutritional attention, on account of both its inulin content and its relevance to diabetic diets, the aerial organs of the plant, its leaves, stems and flowers, have increasingly been recognised as chemically distinct tissues in their own right. Various parts of Jerusalem artichoke have long been used in traditional medicine for digestive complaints, skin inflammation and wound healing, in addition to its established dietary role in diabetes management [13]. More recent pharmacological surveys have extended this traditional profile considerably, reporting antioxidant, anti-inflammatory, antimicrobial and hepatoprotective activity across extracts derived from different organs of the plant, effects generally attributed to its diverse phenolic and terpenoid content rather than to any single constituent [13]. Phytochemically, *Helianthus tuberosus* L. is a compositionally rich species even by the standards of the wider Helianthus genus, yielding hydroxycinnamic acid derivatives, flavonoid glycosides, sesquiterpene lactones and a range of minor phenolic constituents distributed unevenly across its tissues [15]. Comparative organ-level analysis has established that it is specifically the leaves, rather than the more commonly studied tubers, that represent the richest source of phenolic compounds in the plant, with chlorogenic acid and its related dicaffeoylquinic acid esters alone accounting for 72

to 82% of total leaf phenolic content [16]. Mass-spectrometric profiling of leaf tissue has additionally confirmed the presence of the flavone glucoside astragalin alongside this hydroxycinnamic acid family [17], while heliangine, one of eleven structurally related sesquiterpene lactones isolated and characterised from Jerusalem artichoke leaf tissue [18], has independently demonstrated anti-inflammatory activity in macrophage and vascular endothelial cell models, curbing excess nitric-oxide output and dialling down endothelial adhesion-molecule signalling, actions plausibly relevant to the vascular pathology shared by hypertension and CKD [19] has independently demonstrated anti-inflammatory activity.

Put plainly, this body of evidence puts the same families of phenolic and flavonoid compounds already linked to ACE inhibition squarely inside the leaf of a single, well-characterised plant, yet so far as the literature surveyed for this thesis shows, nobody has actually tested Jerusalem artichoke leaf phytochemicals against the enzyme, let alone within a CKD framing, which is precisely the gap this thesis sets out to close [11, 12].

1.1 Problem Statement

Chronic kidney disease, particularly its progression driven by overactivity of the renin-angiotensin-aldosterone system, is a major global health issue with rising prevalence and substantial mortality. Current ACE inhibitor therapies are effective but limited by side effects and reduced tolerability with prolonged use. Hence, there is a need to identify novel natural compounds targeting the same pathway.

1.2 Hypothesis

Jerusalem artichoke (*Helianthus tuberosus* L.) leaves contain numerous bioactive compounds which may have ACE-inhibitory potential. However, their role in chronic kidney disease mechanisms remains underexplored and requires further investigation.

1.3 Aim

To explore phytochemicals in the leaves of Jerusalem artichoke (*Helianthus tuberosus* L.) and evaluate their potential therapeutic association with chronic kidney disease through molecular docking.

1.4 Objectives

i. To identify the phytochemicals of *Helianthus tuberosus* L. leaves through phytochemical database screening.

ii. To select the identified compounds based on their reported medicinal properties.

iii. To analyze the binding affinities and interactions of selected candidates with the target protein and compare them with a clinically established reference drug.

Chapter 2

Literature Review

2.1 Chronic Kidney Disease and the Renin-Angiotensin-Aldosterone System

CKD does not develop in isolation from the RAAS. Long before overt kidney failure sets in, disturbances in this hormonal cascade are already driving many of the changes that eventually damage the nephron,[3–5] and ACE sits at the centre of that cascade as the enzyme most directly responsible for generating angiotensin II. The sections that follow look first at how large the CKD burden actually is, then work through the RAAS pathway step by step to show where ACE fits in, and finally turn to what the clinical evidence says about ACE inhibition as a treatment, including the side effects that, despite four decades of use, still push researchers to look for gentler, plant-derived alternatives[4, 7, 20].

2.1.1 Global Burden and Clinical Significance

The most recent Global Burden of Disease (GBD) estimates put the global prevalence of CKD in adults at approximately 788 million cases in 2023, more than double the 1990 figure, with roughly 4.6 million people receiving kidney replacement therapy, a near threefold increase since 1990, and CKD accounting for close to

1.5 million deaths annually, equivalent to one death every twenty seconds [1, 2]. Forecasting studies indicate that age-standardised mortality rates from CKD may increase by more than 30% compared with 2022 levels. This projected rise contrasts with the expected decline in mortality rates associated with stroke and ischaemic heart disease, potentially making CKD the third leading cause of death in Western Europe by 2050 [2]. This trajectory, combined with the disproportionate burden of CKD in low- and middle-income countries with limited access to renal replacement therapy, underlines the continuing need for affordable, low-toxicity therapeutic options that can complement or extend existing pharmacological management [1].

2.1.2 RAAS Pathophysiology and the Central Role of ACE

RAAS hyperactivation is one of the principal mechanisms implicated in both the initiation and the progression of CKD [3, 21]. The cascade begins when a fall in renal perfusion pressure, reduced sodium delivery to the macula densa, or increased renal sympathetic tone stimulates the juxtaglomerular apparatus of the kidney to release renin. Renin then acts as the rate-limiting enzyme on angiotensinogen, an alpha-2-globulin secreted continuously by the liver, cleaving it to generate the inactive decapeptide angiotensin I. Angiotensin I is subsequently hydrolysed by ACE, a chloride-dependent, zinc metallopeptidase expressed principally on pulmonary and vascular endothelium, to yield angiotensin II, a potent vasoactive octapeptide [3–5]. Angiotensin II then acts through at least three parallel effector pathways. It binds AT1 receptors on vascular smooth muscle to cause direct vasoconstriction and raise peripheral resistance, it stimulates the zona glomerulosa of the adrenal cortex to secrete aldosterone, which promotes renal sodium and water reabsorption and expands circulating blood volume, and it constricts the renal efferent arteriole, raising glomerular capillary pressure and driving hyperfiltration.

Sustained activity along these three branches converges on the same downstream outcome, namely glomerular hypertension, podocyte injury, proteinuria and progressive tubulointerstitial fibrosis in CKD [3–5]. ACE additionally inactivates bradykinin, a vasodilator kinin peptide with independent renoprotective actions,

so that pharmacological ACE inhibition benefits the system through several simultaneous mechanisms rather than a single one. By preventing the conversion of angiotensin I to angiotensin II, ACE inhibition reduces angiotensin II generation across all three effector pathways described above, while simultaneously reducing bradykinin degradation and thereby increasing bradykinin-mediated vasodilation [5, 22]. The combined result is reduced vasoconstriction and lower peripheral vascular resistance, reduced aldosterone-mediated sodium and water retention and hence lower circulating blood volume, and reduced efferent arteriolar constriction and hence lower glomerular capillary pressure, an overall pharmacological outcome associated with reduced glomerular hypertension, less podocyte injury, reduced proteinuria and slowed progression of CKD [3, 7, 21]. Figure 2.1 summarises this cascade, its three downstream branches, and the corresponding effects of ACE inhibition at each point in the pathway.

2.1.3 Evidence and Limitations of ACE Inhibition as a Therapeutic Strategy in CKD

Angiotensin-converting enzyme inhibitors have been used clinically since the discovery and approval of captopril, the first orally active ACE inhibitor, in the early 1980s [6]. Current guidance from Kidney Disease Improving Global Outcomes (KDIGO), issued in 2024, continues to recommend renin-angiotensin system inhibitors, either ACE inhibitors or angiotensin receptor blockers, as first-line antihypertensive and renoprotective therapy for individuals with CKD [7]. Comparative reviews of RAAS-pathway modulators in CKD emphasise that ACE inhibitors may offer marginally superior renoprotection to angiotensin receptor blockers, although both classes reduce cardiovascular risk to a broadly similar degree [21, 23]. A 2024 systematic review and individual participant-level meta-analysis of randomised trials in advanced CKD (estimated glomerular filtration rate below 30 mL/min/1.73 m^2) confirmed that ACE inhibitor or angiotensin receptor blocker therapy reduces the risk of kidney failure requiring replacement therapy relative to comparator antihypertensives, findings echoed by the subsequent STOP-ACEi trial literature

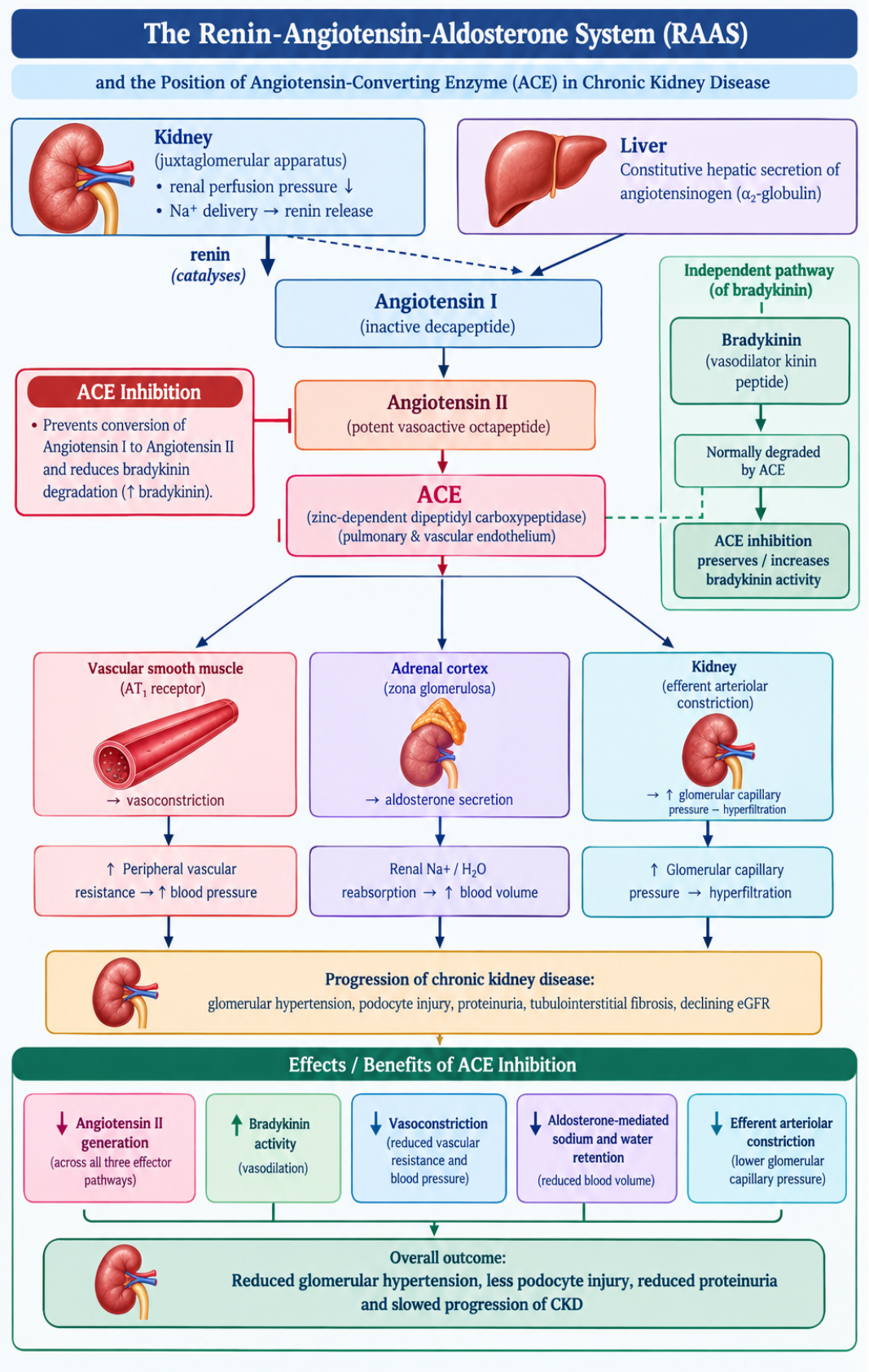


FIGURE 2.1: The renin–angiotensin–aldosterone system (RAAS), showing the role of angiotensin-converting enzyme (ACE) in the cascade and the effects of ACE inhibition in chronic kidney disease progression

on RAAS-inhibitor discontinuation in advanced disease [23–25]. At the same time, a 2024 review tracing the RAAS from its historical discovery to present practice notes that important questions remain regarding how best to individualise RAAS blockade, and that adverse effects, most notably hyperkalaemia, acute kidney injury risk and, for ACE inhibitors specifically, dry cough and rare but serious angioedema, continue to limit tolerability in some patients [4, 7, 20]. It is this combination of well-established efficacy and recognised tolerability limitations that motivates continued interest in structurally distinct, plant-derived ACE inhibitors as complementary or better-tolerated alternatives, discussed further in Section 2.3.

2.2 Angiotensin-Converting Enzyme as a Structure Based Drug Design Target

2.2.1 Structural Biology of ACE

Human somatic ACE is a two-domain, zinc-dependent dipeptidyl carboxypeptidase, with the N- and C-domains sharing high sequence identity but differing subtly in substrate specificity and in their contribution to blood pressure regulation. The C-domain is understood to be primarily responsible for angiotensin I hydrolysis in vivo, which has motivated a research programme into C-domain-selective inhibitors intended to reduce the incidence of angioedema and other side effects associated with dual-domain inhibition [5]. Natesh et al. solved the first high-resolution crystal structures of human testis ACE, reporting both the native, ligand-free enzyme and its complex with the clinically used inhibitor lisinopril within the same study. The lisinopril-bound structure confirmed the catalytic zinc ion at the centre of the substrate-binding channel and provided the structural template subsequently used across the field for structure-based inhibitor design [22]. These structures are deposited in and freely available from the RCSB Protein Data Bank [26], and the two crystal forms from this study, deposited as PDB entries 1O8A (the native structure) and 1O86 (the lisinopril complex), have subsequently

been used as docking receptors in independent computational screening studies, a methodological point returned to in Section 2.6.

2.2.2 Synthetic ACE Inhibitors and Their Limitations

The discovery of captopril, developed by Cushman and Ondetti from peptide leads initially derived from the venom of the Brazilian pit viper (Bothrops jararaca), established ACE as a tractable, rational drug design target and remains a landmark case study in structure-guided medicinal chemistry [6]. Captopril was followed by carboxyl-containing agents such as enalapril and lisinopril and by phosphinyl-containing compounds such as fosinopril, all of which act by chelating the catalytic zinc ion within the ACE active site [5, 6]. Despite their proven efficacy, these agents share a class-wide side-effect profile, namely persistent dry cough attributed to bradykinin and substance P accumulation, hyperkalaemia, first-dose hypotension and, in a small proportion of patients, potentially life-threatening angioedema, which has never been fully eliminated across four decades of clinical use [7]. These limitations, rather than any deficiency in the underlying pharmacological strategy, are what sustain the search reviewed in the remainder of this chapter for structurally distinct, naturally occurring ACE inhibitors that might offer a gentler tolerability profile while acting on the same validated target.

2.3 Natural and Plant-Derived ACE Inhibitors

2.3.1 Rationale for Phytochemical ACE Inhibitors

A 2023 review framed specifically around CKD found that several herbal sources, among them *Rosmarinus officinalis*, *Hibiscus sabdariffa*, *Curcuma longa* and *Moringa oleifera*, show ACE-inhibitory activity comparable to captopril or enalapril in preclinical assays, and argued that natural ACE inhibitors merit continued investigation as adjuncts for hypertension, respiratory distress syndrome and chronic kidney disease specifically [8]. The same review situates this activity within a broader

chemical landscape spanning alkaloids, amino acids, anthocyanidins, flavonoids, glucosinolates, isoflavonoids, phenolic acids, polyphenolics and triterpenoids, and attributes the sustained research interest in this area to the comparatively mild side-effect profile of plant-derived compounds relative to synthetic agents, together with their routine presence in ordinary dietary intake [8]. It is this CKD-specific framing, rather than a generic hypertension framing, that most closely matches the compounds and disease context considered in this chapter, and the closest comparable prior study discussed in Section 2.1.3.

2.3.2 Structure-Activity Relationships of Phenolic and Flavonoid ACE Inhibitors

The mechanistic basis for ACE inhibition by phenolic compounds has been examined systematically in several structure-activity relationship (SAR) studies. Al Shukor et al. tested 22 phenolic compounds spanning hydroxybenzoic acids, hydroxycinnamic acids and flavonoids, and found that the number of hydroxyl groups on the aromatic ring is a key determinant of ACE-inhibitory potency, that methoxy substitution reduces activity, and that molecular docking confirmed a shared binding mode in which phenolic acids and flavonoids coordinate the catalytic zinc ion, with this interaction further stabilised by hydrogen bonding and hydrophobic contacts with surrounding active-site residues [9].

Complementary in vitro work by Guerrero et al. on 17 flavonoids spanning five structural subclasses found the highest ACE-inhibitory activity for luteolin (IC50 = 23 μM), followed by quercetin, rutin and kaempferol, establishing that flavonoid aglycones are generally more potent ACE inhibitors than their corresponding glycosides [27]. This pattern was refined further in a 2025 study by Zielińska et al., which directly compared phenolic acids, flavonoid aglycones, their O-glucosides, and low-molecular-weight phenolic metabolites using a fluorescence-based ACE assay. Among phenolic acids, the potency ranking was chlorogenic acid > p-coumaric acid > sinapic acid > gentisic acid > ferulic acid > syringic acid > vanillic acid > protocatechuic acid > caffeic acid, while among flavonoid aglycones the ranking

was luteolin > quercetin > kaempferol > cyanidin > delphinidin > pelargonin > naringenin. The 3-O-glucosides of these flavonoids were consistently less active than their parent aglycones, although certain 7-O-glucosides retained or even exceeded aglycone-level activity [10]. These two rankings are directly relevant to the compounds discussed in this chapter. They place chlorogenic acid at the top of the phenolic-acid series and caffeic acid at the bottom, and they identify kaempferol, the aglycone of astragalin, as a comparatively potent flavonoid ACE inhibitor whose 3-O-glucoside form would, on this SAR pattern, be expected to show reduced but not necessarily negligible activity. This expectation is revisited compound-by-compound in Section 2.5.

2.3.3 Recent *In Silico* and In Vitro Studies of Plant-Derived ACE Inhibitors

A cluster of recent computational studies has applied structure-based virtual screening pipelines, combining drug-likeness filtering, ADMET prediction and molecular docking against an ACE crystal structure, to identify candidate natural ACE inhibitors from a range of plant sources. Among these, the study whose disease framing and compound interests align most closely with the focus of this chapter is a 2026 study by Islam et al., which computationally evaluated phytochemicals from Nypa fruticans (nipa palm) leaves as ACE inhibitors explicitly in the context of hypertension and chronic kidney disease [11]. That study identified 36 compounds by HPLC and GC-MS profiling, of which quercetin, rosmarinic acid and caffeic acid were carried forward as key bioactive candidates.

Pharmacokinetic and toxicity screening was performed with SwissADME, pkCSM and ProTox 3.0, and molecular docking against ACE (PDB code 1O86) found binding affinities of -8.28 kcal/mol for quercetin and -8.95 kcal/mol for rosmarinic acid, both stronger than the enalapril reference (-8.1 kcal/mol). Density functional theory (DFT) analysis additionally showed that rosmarinic acid had a HOMO-LUMO energy gap (0.1342 eV) similar to that of enalapril (0.1488 eV), interpreted as evidence of comparable chemical reactivity [11]. A companion 2026 study from

the same research group went further, testing an ethyl acetate extract of *Nypa fruticans* leaves in a gentamicin-induced nephrotoxicity rat model and reporting significant improvement in renal function biomarkers alongside reduced tubular necrosis and glomerular damage, with rosmarinic acid, quercetin and (-)-epicatechin again highlighted as the leading computationally and experimentally supported candidates [12]. Because this pair of studies shares the same disease framing (CKD via RAAS/ACE hyperactivation) and the same core computational toolkit (SwissADME, pkCSM, ACE-crystal-structure docking), it is treated throughout the remainder of this chapter as the most directly comparable prior work in this literature, summarised alongside other studies in Table 2.4, without at any point representing the same plant species or the same compound panel.

Several other recent studies illustrate the methodological range found elsewhere in this literature. Yue et al. combined 3D-QSAR pharmacophore modelling, untargeted UPLC-based metabolomics, molecular docking (cross-validated between AutoDock Vina, CB-Dock2 and Schrödinger Glide) and 100-nanosecond molecular dynamics simulations to screen 680 compounds identified in *Suaeda salsa*, narrowing to six top-hit ACE-binding candidates docked against ACE structure PDB 1O86 [28]. A 2024 study of 1,526 in-house phytoconstituents from edible plants combined virtual screening with domain-selective docking against the ACE N- and C-domains and in vitro validation, isolating 4-O-caffeoylquinic acid, a positional isomer of 5-p-coumaroylquinic acid, as a C-domain-selective inhibitor (IC50 = 62.92 μM) that acted synergistically with captopril [29].

A 2026 study of the medicinal plant *Pluchea indica* (Beluntas) screened 110 phytoconstituents through an ADMET funnel that reduced the candidate set to 20 compounds prior to docking against ACE, illustrating a large-panel triage strategy for candidate selection [30]. Earlier work on soybean (*Glycine max*) phytomolecules combined docking with molecular dynamics simulation across 34 candidate compounds and identified beta-sitosterol as the most potent predicted ACE inhibitor of the panel [31], while a 2024 network pharmacology and docking study of Fabaceae species demonstrated the growing popularity of combining pathway-level network analysis with target-specific docking in antihypertensive phytochemical research

[32]. Collectively, these studies confirm that structure-based virtual screening of plant phytochemicals against ACE is active and rapidly developing research area, but none of them screens Jerusalem artichoke leaf phytochemicals specifically, and none evaluates the particular five-compound panel considered in this chapter, a gap returned to explicitly in Section 2.7.

2.4 Jerusalem Artichoke: Phytochemistry and Bioactivity

Helianthus tuberosus L. (Jerusalem artichoke) belongs to the genus Helianthus within the family Asteraceae and subfamily Asteroideae, a genus comprising approximately 50 species of which only two, Jerusalem artichoke and the common sunflower (Helianthus annuus), are widely cultivated for medicinal and nutritional value [13].

Unlike H. annuus, which is grown principally as an oilseed crop, Jerusalem artichoke is a perennial, tuberous herbaceous plant cultivated across temperate regions worldwide for a considerably wider range of beneficial traits [13]. Table 2.1 sets out its standard taxonomic classification, verified directly against the GBIF Backbone Taxonomy species record for *Helianthus tuberosus* L. [14].

TABLE 2.1: Taxonomic Classification of *Helianthus tuberosus* L. [14]

Rank	**Classification**
Kingdom	Plantae
Phylum	Tracheophyta
Class	Magnoliopsida
Order	Asterales
Family	Asteraceae
Genus	Helianthus
Species	*Helianthus tuberosus* L.

2.4.1 Morphological Features

The plant's aerial parts comprise an erect, pubescent stem bearing opposite, ovate-lanceolate leaves with serrate margins and a terminal yellow flower head (capitulum) characteristic of the Asteraceae, while its underground portion consists of a fibrous root system, stolons and fleshy tubers [13]. The tubers themselves are irregular in shape, variously described as round, pear-shaped or oval and resembling potatoes, and their colour ranges from pale brown to dark brown, red, purple or white depending on cultivar and local growing conditions [13]. Figure 2.2 illustrates these principal organs, namely the whole plant, leaves, flowers and tubers. It is this same organ-level distinction between aerial tissue (leaves, flowers, stems) and the underground tuber that underlies the leaf-specific phytochemical focus of this chapter, developed further in Section 2.4.5.

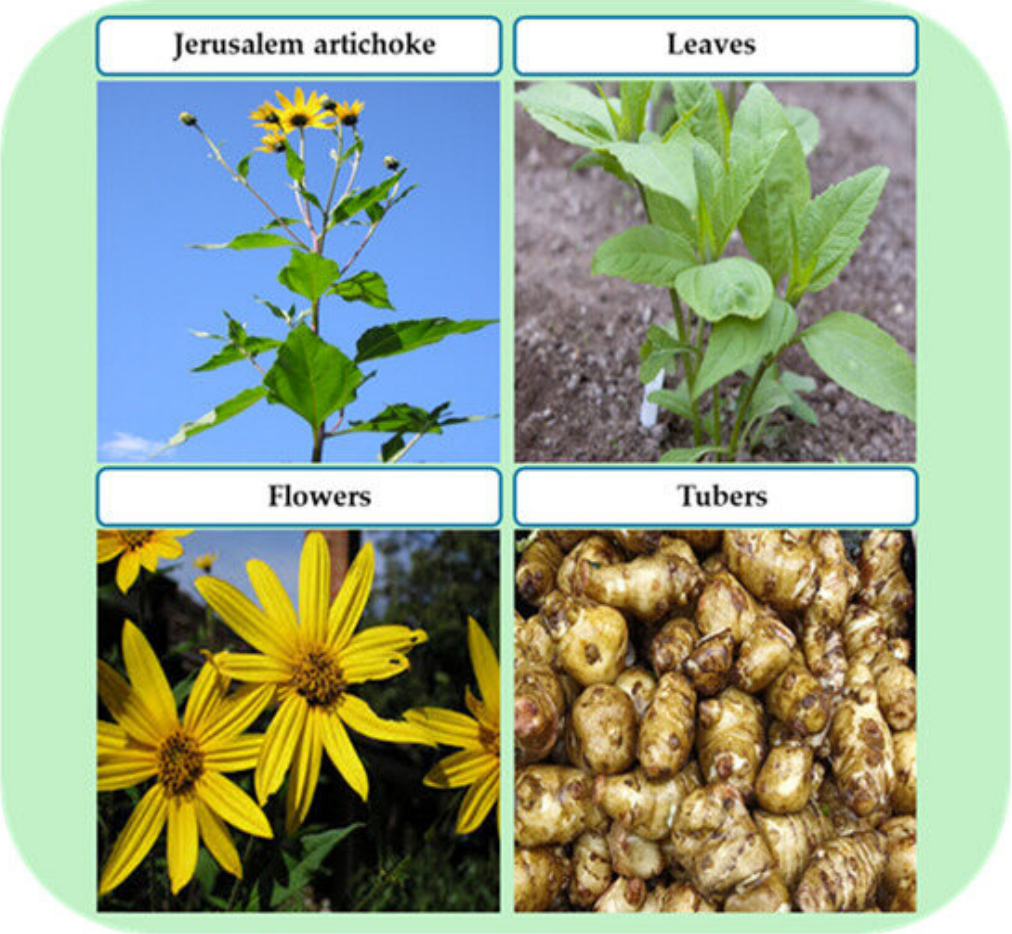


FIGURE 2.2: Principal organs of *Helianthus tuberosus* L. (Jerusalem artichoke), including the whole plant, leaves, flowers and tubers [13]

2.4.2 Life Cycle and Growth Pattern

The species is notably hardy. It tolerates a broad range of soil types without requiring chemical fertilisers or pesticides, shows strong frost resistance, requires minimal agronomic maintenance, and demonstrates high tolerance to pests and diseases, growing well even in semi-arid conditions under annual precipitation of 31 to 282 cm, temperatures of 6.3 to 26.6 degrees Celsius, and soil pH between 4.5 and 8.2 [13].

These growing-condition differences have themselves been reported to influence the plant's growth characteristics and the content and composition of its bioactive compounds, meaning phytochemical yield can vary with climate, soil and cultivar [13]. As a perennial, Jerusalem artichoke persists from season to season through its underground tuber system while completing its above-ground growth cycle annually, typically reaching a mature height of 300 to 450 cm within a single growing season [13].

2.4.3 Traditional and Medicinal Uses

Beyond its contemporary phytochemical characterisation, Jerusalem artichoke has a documented history of use in traditional and folk medicine, where it has been applied to pain, wounds, digestive complaints, arthritis, rheumatism and skin disorders, with the specific mode of preparation varying by region [13]. In European and Russian folk practice, the plant was most commonly consumed raw or boiled to relieve digestive disorders and joint pain, whereas in East Asian traditional use it was more often prepared in dried or sliced form to treat skin conditions and reduce inflammation [13]. Table 2.2 correlates these traditional applications of Jerusalem artichoke with the modern pharmacological findings identified for each, organised here by the strength of the underlying evidence, from human studies through to in vitro assays, and compiled from the same source.

These regional traditional applications are broadly consistent with the antioxidant, anti-inflammatory and antimicrobial bioactivities subsequently reported for the

plant's phenolic acid and flavonoid constituents, discussed further in Section 2.4.6, although the review from which this evidence is drawn is careful to note that rigorous pharmacological validation of individual traditional claims remains limited to date [13].

TABLE 2.2: Ethnomedicinal Applications of Jerusalem Artichoke Correlated with Modern Pharmacological Findings [13]

Plant Part Used	**Traditional Application**	**Principal Constituents**	**Modern Pharmacological Correlate**
Tuber (consumed raw, boiled or pickled)	Relief of digestive discomfort	Inulin, dietary fibre	Supports gut-microbiota balance and improves digestive and lipid-metabolic function (human, in vivo evidence)
Tuber (dietary intake or extract)	Management of elevated blood glucose	Inulin	Helps regulate circulating glucose and enhances insulin sensitivity (human, in vivo evidence)
Tuber (whole extract)	Weight and metabolic management	Inulin, polysaccharides	Limits lipid accumulation and favourably alters lipid profile, appetite and body weight (human, in vivo evidence)
Leaves and tuber (extract)	General anti-inflammatory use	Polyphenols, flavonoids, phenolic acids	Reduces inflammatory mediators and oxidative stress (in vitro and in vivo evidence)
Tuber (applied topically)	Wound care and skin conditions	Polyphenols, sesquiterpene lactones	Promotes wound closure and skin barrier repair alongside antioxidant and anti-inflammatory action (in vitro and in vivo evidence)

Continued on next page

TABLE 2.2: Ethnomedicinal Applications of Jerusalem Artichoke Correlated with Modern Pharmacological Findings [13] (continued)

Plant Part Used	**Traditional Application**	**Principal Constituents**	**Modern Pharmacological Correlate**
Leaves and tuber (prepared as a decoction)	Relief of joint pain, arthritis and rheumatism	Polyphenols, sesquiterpenes	May relieve pain and inflammation through antioxidant and anti-inflammatory mechanisms (in vitro and in vivo evidence)
Leaves and tuber (extract)	Antioxidant and skin-ageing prevention	Polyphenols, flavonoids	Scavenges free radicals and protects cells from oxidative damage (in vitro and in vivo evidence)
Leaves (extract)	Antimicrobial use	Polyphenols, sesquiterpenes	Inhibits growth of selected bacterial and fungal pathogens (in vitro evidence)

2.4.4 General Phytochemical Composition

Jerusalem artichoke is best known agronomically for the high inulin content of its tubers, a fructose-based storage polysaccharide that underlies much of the plant's traditional and functional-food use [13]. Beyond inulin, however, extracts derived from the tubers, leaves, flowers and aerial biomass collectively contain a diverse array of bioactive compounds, including phenolic acids, flavonoids, sesquiterpene lactones and amino acids, that have been associated in preclinical studies with antioxidant, anti-inflammatory, antihyperglycaemic, nutraceutical and pharmaceutical applications beyond its traditional role as an inulin source [13]. The relative abundance of these compound classes nonetheless varies substantially by plant organ, a distinction examined in detail for the leaves specifically in Section 2.4.5.

2.4.5 Leaf-Specific Phytochemical Profile

Ultra-high-performance liquid chromatography electrospray ionisation Orbitrap mass spectrometry (UHPLC-ESI-Orbitrap-MS/MS) profiling of a leaf protein concentrate isolated from Jerusalem artichoke green biomass identified 53 distinct phytochemicals, dominated by mono- and di-hydroxycinnamic acid esters of quinic acid alongside several hydroxylated methoxyflavones and flavone glucosides, including kaempferol-3-O-glucoside (astragalin) and quercetin-3-O-glucoside (isoquercetin) [17]. Comparative organ-level analysis has likewise found the leaves, rather than the tubers, to be the richest source of phenolic compounds specifically, with total phenolic content reported as highest in leaf extracts, followed by flower, then tuber, then stem, and chlorogenic acid together with its related dicaffeoylquinic acid esters accounting for 72-82% of corrected total phenolic content in leaf and tuber extracts [16]. This UHPLC-MS/MS characterisation is the primary literature basis confirming that both a hydroxycinnamoyl-quinic acid family of compounds and the specific flavone glucoside astragalin co-occur naturally in Jerusalem artichoke leaf tissue, directly supporting chlorogenic acid, caffeic acid, 5-p-coumaroylquinic acid and astragalin as a chemically coherent, leaf-representative set of Jerusalem artichoke phytochemicals.

2.4.6 Reported Pharmacological Properties

Beyond the specific traditional applications discussed in Section 2.4.3, more recent pharmacological studies have examined several of these medicinal properties in greater mechanistic detail. Table 2.3 compiles compound-level findings from the same source, spanning human, in vivo and in vitro evidence and including heliangin and kaempferol-3-O-glucoside among the compounds already discussed in this chapter, as it corresponds to that paper's reference list rather than to the reference list of this chapter. The sub-sections below then summarise the properties most consistently reported for Jerusalem artichoke extracts, with particular attention to the antihypertensive and cardiovascular activity most directly relevant to the ACE-inhibition focus of this chapter [13].

TABLE 2.3: Compound-Level Evidence for the Bioactivity of Jerusalem Artichoke Constituents [13]

Compound / Extract	**Plant Source**	**Study Model (Evidence Level)**	**Endpoints Assessed**	**Principal Finding**
Inulin-rich extract	Tuber	Older human adults (human, in vivo)	Postprandial glucose, gut microbiota composition	A single morning dose lowered post-meal glucose and favourably shifted gut microbial composition
Phenolic-rich extract	Tuber and leaf	HaCaT and BJ fibroblast cell lines (in vitro)	Antioxidant capacity, cytotoxicity	Strong radical-scavenging activity was observed alongside minimal cytotoxic effect, favourably composition
Kaurenoic acid	Flowers	Bacterial and immune cell models (in vitro)	Inflammatory markers, microbial growth inhibition	Displayed combined antibacterial and anti-inflammatory action
Heliangin	Aerial parts	LPS-stimulated RAW 264.7 macrophages (in vitro)	Nitric oxide production, inflammatory mediators	Suppressed inflammatory signalling through inhibition of the NF-κB pathway
Ethyl acetate fraction	Tuber	HepG2 and NIH 3T3 cell lines (in vitro)	Glucose uptake, wound closure	Enhanced cellular glucose handling and accelerated wound healing

Continued on next page

TABLE 2.3: Compound-Level Evidence for the Bioactivity of Jerusalem Artichoke Constituents [13] (continued)

Compound / Extract	**Plant Source**	**Study Model (Evidence Level)**	**Endpoints Assessed**	**Principal Finding**
Chlorogenic acid	Tuber	Inflammatory cell models (in vitro)	Cytokine release, reactive oxygen species	Reduced inflammatory cytokine output and oxidative stress markers
Ferulic acid	Tuber	Cancer and metabolic cell models (in vitro)	Oxidative stress, glucose metabolism	Showed antioxidant activity together with glucose-lowering effects
Butein	Leaves	Cancer cell lines (in vitro)	Apoptosis	Induced programmed cell death in cancer cells
Kaempferol 3-O-glucoside	Leaves	Microbial and oxidative-stress assays (in vitro)	Microbial growth inhibition, reactive oxygen species	Combined antioxidant and antimicrobial action was observed
Heliangin	Leaves	Vascular and immune cell models (in vitro)	Inflammatory signalling pathways	Reduced markers linked to inflammation and atherosclerotic vascular injury
Vanillin	Whole plant	Cell-based assays (in vitro)	Glucose metabolism, inflammatory markers	Exhibited antidiabetic and anti-inflammatory effects

Continued on next page

TABLE 2.3: Compound-Level Evidence for the Bioactivity of Jerusalem Artichoke Constituents [13] (continued)

Compound / Extract	**Plant Source**	**Study Model (Evidence Level)**	**Endpoints Assessed**	**Principal Finding**
4,15-Isoatriplicolide	Whole plant	Cancer cell lines (in vitro)	Cell proliferation	Inhibited proliferation of cancer cells
Inulin (selenium nanoparticle formulation)	Tuber-derived nanoparticle preparation	Cancer cells and murine model (in vitro and in vivo)	Tumour growth	Enhanced targeted delivery and suppressed tumour growth

2.4.6.1 Antioxidant Activity

Antioxidant activity is among the most consistently reported bioactivities of Jerusalem artichoke and has been demonstrated across multiple plant organs. Comparative analysis of tuber, leaf, flower and stem extracts attributes this activity principally to phenolic acid content, with leaf extracts showing the strongest free-radical-scavenging capacity of the organs tested, tracking closely with their higher total phenolic content [16]. The 2026 phytochemistry review attributes this activity broadly to the plant's phenolic acid and flavonoid constituents and notes that antioxidant capacity underlies several of the plant's other reported effects, including its anti-inflammatory and skin-protective properties [13].

2.4.6.2 Anti-Inflammatory Activity

Anti-inflammatory activity has been reported for Jerusalem artichoke extracts generally [13], and has been characterised in the most mechanistic detail for heliangin, the major sesquiterpene lactone of the leaves.

In lipopolysaccharide-stimulated macrophages, heliangin suppressed nitric oxide overproduction, and in TNF-alpha-stimulated vascular endothelial cells it inhibited expression of the adhesion molecules ICAM-1, VCAM-1 and E-selectin together with the chemokine MCP-1, acting through inhibition of NF-kB and IkB-alpha phosphorylation [19]. Because this adhesion-molecule and NF-kB signalling cascade is a recognised early step in atherosclerotic vascular injury, the study's authors proposed heliangin as a candidate for preventing the vascular inflammation that underlies atherosclerosis, an effect with plausible relevance to the vascular pathology of CKD given the endothelial dysfunction implicated in both conditions [19].

A broader review of Helianthus genus phytochemistry situates heliangin within the germacranolide class of sesquiterpene lactones characteristic of Asteraceae secondary metabolism, while noting that terpenoid bioactivities within this genus remain comparatively less thoroughly characterised than the genus's phenolic constituents [15], a point returned to in Section 2.5.5.

2.4.6.3 Antimicrobial and Antifungal Activity

Antifungal activity is listed among the biological effects reported for Jerusalem artichoke extracts in the 2026 phytochemistry review, alongside the antioxidant, anti-inflammatory, antihyperglycaemic and antihypertensive activities discussed elsewhere in this section [13].

Compound-specific antimicrobial or antifungal evidence for the five phytochemicals considered in this chapter was not identified in the literature reviewed for this chapter, and this is noted here as a gap rather than inferred.

2.4.6.4 Antihyperglycaemic and Metabolic Activity

Antihyperglycaemic activity is one of the most frequently cited properties of Jerusalem artichoke, reported alongside broader metabolic relevance to obesity and colorectal cancer prevention [13]. These metabolic effects have been linked in the

literature to both the plant's inulin content, fermented by gut microbiota to influence postprandial glucose response, and to its phenolic acid and flavonoid constituents [13]. The 2026 review further notes emerging evidence for immune modulation through alteration of intestinal microbiota composition, and for skin-protective, anti-aging effects attributed to the plant's antioxidant capacity, indicating a broader functional-food relevance that extends beyond the cardiovascular and renal focus of this chapter [13].

2.4.6.5 Antihypertensive and Cardiovascular Activity

Antihypertensive activity is explicitly listed among the biological effects reported for Jerusalem artichoke extracts [13], and is the property most directly relevant to the ACE-inhibition focus of this chapter. This general antihypertensive claim is reinforced mechanistically by heliangin's endothelial-protective, anti-inflammatory activity described above, and independently by the class-level ACE-inhibitory evidence available for the plant's phenolic acid and flavonoid constituents reviewed in Section 2.3.2. Because vascular endothelial dysfunction and inflammation are recognised contributors to the hypertension-CKD axis, this combined evidence, although not itself a direct ACE-inhibition assay for Jerusalem artichoke as a whole, provides an independent cardiovascular and renal rationale for the phytochemical panel investigated in this chapter.

2.5 ACE-Relevant Evidence for the Five Compounds of Interest

The five compounds discussed in this chapter are not a structurally arbitrary set. As Figure 2.3 illustrates, they fall into two chemical classes, both well represented in Jerusalem artichoke leaf tissue and both previously implicated, at the level of their chemical class, in ACE inhibition. Three are hydroxycinnamic acid derivatives (chlorogenic acid, caffeic acid and 5-p-coumaroylquinic acid), one is a flavonol

glucoside (astragalin), and one is a sesquiterpene lactone (heliangine). The subsections below examine each compound individually against the literature identified in Sections 2.3 and 2.4, and Table 2.4, presented in Section 2.6, situates these compounds alongside the wider literature on natural ACE inhibitors.

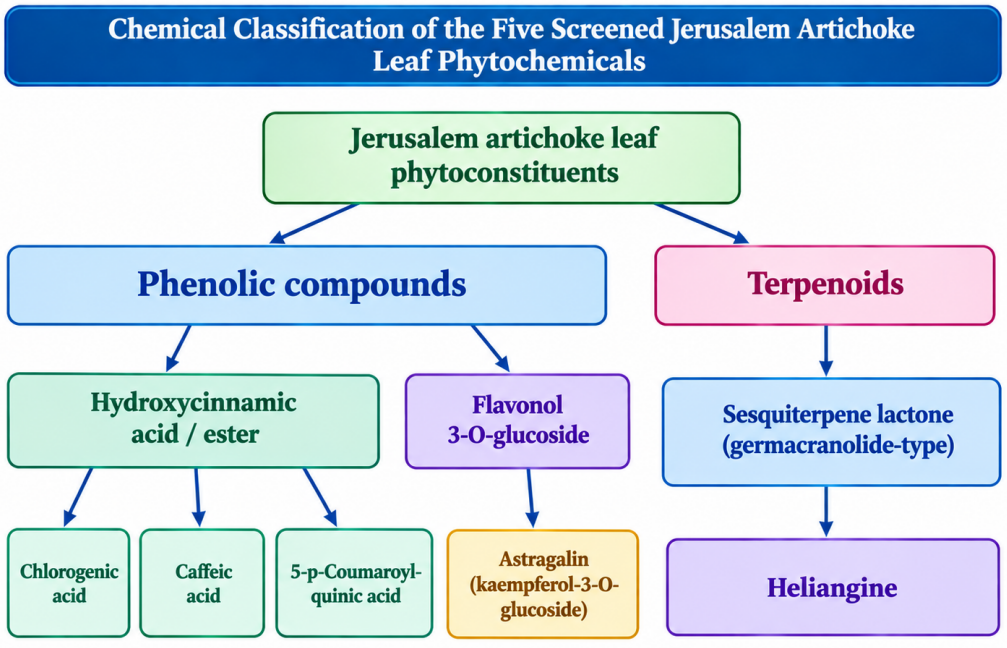


FIGURE 2.3: Structural classification of five Jerusalem artichoke leaf phytochemicals by chemical class.

2.5.1 Chlorogenic Acid

Chlorogenic acid (5-O-caffeoylquinic acid) is, together with its related dicaffeoylquinic acid isomers, the dominant phenolic constituent of Jerusalem artichoke leaves, accounting for the large majority of total leaf phenolic content [16]. In the direct ACE-inhibition ranking reported by Zielińska et al., chlorogenic acid was the most potent of nine phenolic acids tested [10], and a 2025 network pharmacology study modelling chlorogenic acid's mechanism of action in an unrelated inflammatory-injury context found favourable predicted molecular docking binding between chlorogenic acid and several protein targets including ACE, among a panel of ten shared targets identified computationally [33]. Although that docking result was generated for a different disease indication and does not by itself establish

antihypertensive efficacy, it is nonetheless independent computational evidence that chlorogenic acid is capable of favourable *In Silico*binding to the ACE protein.

2.5.2 Caffeic Acid

Caffeic acid is the simplest hydroxycinnamic acid discussed in this chapter and is present in Jerusalem artichoke leaves both as the free acid and as the biosynthetic precursor of chlorogenic acid and its related quinic acid esters [16]. In the same comparative ACE-inhibition ranking that placed chlorogenic acid first among phenolic acids, caffeic acid was ranked last of the nine acids tested, indicating comparatively weak ACE-inhibitory activity relative to its more highly esterified relatives [10]. This class-level evidence positions caffeic acid as the weakest ACE-inhibitory candidate among the hydroxycinnamic acid derivatives considered here, and as a useful lower-bound reference point for interpreting the other compounds in this group.

2.5.3 5-p-Coumaroylquinic Acid

5-p-Coumaroylquinic acid is a cinnamate ester formed from the condensation of p-coumaric acid with quinic acid, structurally analogous to chlorogenic acid but bearing a single hydroxyl group on the aromatic ring rather than the catechol pair present in caffeic acid derivatives, and it has been reported among the hydroxycinnamate profile of *Helianthus tuberosus* L. leaf tissue [16]. A recent review of the broader caffeoylquinic acid family notes that this class of hydroxycinnamate esters, of which 5-p-coumaroylquinic acid is a structural relative, is associated with antioxidant, antimicrobial, anti-diabetic and anti-inflammatory pharmacological activity, although the review does not extend to ACE-specific evidence for individual positional isomers [34]. No compound-specific ACE-inhibition assay for 5-p-coumaroylquinic acid itself was identified in the literature reviewed for this chapter. This is noted here as a genuine evidence gap rather than inferred or filled with an unverifiable claim. Two indirect lines of class-level evidence are

nonetheless available. First, in the phenolic-acid ACE-inhibition ranking discussed above, the parent acid p-coumaric acid ranked second only to chlorogenic acid, ahead of caffeic acid [10]. Second, the positional isomer 4-O-caffeoylquinic acid, differing from 5-p-coumaroylquinic acid only in the position of esterification and in bearing a catechol rather than a single hydroxyl, was shown by domain-selective docking to bind preferentially to the ACE C-domain, the domain primarily responsible for angiotensin I hydrolysis in vivo [5, 29]. Together, this positions 5-p-coumaroylquinic acid as a chemically plausible but not yet directly confirmed ACE-inhibitory candidate.

2.5.4 Astragalin (Kaempferol-3-O-glucoside)

Astragalin, the 3-O-glucoside of the flavonol kaempferol, was among the flavone glucosides identified by UHPLC-ESI-Orbitrap-MS/MS profiling of Jerusalem artichoke leaf protein concentrate [17]. Kaempferol itself, astragalin's aglycone, ranked third among seven flavonoid aglycones tested for ACE inhibition, behind only luteolin and quercetin [10]. The same comparative study found that 3-O-glucosylation of flavonoids generally reduces ACE-inhibitory potency relative to the parent aglycone, although select 7-O-glucosides were exceptions to this pattern [10]. On this structure-activity basis, astragalin would be expected to retain some, but likely reduced, ACE-inhibitory activity relative to free kaempferol, an expectation that underlines the value of testing glucoside derivatives such as astragalin directly rather than relying on aglycone data alone.

2.5.5 Heliangine

Heliangine is a germacranolide-type sesquiterpene lactone first isolated and characterised from Jerusalem artichoke leaves, and remains one of the compounds most closely associated with this specific plant tissue in the phytochemical literature [15, 18]. No published assay of heliangine's direct ACE-inhibitory activity was identified in the course of this review, which is again noted openly rather than inferred.

The available bioactivity evidence for heliangine is instead cardiovascular-adjacent. As discussed in Section 2.4.6, heliangine has been shown to suppress nitric-oxide overproduction in macrophages and to inhibit TNF-α-induced adhesion-molecule expression in vascular endothelial cells via the NF-κB pathway, a mechanism proposed to be protective against atherosclerosis [19]. A 2026 review of Helianthus genus phytochemistry further notes that terpenoid constituents of this genus have received comparatively less pharmacological characterisation against cardiovascular and renal targets than the genus's phenolic acids and flavonoids [15]. Heliangine is accordingly best understood as an exploratory extension of ACE-inhibitor interest into a chemical class, namely sesquiterpene lactones, that is under-represented in the existing plant-derived ACE-inhibitor literature relative to phenolics, rather than as a compound with pre-existing direct ACE evidence.

2.6 Computational and Experimental Approache in the Literature

2.6.1 Structured Virtual Screening and Docking Platforms

Structure-based virtual screening of ACE inhibitors depends first on the availability of a validated three-dimensional receptor structure, and the RCSB Protein Data Bank has served as the universal repository for such structures since its establishment [26], with candidate compound structures typically retrieved from public chemical repositories such as PubChem [35]. As noted in Section 2.2.1, both PDB 1O8A and PDB 1O86 have been used as ACE docking receptors in independently published studies [11, 22, 28]. Binding-site prediction tools such as DoGSiteScorer apply automated cavity-detection algorithms to flag candidate druggable pockets prior to docking [36]. For the docking step itself, the literature reviewed in this chapter uses a range of platforms, including CB-Dock2, a cavity-detection-guided blind docking server that automatically identifies and ranks candidate binding cavities on the receptor surface [37], and AutoDock Vina and Schrödinger Glide,

which are more commonly paired with a manually defined or homology-guided binding site [28].

2.6.2 ADMET and Drug-Likeness Prediction Tools

Across the plant-derived ACE-inhibitor literature reviewed in this chapter, drug-likeness triage is almost universally performed against Lipinski's Rule of Five, comprising molecular weight, hydrogen-bond donor and acceptor counts, calculated LogP and rotatable bond count, most commonly implemented through the freely available SwissADME web server [38, 39]. Detailed absorption, distribution, metabolism, excretion and toxicity (ADMET) profiling is most frequently performed using pkCSM, a graph-based signature method for small-molecule pharmacokinetic and toxicity prediction [40], often supplemented in more recent studies by ProTox 3.0 for additional toxicity endpoints [11]. Some comparator studies extend this toolkit further still, for example incorporating density functional theory (DFT) calculation of frontier molecular orbital energy gaps as a secondary indicator of chemical reactivity alongside docking scores [11, 28].

2.6.3 Summary of Reviewed Literature

Table 2.4 consolidates the studies discussed throughout this chapter into a single summary, drawing together structure-activity relationship studies of phenolic acids and flavonoids, computational virtual-screening studies of plant phytochemicals against ACE, and the Jerusalem artichoke phytochemistry and bioactivity studies that establish the occurrence and pharmacological relevance of the five compounds considered in Section 2.5. Studies are grouped by theme and ordered by publication year within each theme, and entries recorded as ”not stated” reflect information not available in the abstracts and summaries accessible for this review rather than an assumed value. Read as a whole, the table highlights the range of plant sources, panel sizes and computational approaches already applied across this field,

providing the basis for the more detailed positioning of the compounds that follows in Section 2.7.

TABLE 2.4: Summary of Structure-Activity, Computational-Screening and Jerusalem Artichoke Phytochemistry Studies

Study	**Compound(s) / source**	**Approach**	**Key finding**
Al Shukor et al., 2013 [9]	22 phenolic compounds (hydroxybenzoic acids, hydroxycinnamic acids, flavonoids)	In vitro ACE assay and molecular docking	Zinc coordination is the shared ACE-inhibitory mechanism, hydroxylation increases potency and methoxylation reduces it
Guerrero et al., 2012 [27]	17 flavonoids across 5 structural subclasses	In vitro ACE inhibition assay	Luteolin most potent (IC50 = 23 μM), aglycones generally more potent
Zielińska et al., 2025 [10]	9 phenolic acids, 7 flavonoid aglycones and their O-glucosides	Fluorescence-based ACE inhibition assay	Chlorogenic acid ranked most potent phenolic acid and caffeic acid least potent, kaempferol ranked third among flavonoid aglycones, glucosylation generally reduces potency
Khaled et al., 2023 [8]	Multiple herbal sources (*Rosmarinus, Hibiscus, Curcuma, Moringa* and others)	Narrative literature review	Several natural sources show ACE-inhibitory activity comparable to captopril or enalapril, proposed as adjuncts for hypertension, respiratory distress syndrome and CKD

Continued on next page

TABLE 2.4: Summary of Structure-Activity, Computational-Screening and Jerusalem Artichoke Phytochemistry Studies (continued)

Study	Compound(s) / source	Approach	Key finding
Islam et al., 2026 [11]	*Nypa fruticans* leaves, 36 compounds, quercetin, rosmarinic acid and caffeic acid prioritised	SwissADME, pkCSM and ProTox 3.0 filtering, molecular docking against ACE (PDB 1O86), DFT analysis	Rosmarinic acid (-8.95 kcal/mol) and quercetin (-8.28 kcal/mol) outperformed the enalapril reference (-8.1 kcal/mol)
Islam et al., 2026 (companion study) [12]	*Nypa fruticans* leaf extract	In vivo gentamicin-induced nephrotoxicity rat model with docking against AT1 receptor and SGLT2, combined with molecular docking	Improved renal function biomarkers, rosmarinic acid the strongest binder with stability confirmed by 100 ns molecular dynamics
Yue et al., 2024 [28]	*Suaeda salsa*, 680 metabolomics-derived compounds	3D-QSAR pharmacophore modelling, docking (AutoDock Vina, CB-Dock2, Schrödinger Glide) and 100 ns molecular dynamics	Six top-hit compounds identified with strong predicted ACE binding

Continued on next page

TABLE 2.4: Summary of Structure-Activity, Computational-Screening and Jerusalem Artichoke Phytochemistry Studies (continued)

Study	Compound(s) / source	Approach	Key finding
Darwish et al., 2024 [29]	1,526 phytoconstituents from 19 edible plants	Domain-selective docking (ACE N-domain versus C-domain), in vitro ACE assay, combined with captopril synergy testing	4-O-caffeoylquinic acid (from *Moringa oleifera*) is C-domain selective (IC50 = 62.92 μM) and synergistic with captopril
Rasjava et al., 2026 [30]	*Pluchea indica* (Beluntas), 110 phytoconstituents, 20 retained after ADMET triage	ADMET triage followed by molecular docking against ACE	Caffeoylquinic acid derivatives closely mimicked the binding mode of the ramiprilat reference, while quercetin glycosides showed a distinct interaction pattern binding
Ramlal et al., 2023 [31]	Soybean (*Glycine max*), 34 phytomolecules	Molecular docking and molecular dynamics simulation	Beta-sitosterol identified as the most potent predicted ACE inhibitor of the panel
Shahzadi et al., 2024 [32]	Fabaceae species, 414 compounds	Network pharmacology combined with molecular docking	Six compounds, including dihydrokaempferol, identified as effective agents against antihypertensive-pathway targets

Continued on next page

TABLE 2.4: Summary of Structure-Activity, Computational-Screening and Jerusalem Artichoke Phytochemistry Studies (continued)

Study	**Compound(s) / source**	**Approach**	**Key finding**
Kaszás et al., 2020 [17]	Jerusalem artichoke leaf protein concentrate	UHPLC-ESI-Orbitrap-MS/MS profiling	Identified 53 phytochemicals including chlorogenic-acid family esters, astragalin and quercetin-3-O-glucoside (isoquercetin)
Showkat et al., 2019 [16]	Jerusalem artichoke tuber, leaf, flower and stem	HPLC-UV and Folin-Ciocalteu antioxidant assay across plant organs	Leaves are the richest phenolic source, chlorogenic and dicaffeoylquinic acids account for 72-82% of leaf total phenolic content present
Yuan et al., 2013 [18]	Jerusalem artichoke leaves, 11 sesquiterpene lactones and 2 flavones	Bioassay-directed isolation and cytotoxicity assay	Isolated and structurally characterised heliangine-related sesquiterpene lactones, with structure-activity patterns established for cytotoxicity structured characteristics
Saiki et al., 2022 [19]	Heliangin isolated from Jerusalem artichoke leaves	In vitro macrophage and vascular endothelial cell assays	Heliangin suppressed nitric-oxide overproduction and adhesion-molecule expression via the NF-κB pathway

2.7 Research Gap in the Literature

Three separate strands of literature have been reviewed in this chapter. These are the pathophysiological and clinical case for ACE inhibition in CKD (Sections 2.1-2.2), the growing body of computational and experimental work on plant-derived ACE inhibitors in general (Section 2.3), and the phytochemistry of Jerusalem artichoke specifically, including leaf-specific compositional data and the individual evidence available for each of the five compounds of interest (Sections 2.4-2.5). Considered together, these strands establish that each individual element needed to justify a Jerusalem-artichoke-focused, ACE-targeted investigation is well supported by precedent. ACE is a validated CKD-relevant drug target, plant phenolics and flavonoids are established, mechanistically plausible ACE inhibitors, and Jerusalem artichoke leaves are a documented, chemically characterised source of exactly the compound classes shown elsewhere to inhibit ACE, while also showing that no single prior peer-reviewed study combines all three elements together.

Specifically, the closest identified prior work, Islam et al.'s 2026 computational evaluation of *Nypa fruticans* phytochemicals as ACE inhibitors in hypertension and CKD [11, 12], shares the disease framing and general computational strategy relevant to the compounds discussed in this chapter, but examines an entirely different plant species and a materially different, only partially overlapping compound panel (quercetin, rosmarinic acid and caffeic acid, of which only caffeic acid is common to both). No study identified in this review screens the specific combination of chlorogenic acid, caffeic acid, 5-p-coumaroylquinic acid, astragalin and heliangine against ACE, and no study restricts its candidate selection specifically to Jerusalem artichoke leaf phytochemistry with an explicit CKD framing. There is therefore a narrow but genuine and clearly delineated gap in this literature. To the knowledge gathered in this review, no structure-based virtual screening study of Jerusalem artichoke leaf phytochemicals against ACE has yet been published in the specific context of chronic kidney disease. Section 2.5 has also been explicit about where the existing literature does not yet extend. No direct ACE-inhibition assay was identified for 5-p-coumaroylquinic acid or for heliangine, and the expected reduction

in ACE-inhibitory potency on glucosylation of flavonoids such as astragalin, discussed in Section 2.5.4, has not yet been directly tested for this specific compound. These points highlight specific, well-defined directions for future experimental and computational work rather than being glossed over here.

Chapter 3

Methodology

This chapter presents the complete computational workflow followed in this study, from the selection of the disease and the therapeutic target through to the identification and validation of lead phytochemical candidates against a standard reference drug. The overall approach followed a structure-based virtual screening pipeline, in which a validated protein target was prepared computationally, a panel of plant-derived phytochemicals was screened for drug-likeness and pharmacokinetic suitability, and the surviving candidates were evaluated by molecular docking and protein-ligand interaction analysis. Every stage of this workflow is described in the sections that follow. Figure 3.1 summarises the overall sequence as a single, colour-coded workflow diagram, showing the parallel disease-selection and plant-selection tracks converging through molecular docking and interaction analysis into a final comparison against the reference drug, lisinopril.

3.1 Selection of the Disease

Chronic kidney disease (CKD) was selected as the disease for this study. CKD is a progressive condition in which renal function declines over time, and the renin-angiotensin-aldosterone system (RAAS) is one of the central physiological pathways implicated in both the initiation and the progression of the disease [3]. Because

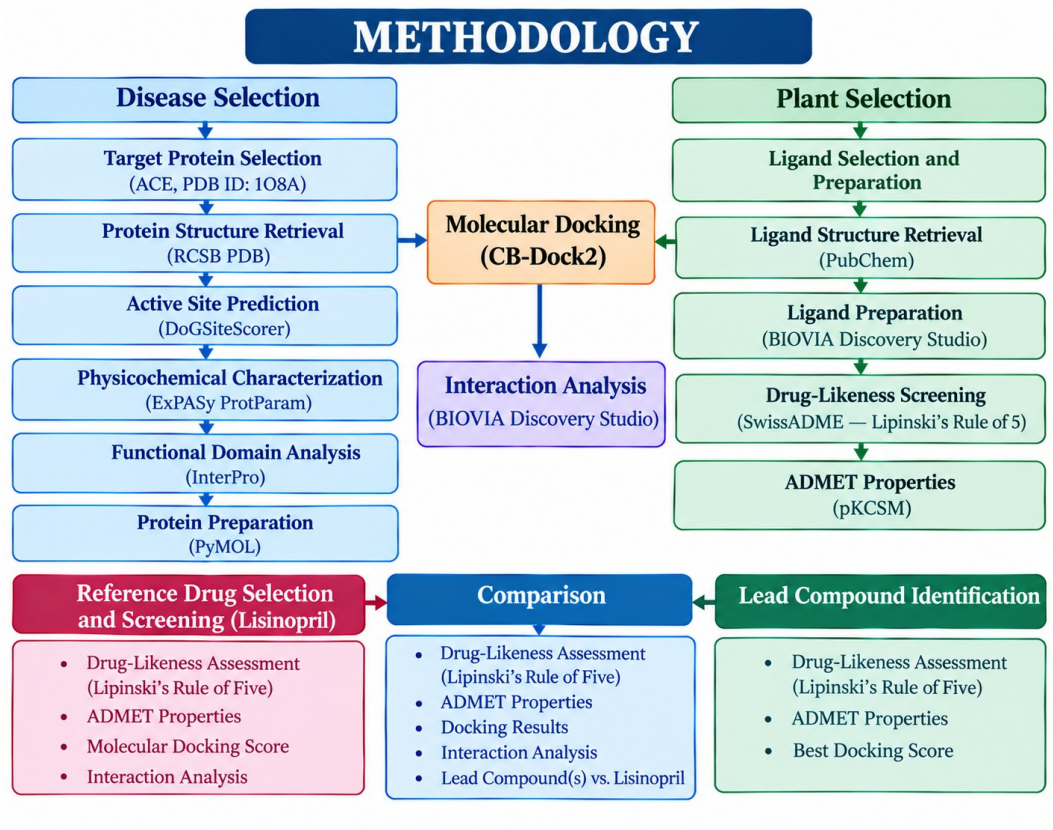


FIGURE 3.1: Overall methodological workflow followed in this study, showing the parallel Disease Selection and Plant Selection tracks converging through Molecular Docking and Interaction Analysis into a final Comparison against the reference drug, lisinopril

angiotensin-converting enzyme (ACE) sits at a pivotal point within the renin-angiotensin-aldosterone system, ACE inhibition was chosen as the therapeutic strategy of interest, and the remainder of the methodology was built around identifying plant-derived compounds capable of inhibiting this enzyme.

3.2 Preparation of the Target Protein

3.2.1 Selection of Target Protein

Angiotensin-converting enzyme (ACE) was selected as the target protein for this study, given its established, direct role within the renin-angiotensin-aldosterone system and its long-standing status as a validated drug target in hypertension and, by extension, in CKD management. The three-dimensional structure of human

ACE was retrieved from the RCSB Protein Data Bank [26], corresponding to the crystal structure deposited under PDB ID 1O8A [22], described in the Protein Data Bank as the native (ligand-free) structure of human angiotensin-converting enzyme. The structure file was downloaded in PDB format for use in all subsequent preparation and docking steps.

3.2.2 Active Site Prediction

The active site of the prepared ACE structure was predicted using DoGSiteScorer [36], a web-based cavity-detection tool accessed through the ProteinsPlus server. This step was carried out to independently confirm the location and approximate volume of the catalytic pocket prior to docking, so that the cavity subsequently selected by the docking software itself could be cross-checked against a structurally grounded prediction rather than accepted on faith.

3.2.3 Physicochemical Characterization

The amino acid sequence of ACE, retrieved in FASTA format from the same PDB entry (1O8A), was submitted to the web-based ExPASy ProtParam server [41] to determine the physicochemical properties of the protein. Parameters obtained through this analysis included the number of amino acid residues, molecular weight, instability index, and grand average of hydropathicity(GRAVY), among other standard descriptors. These values were used to characterise the general biochemical nature of the protein before proceeding to structural preparation.

3.2.4 Functional Domain Analysis

The same FASTA sequence was submitted to the web-based InterPro resource [42] for functional domain and family classification. This step served to confirm, independently of the structural data, that the retrieved sequence corresponds to a member of the M2 family of zinc-dependent metallopeptidases, consistent with the

established catalytic mechanism of ACE, and to identify the residue range over which this family-level classification held across multiple independent signature databases.

3.2.5 Protein Structure Preparation

The raw, as-deposited PDB structure was visualised and prepared in PyMOL, version 2.6.2 (Incentive build) [43], a molecular visualisation program installed locally under an academic licence rather than accessed as a web service. From this stage onward, ACE is referred to as the receptor, reflecting its specific role as the docking target rather than as a protein under general biochemical characterisation, as in Sections 3.2.1-3.2.4. Preparation involved the removal of crystallographic water molecules, any co-crystallised ligand, and other non-essential heteroatoms present in the original deposition, while the catalytic zinc ion (Zn2+) was deliberately retained throughout. This distinction was treated as a fixed rule during preparation rather than a case-by-case judgement. The zinc ion occupies the catalytic centre of the enzyme and is the site with which candidate inhibitors are expected to coordinate, so its removal would have rendered the docking exercise mechanistically meaningless, whereas the surrounding waters and incidental heteroatoms carry no such requirement and were cleared to leave an unobstructed binding pocket. Polar hydrogens were added to the cleaned structure, and the resulting prepared receptor was exported in PDB format for use in the docking stage.

3.3 Selection and Preparation of Ligands

3.3.1 Selection of Ligands

Candidate ligands were selected from phytochemicals previously reported specifically in the leaves of Jerusalem artichoke (*Helianthus tuberosus* L.), drawn from the existing phytochemical literature on this species. For each selected compound, both the three-dimensional structure and the two-dimensional structure were retrieved

from the web-based PubChem Compound database [35] using its corresponding PubChem CID. The 3D structure was downloaded in SDF format for use in ligand preparation and docking, ensuring that the geometry used for docking reflected an energetically reasonable three-dimensional conformation rather than a flat depiction, while the 2D structure image was downloaded separately for use in the compound identity table presented in Chapter 4.

3.3.2 Ligand Refinement and Preparation

Each downloaded ligand structure was imported into BIOVIA Discovery Studio Visualizer 2025 [44], installed locally under an academic licence rather than accessed as a web service, for visual inspection and refinement prior to screening. This step allowed each structure to be checked for chemical plausibility, and the refined structure was saved for use in the subsequent virtual screening and docking stages.

3.4 Virtual Screening of Phytochemicals

Virtual screening was carried out in two stages, assessing drug-likeness and pharmacokinetic/toxicological suitability in turn, before any compound was carried forward to molecular docking.

3.4.1 Drug-Likeness Assessment (Lipinski's Rule of Five)

The canonical SMILES notation for each selected phytochemical was retrieved from its PubChem record [35] and submitted to the web-based SwissADME server [38]. SwissADME was used specifically to evaluate compliance with Lipinski's Rule of Five [39], examining molecular weight, the number of hydrogen-bond donors and acceptors, the calculated partition coefficient (consensus LogP), and the number of rotatable bonds for each compound, in order to obtain an initial indication of oral drug-likeness before proceeding to more detailed pharmacokinetic profiling.

3.4.2 ADMET Profiling

The same SMILES data were subsequently submitted to the web-based pkCSM server [40] to generate a full absorption, distribution, metabolism, excretion, and toxicity (ADMET) profile for each compound. This stage produced predictions across all five ADMET categories, including intestinal absorption, plasma protein binding and distribution parameters, cytochrome P450 substrate and inhibitor status, renal clearance behaviour, and a panel of toxicity endpoints such as AMES mutagenicity, cardiotoxicity (hERG I/II inhibition), and hepatotoxicity.

3.5 Molecular Docking

Molecular docking of the prepared ligands against the prepared ACE receptor was performed using the web-based CB-Dock2 server [37], a cavity-detection-guided blind docking platform. Rather than requiring the binding site to be manually specified in advance, CB-Dock2 automatically detects candidate cavities on the submitted receptor surface and ranks them, allowing the top-ranked predicted cavity to be compared directly against the independently predicted active site obtained earlier from DoGSiteScorer [36]. Each ligand was docked against the prepared receptor in turn, and the resulting binding affinity, expressed as a Vina score in kcal/mol, was recorded for the best-ranked binding pocket returned for each compound.

3.6 Protein-Ligand Interaction Analysis

The top-ranked docked pose obtained for each compound was subsequently visualised in the locally installed BIOVIA Discovery Studio Visualizer 2025 [44] to generate a two-dimensional protein-ligand interaction diagram. This analysis identified the specific ACE residues involved in binding and characterised the nature of each interaction, including conventional hydrogen bonds, van der Waals

contacts, and electrostatic and hydrophobic interactions such as pi-alkyl, pi-sigma, and pi-cation contacts, providing a mechanistic basis for interpreting the docking scores obtained in the preceding stage.

3.7 Lead Compound Identification

Lead compounds were identified by weighing the docking score, Lipinski's Rule of Five [39] profile, and full ADMET/toxicity results together, rather than ranking compounds on docking score alone. A compound combining a favourable docking score with a broadly acceptable pharmacokinetic and toxicity profile was treated as a strong lead candidate. Where a compound returned a specific toxicity or drug-likeness flag despite an otherwise strong overall profile, this was reported explicitly alongside the recommendation, as a stated limitation requiring further experimental confirmation, rather than applied as an automatic, unstated exclusion criterion. A compound was set aside only when the panel's own weakest performer failed to improve on the reference drug on any measure. This combined evaluation, including any compound carried forward with an explicit caveat, is described in full, with the supporting comparative data, in Chapter 4.

3.8 Reference Drug Selection and Screening

3.8.1 Identification of Reference Drug

Lisinopril, a clinically established ACE inhibitor, was selected as the reference drug for this study. Lisinopril was chosen specifically because it is the ligand co-crystallised in several ACE crystal structures reported in the literature [22] and is widely used as the benchmark inhibitor in comparable *In Silico* ACE-inhibitor screening studies, making it an appropriate standard against which the binding behaviour of the candidate phytochemicals could be judged.

3.8.2 Screening of Reference Drug

Lisinopril was subjected to the same screening pipeline applied to the candidate phytochemicals, to ensure a fair, like-for-like comparison. Its canonical SMILES was retrieved from its PubChem record [35] and submitted to SwissADME [38] for Lipinski's Rule of Five [39] assessment, and separately to pkCSM [40] for full ADMET profiling. The compound was then docked against the same prepared ACE receptor using CB-Dock2 [37], and its top-ranked docked pose was analysed in the locally installed BIOVIA Discovery Studio Visualizer 2025 [44] to generate its own two-dimensional protein-ligand interaction diagram, following exactly the same procedure described in Sections 3.4 through 3.6.

3.9 Comparative Analysis of Lead Compounds with the Reference Drug

Once the lead phytochemical candidates had been identified, their docking scores, drug-likeness profiles, and ADMET/toxicity results were compared directly against those obtained for lisinopril. This comparison was used to assess whether the selected leaf phytochemicals showed binding affinity and pharmacokinetic behaviour comparable to, or more favourable than, an established clinical ACE inhibitor, and forms the basis of the results and discussion presented in Chapter 4.

Chapter 4

Results

This chapter reports the findings obtained by following the computational workflow described in Chapter 3, from preparation and characterisation of the target protein through to comparative evaluation of the lead phytochemical candidates against the reference drug, lisinopril. Chronic kidney disease (CKD) was the disease context motivating this study, given the established role of the renin-angiotensin-aldosterone system (RAAS) in its onset and progression [3], and angiotensin-converting enzyme (ACE) was accordingly the therapeutic target against which phytochemicals from the leaves of Jerusalem artichoke were screened. Results are presented in the same order the workflow was carried out: target protein characterisation and preparation, ligand selection and screening, molecular docking, protein–ligand interaction analysis, lead compound identification, reference drug screening, and finally the comparative analysis of the identified leads against lisinopril.

Overall, four of the five phytochemicals emerged as leads, with astragalin (-8.6 kcal/mol), heliangine and chlorogenic acid (-7.9) and 5-p-coumaroylquinic acid (-7.7) all docking more favourably than lisinopril (-7.3), while caffeic acid (-6.3) did not. All ligands occupied the same cavity predicted as the active site. Astragalin bound most strongly, though its two Lipinski violations tempered its overall profile. Heliangine showed the best predicted absorption (97.9%) but carried an AMES-positive flag, whereas lisinopril was the only compound predicted to be hepatotoxic as the active state.

4.1 Selection and Preparation of the Target Protein

4.1.1 Selection of Target Protein

Angiotensin-converting enzyme (ACE) was the target protein for this study. Its three-dimensional structure was retrieved from the RCSB Protein Data Bank [26], corresponding to the crystal structure deposited under PDB ID 1O8A [22], the native (ligand-free) structure of human ACE. Figure 4.1 shows this structure as retrieved, prior to any preparation.

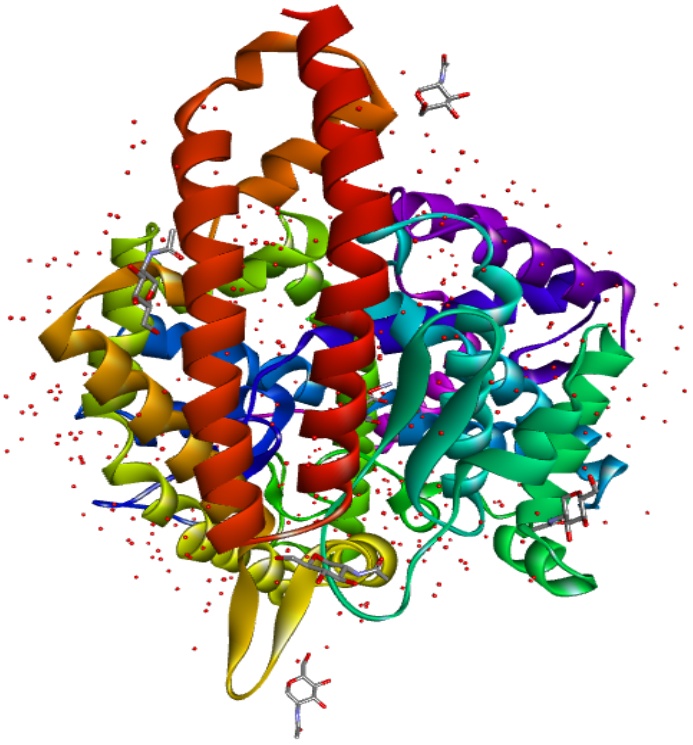


FIGURE 4.1: 3D structure of ACE

4.1.2 Active Site Prediction

The active site of the prepared ACE structure was predicted using DoGSiteScorer [36], a cavity-detection tool accessed through the ProteinsPlus server. Thirteen

cavities were detected across the protein surface, labelled P_0 through P_12. As shown in Figure 4.2, one cavity stood out visually and spatially from the rest, forming a single large, contiguous surface patch well beyond the size of any of the smaller pockets scattered around the periphery. This central cavity was predicted as the ACE active site and used as the docking target for the molecular docking reported in Section 4.3.

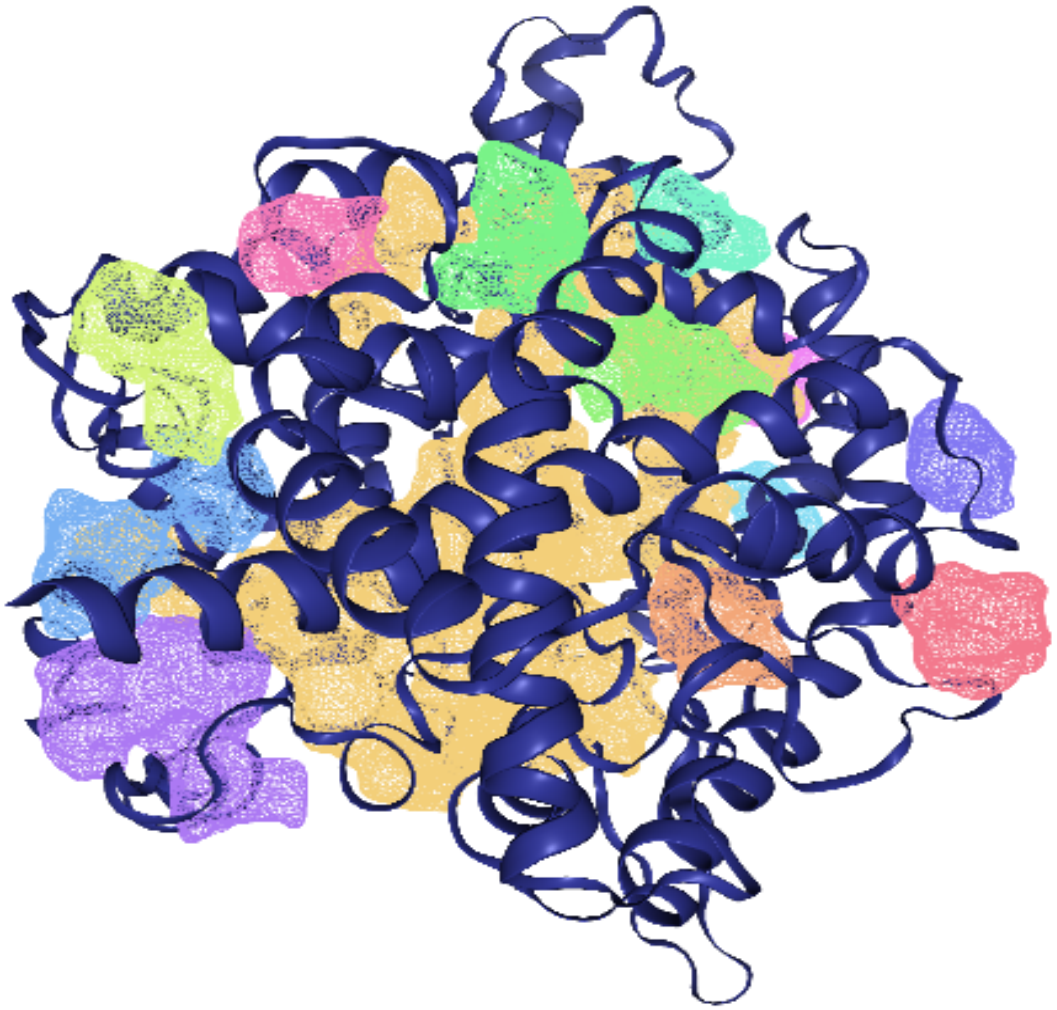


FIGURE 4.2: Cavities detected on the target protein

4.1.3 Physicochemical Characterization

The amino acid sequence of ACE, retrieved from PDB in FASTA format entry 1O8A, was submitted to ExPASy ProtParam [41] to determine the physicochemical properties of the protein. Results are given in Table 4.1.

TABLE 4.1: Physicochemical parameters of the ACE protein sequence

Property	**Value**
Number of amino acids	589
Molecular weight	67,993.20 Da
Theoretical pI	5.82
Total negatively charged residues (Asp + Glu)	70
Total positively charged residues (Arg + Lys)	56
Formula	C3076H4656N818O883S24
Total number of atoms	9,457
Extinction coefficient (all Cys residues form cystines), 280 nm	143,615 M^{-1} cm^{-1} (Abs 0.1% = 2.112)
Extinction coefficient (all Cys residues reduced), 280 nm	143,240 M^{-1} cm^{-1} (Abs 0.1% = 2.107)
Estimated half-life, mammalian reticulocytes, in vitro	5.5 hours
Estimated half-life, yeast, in vivo	3 minutes
Estimated half-life, Escherichia coli, in vivo	2 minutes
Instability index (II)	39.46 (classified as stable)
Aliphatic index	78.86
Grand average of hydropathicity (GRAVY)	-0.441

4.1.4 Functional Domain Analysis

The same FASTA sequence was submitted to InterPro [42] for functional domain and family classification. The result, shown in Figure 4.3, confirms that the sequence is classified within the M2 family of zinc-dependent metallopeptidases, consistent

with the established catalytic mechanism of ACE. Multiple independent signature databases converged on this family assignment (Peptidase_M2, IPR001548) across roughly residues 3–586, and a separate track identified the zinc-metalloprotease catalytic domain spanning residues 5–581.

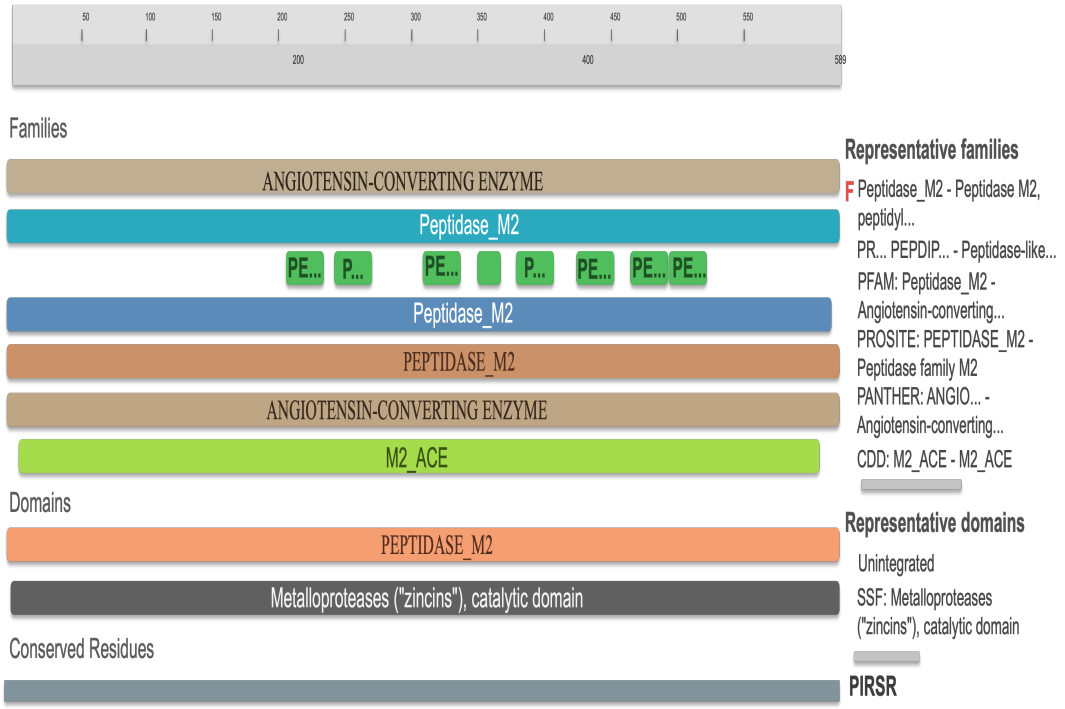


FIGURE 4.3: Domain and family organisation of the ACE protein sequence

4.1.5 Protein Structure Preparation

The raw, as-deposited structure was visualised and prepared in PyMOL, version 2.6.2 (Incentive build) [43]. From this stage onward, ACE is referred to as the receptor, reflecting its specific role as the docking target rather than as a protein under general biochemical characterisation, as in Sections 4.1.1–4.1.4. Preparation involved removal of crystallographic water molecules and other non-essential heteroatoms, while the catalytic zinc ion (Zn^{2+}) was retained throughout, since it occupies the catalytic centre with which candidate inhibitors are expected to coordinate. Polar hydrogens were added to the cleaned structure, and the resulting prepared receptor, shown in Figure 4.4, was exported in PDB format for use in the docking stage.

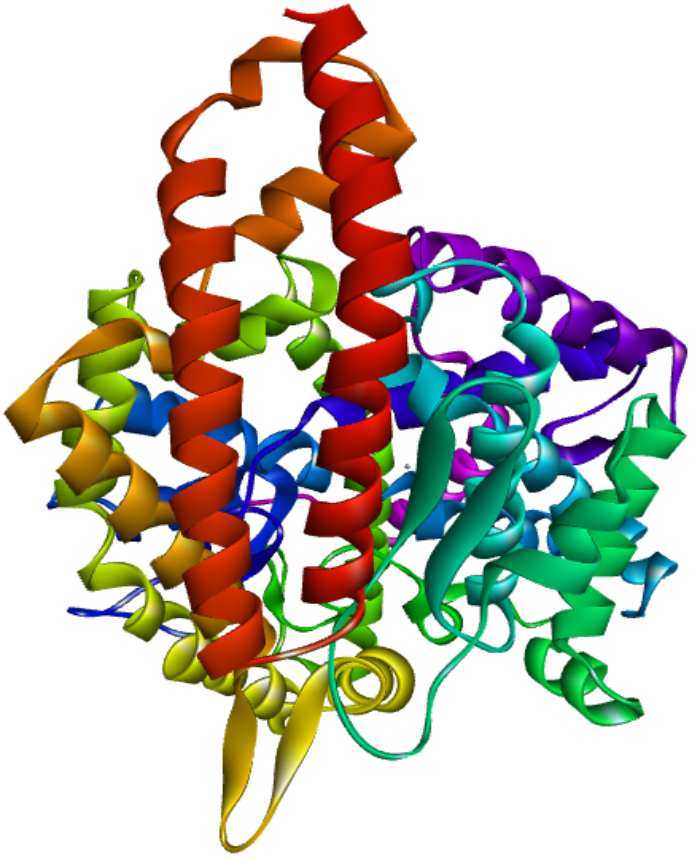


FIGURE 4.4: Prepared 3D structure of ACE

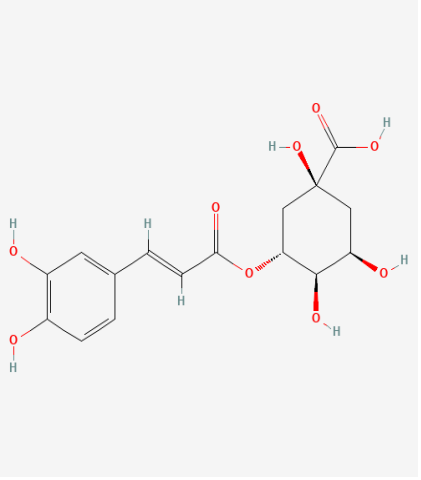
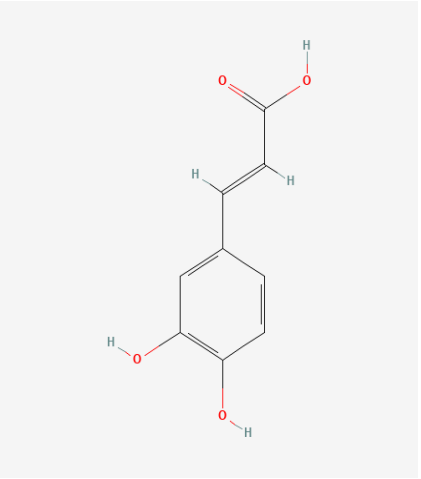
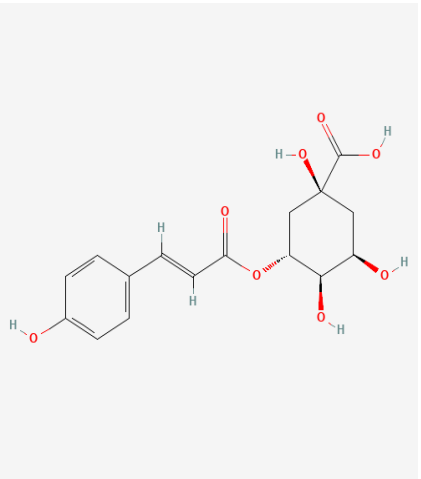
4.2 Selection and Screening of Ligands (Phytochemicals)

Candidate ligands were selected from phytochemicals previously reported *Helianthus tuberosus* L. (Jerusalem artichoke) leaf. For each compound, both the three-dimensional structure (SDF format, for docking) and the two-dimensional structure (for the identity table below) were retrieved from PubChem [35] using its PubChem CID.

4.2.1 Molecular Identity

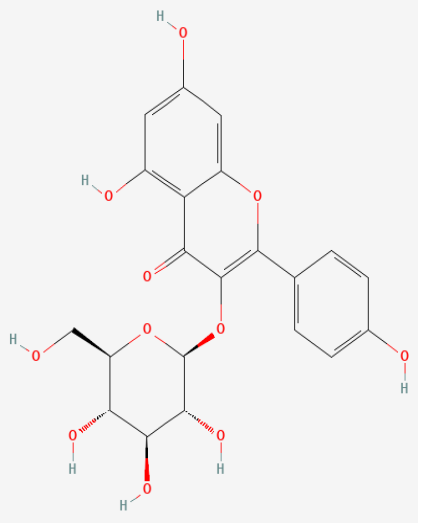
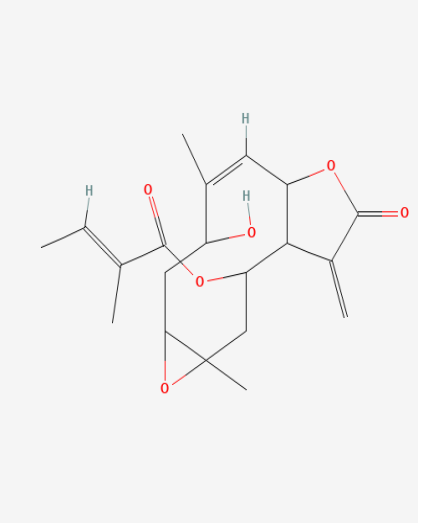
Table 4.2 lists each ligand together with its PubChem identifier, molecular formula, and two-dimensional structure.

TABLE 4.2: Ligand identity, PubChem CID, molecular formula, and two-dimensional structure

Sr. No.	Ligand	PubChem CID	Molecular Formula	2D Structure
1	Chlorogenic acid	1794427	C16H18O9	
2	Caffeic acid	689043	C9H8O4	
3	5-p-Coumaroylquinic acid	6441280	C16H18O8	

Continued on next page

TABLE 4.2: Ligand identity, PubChem CID, molecular formula, and two-dimensional structure (continued)

Sr. No.	Ligand	PubChem CID	Molecular Formula	2D Structure
4	Astragalin	5282102	C21H20O11	
5	Heliangine	5838160	C20H26O6	

4.2.2 Ligand Refinement and Preparation

Each downloaded ligand structure was imported into BIOVIA Discovery Studio Visualizer 2025 [44] for visual inspection and refinement prior to screening, checking each structure for chemical plausibility before it was carried forward to virtual screening.

4.2.3 Drug-Likeness Assessment (Lipinski's Rule of Five)

The canonical SMILES notation for each ligand was retrieved from its PubChem record [35] and submitted to SwissADME [38] to assess compliance with Lipinski's Rule of Five [39]: molecular weight at or below 500 g/mol, no more than ten hydrogen-bond acceptors, no more than five hydrogen-bond donors, and a calculated LogP at or below 5.

The findings are presented in Table 4.3.

TABLE 4.3: Lipinski's Rule of Five parameters of ligands

Parameter	**Chlorogenic acid**	**Caffeic acid**	**5-p-Coumaroylquinic acid**	**Astragalin**	**Heliangine**
MW (≤500 g/mol)	354.31	180.16	338.31	448.38	362.42
H-Bond Donors (≤5)	6	3	5	7	1
H-Bond Acceptors (≤10)	9	4	8	11	6
Consensus LogP (≤5)	-0.71	0.92	-0.31	-0.94	2.12
Rotatable Bonds	5	2	5	4	3
Lipinski Violations	1: NHorOH->5	0	0	2: NorO>10, NHorOH->5	0

Four of the five compounds satisfied all four criteria outright.Astragalin was the exception, exceeding both the acceptor and donor limits (11 acceptors, 7 donors).

4.2.4 ADMET Profiling

The same SMILES data were submitted to pkCSM [40] to generate a full absorption, distribution, metabolism, excretion, and toxicity (ADMET) profile for each compound, reported below by category.

4.2.4.1 Absorption

TABLE 4.4: Absorption parameters of ligands

Parameter	**Chlorogenic acid**	**Caffeic acid**	**5-p-Coumaroylquinic acid**	**Astragalin**	**Heliangine**
Water Solubility (log mol/L)	-2.449	-2.33	-1.991	-2.863	-3.831
Caco-2 Permeability (log Papp, 10^{-6} cm/s)	-0.84	0.634	-0.656	0.306	1.178
Intestinal Absorption – Human (%)	36.377	69.407	43.925	48.052	97.894
Skin Permeability (log Kp)	-2.735	-2.722	-2.735	-2.735	-3.306
P-glycoprotein Substrate	Yes	No	Yes	Yes	Yes
P-glycoprotein I Inhibitor	No	No	No	No	No
P-glycoprotein II Inhibitor	No	No	No	No	No

As given in Table 4.4, predicted intestinal absorption ranged widely across the panel, from 36.4% for chlorogenic acid to 97.9% for heliangine. None of the five compounds was predicted to inhibit either P-glycoprotein isoform, although four of the five (all except caffeic acid) were themselves substrates of the transporter.

4.2.4.2 Distribution

TABLE 4.5: Distribution parameters of ligands

Ligand	VDss Human (log L/kg)	Fraction Unbound Human (Fu)	BBB Permeability (log BB)	CNS Permeability (log PS)
Chlorogenic acid	0.581	0.658	-1.407	-3.856
Caffeic acid	-1.098	0.529	-0.647	-2.608
5-p-Coumaroylquinic acid	0.034	0.612	-1.16	-3.693
Astragalin	1.444	0.218	-1.514	-3.908
Heliangine	-0.086	0.363	-0.482	-2.95

As Table 4.5 shows, all five compounds returned negative log BB and log PS values, indicating limited predicted penetration of the blood–brain barrier.

4.2.4.3 Metabolism

TABLE 4.6: Metabolism parameters of ligands

Parameter	Chlorogenic acid	Caffeic acid	5-p-Coumaroylquinic acid	Astragalin	Heliangine
CYP2D6 Sub.	No	No	No	No	No
CYP3A4 Sub.	No	No	No	No	Yes
CYP1A2 Inh.	No	No	No	No	No
CYP2C19 Inh.	No	No	No	No	No

Continued on next page

TABLE 4.6: Metabolism parameters of ligands (continued)

Parameter	**Chlorogenic acid**	**Caffeic acid**	**5-p-Coumaroylquinic acid**	**Astragalin**	**Heliangine**
CYP2C9 Inh.	No	No	No	No	No
CYP2D6 Inh.	No	No	No	No	No
CYP3A4 Inh.	No	No	No	No	No

Table 4.6 shows that heliangine was the only compound predicted to act as a CYP3A4 substrate, and that none of the five compounds was predicted to inhibit any of the five isoforms screened.

4.2.4.4 Excretion

Excretion parameters describe how quickly a compound would be cleared from the body once absorbed, and whether that clearance depends on active renal transport rather than simple filtration. These are summarised in Table 4.7.

TABLE 4.7: Excretion parameters of ligands

Ligand	**Total Clearance (log mL/min/kg)**	**Renal OCT2 Substrate**
Chlorogenic acid	0.307	No
Caffeic acid	0.508	No
5-p-Coumaroylquinic acid	0.453	No
Astragalin	0.462	No
Heliangine	1.312	No

Clearance values fell within a fairly narrow band across the panel (0.307–1.312 log mL/min/kg), and none of the five compounds was predicted to be a substrate of the renal organic cation transporter OCT2.

4.2.4.5 Toxicity

The toxicity panel covers genetic toxicity (AMES), cardiac liability (hERG I/II), acute and chronic oral toxicity in rodent models, organ-specific toxicity, skin sensitisation, and two aquatic toxicity endpoints, given in Table 4.8, with parameters as rows and compounds as columns.

TABLE 4.8: Toxicity parameters of ligands

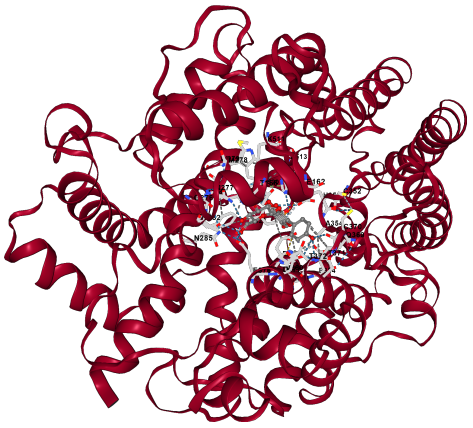
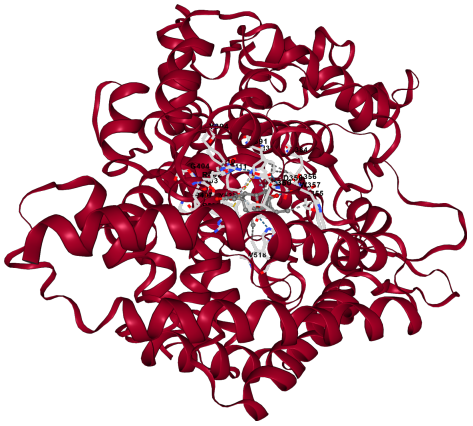
Toxicity Parameter	**Chlorogenic acid**	**Caffeic acid**	**p-Coumaroylquinic acid**	**Astragalin**	**Heliangine**
AMES Toxicity	No	No	No	No	Yes
Max. Tolerated Dose (log mg/kg/day)	-0.134	1.145	-0.09	0.582	-0.202
hERG I Inhibitor	No	No	No	No	No
hERG II Inhibitor	No	No	No	No	No
LD50 (mol/kg)	1.973	2.383	1.737	2.546	2.997
LOAEL (log mg/kg_bw/day)	2.982	2.092	2.508	4.53	1.286
Hepatotoxicity	No	No	No	No	No
Skin Sensitisation	No	No	No	No	No
T.Pyriformis Toxicity (log μg/L)	0.285	0.293	0.285	0.285	0.401
Minnow Toxicity (log mM)	5.741	2.246	4.611	6.735	2.535

Heliangine was the only compound flagged positive for AMES mutagenicity. The remaining four compounds were clean across every toxicity endpoint tested non-mutagenic, non-hepatotoxic, and negative for both hERG channels with only modest differences between them in acute and chronic dosing thresholds.

4.3 Molecular Docking

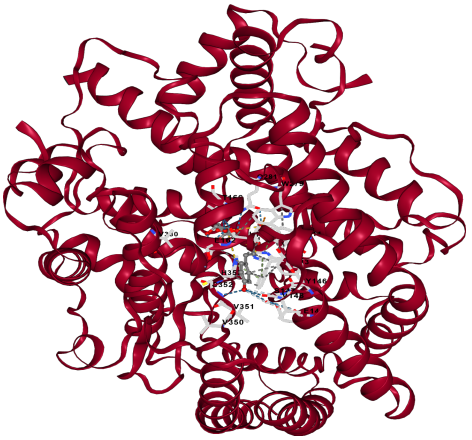
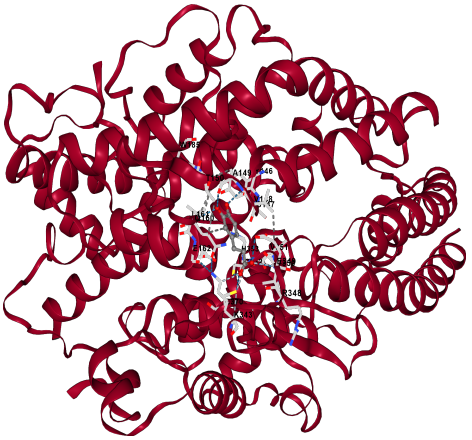
Molecular docking of the prepared ligands against the prepared ACE receptor was performed using CB-Dock2 [37], a cavity-detection-guided blind docking platform that automatically detects candidate cavities on the submitted receptor surface and ranks them, rather than requiring the binding site to be specified manually. Results are given in Table 4.9. All five compounds independently converged on the same cavity, designated C1 by the server as the top-ranked predicted cavity, consistent with the active site independently predicted by DoGSiteScorer in Section 4.1.2.

TABLE 4.9: Docking scores and the volume of cavity C1, ordered from strongest to weakest predicted binder, together with the corresponding docked complex for each compound

Ligand	**Docking Score (kcal/mol)**	**Cavity Volume (Å³)**	**Docked Complex (Receptor + Ligand)**
Astragalin	-8.6	13,542	
Heliangine	-7.9	13,542	

Continued on next page

TABLE 4.9: Docking scores and the volume of cavity C1, ordered from strongest to weakest predicted binder, together with the corresponding docked complex for each compound (continued)

Ligand	**Docking Score (kcal/mol)**	**Cavity Volume (Å³)**	**Docked Complex (Receptor + Ligand)**
Chlorogenic acid	-7.9	13,542	
5-p-Coumaroyl-quinic acid	-7.7	13,542	
Caffeic acid	-6.3	13,542	

Astragalin produced the strongest score in the panel at -8.6 kcal/mol, with heliangine and chlorogenic acid tied for second at -7.9 kcal/mol, followed by 5-p-coumaroylquinic acid at -7.7 kcal/mol. Caffeic acid was the weakest binder at -6.3 kcal/mol.

4.4 Protein–Ligand Interaction Analysis

The top-ranked docked pose obtained for each compound was visualised in BIOVIA Discovery Studio Visualizer 2025 [44] to generate a two-dimensional receptor–ligand interaction diagram, identifying the specific ACE residues contributing to binding and characterising the interactions, including conventional hydrogen bonds, van der Waals contacts, and electrostatic and hydrophobic interactions such as pi-alkyl, pi-sigma, and pi-cation contacts.

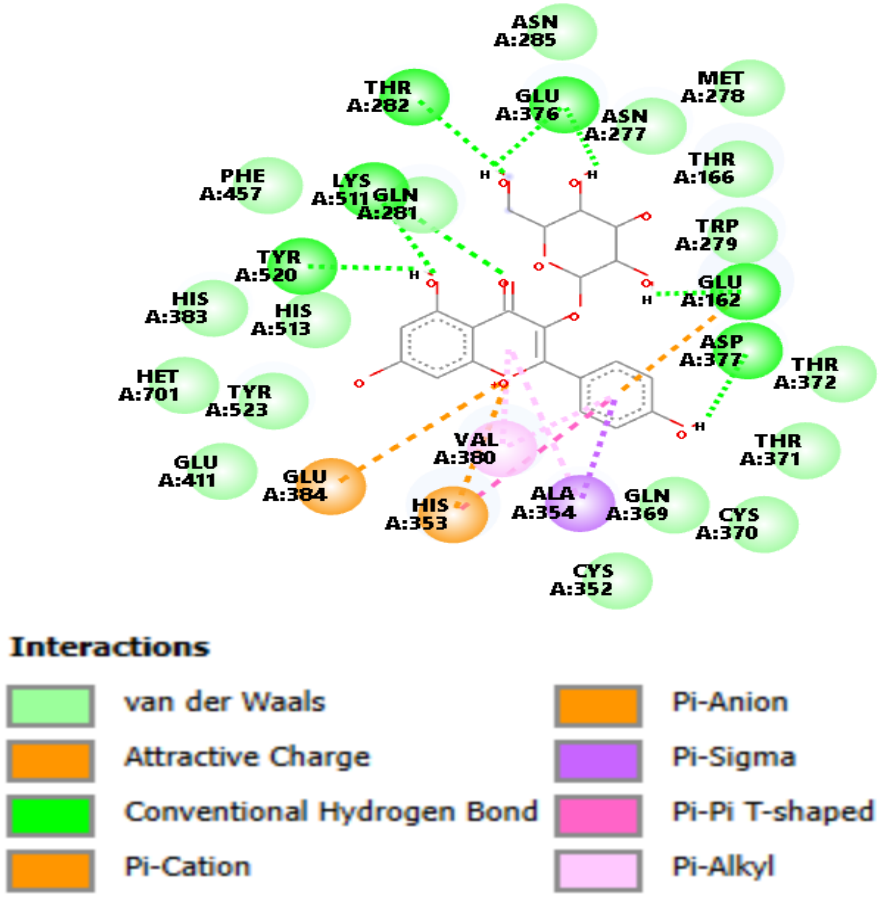


FIGURE 4.5: Molecular interaction analysis of Astragalin with ACE

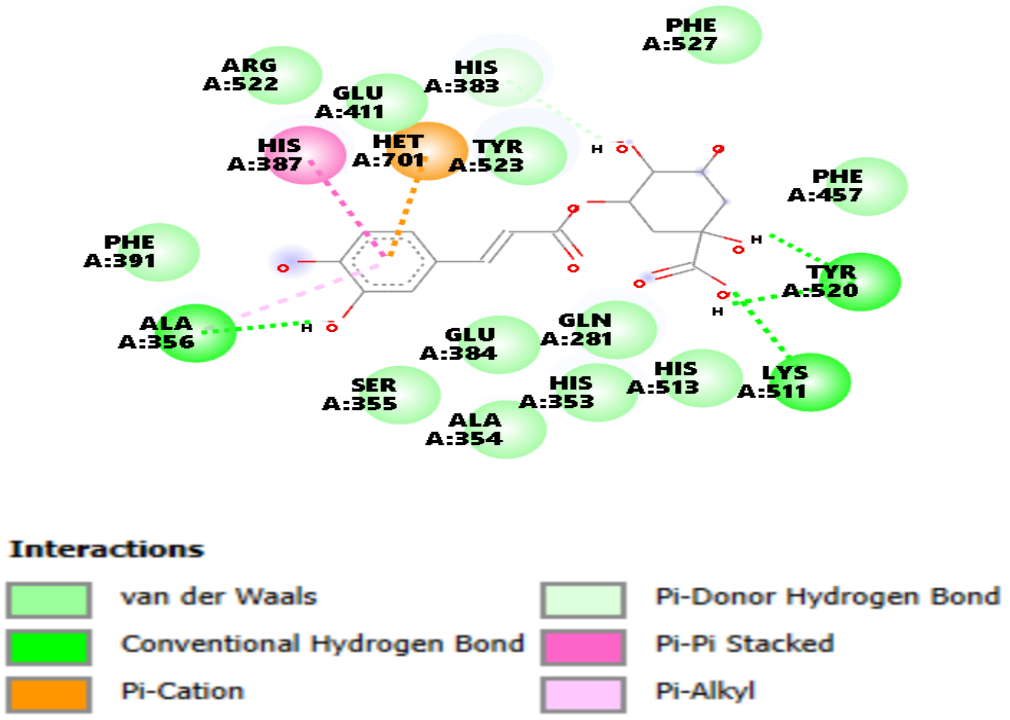


FIGURE 4.6: Molecular interaction analysis of Chlorogenic acid with ACE

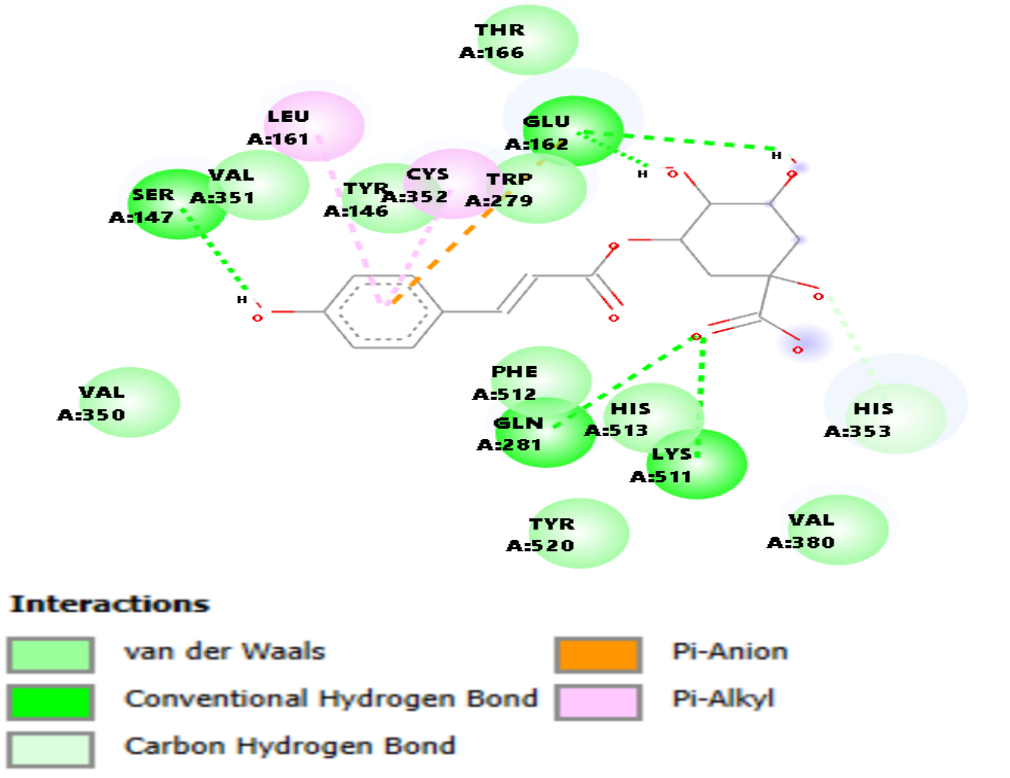


FIGURE 4.7: Molecular interaction analysis of 5-p-Coumaroylquinic acid with ACE

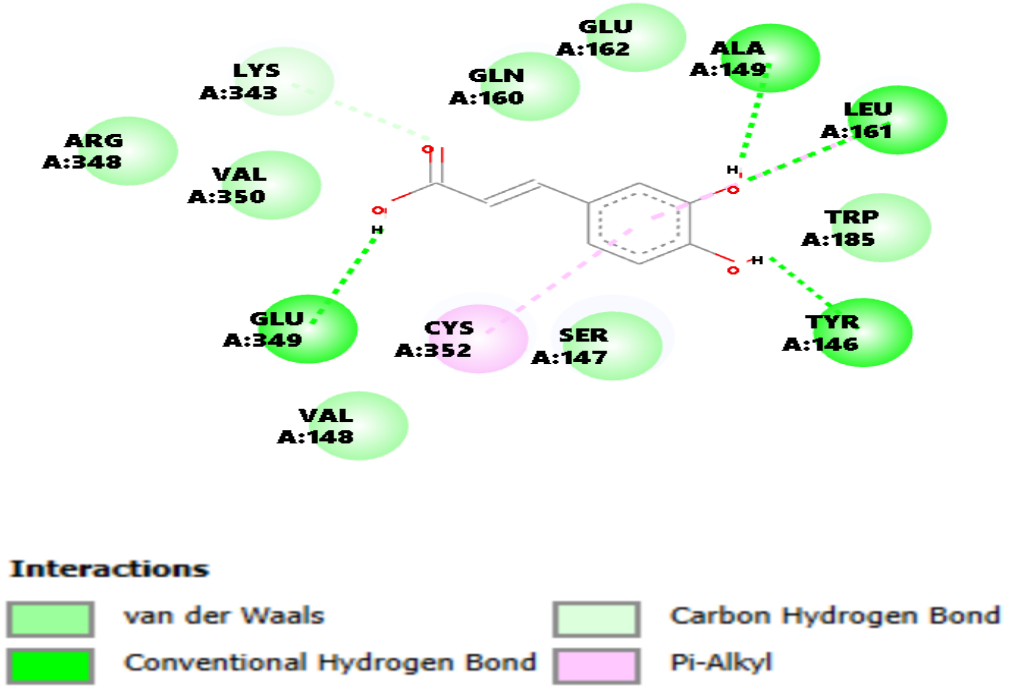


FIGURE 4.8: Molecular interaction analysis of Caffeic acid with ACE

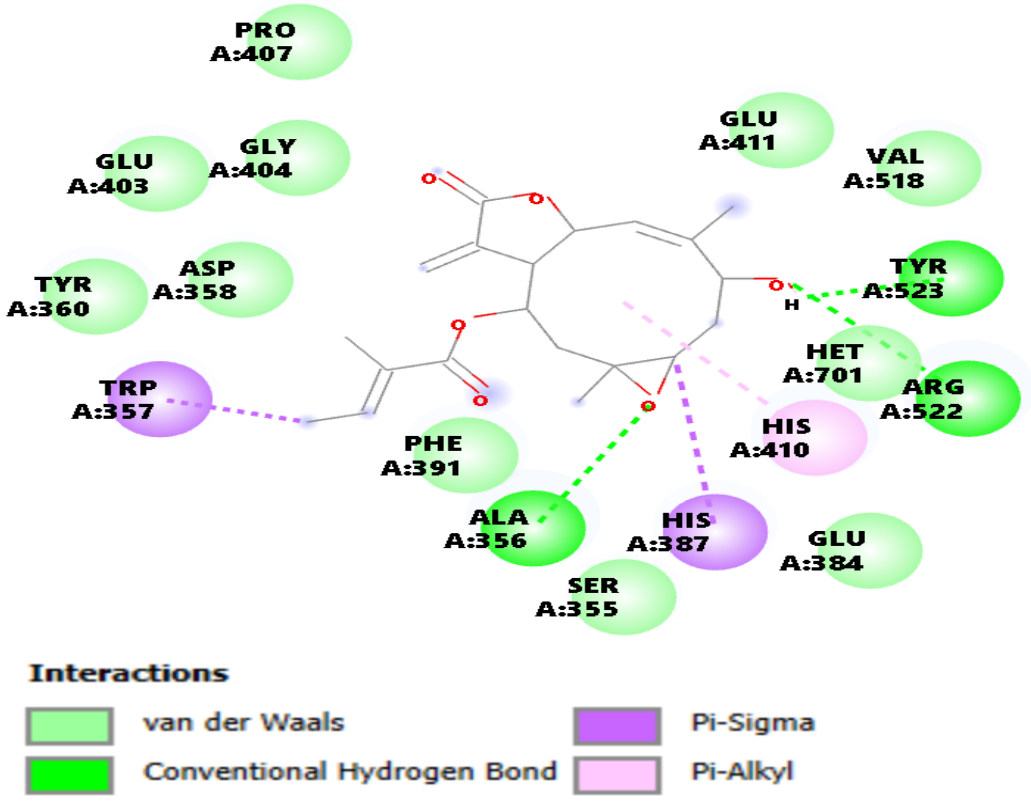


FIGURE 4.9: Molecular interaction analysis of Heliangine with ACE

Across the panel (Figures 4.5–4.9), hydrogen bonding and van der Waals contact with residues lining the C1 pocket recurred as the main contact types observed. The strongest binders (astragalin, heliangine, chlorogenic acid) each formed a wider spread of conventional hydrogen bonds than caffeic acid.

4.5 Lead Compound Identification

Lead compounds were identified by considering the docking, drug-likeness, and ADMET/toxicity results together rather than ranking compounds on docking score alone. On this basis, four of the five screened phytochemicals astragalin, heliangine, chlorogenic acid, and 5-p-coumaroylquinic acid were carried forward as lead candidates for comparison against the reference drug in Section 4.7 caffeic acid, the weakest binder of the panel (-6.3 kcal/mol) and the only compound to score below the reference drug, was not carried forward.

Astragalin returned the strongest docking score of the panel (-8.6 kcal/mol) but carried two Lipinski violations and the weakest predicted intestinal absorption (48.1%). Heliangine matched chlorogenic acid for the second-best docking score (-7.9 kcal/mol) and gave the best absorption of the whole panel (97.9%), but returned a positive AMES mutagenicity result; this result is carried forward as a flag requiring experimental confirmation rather than as grounds for exclusion at this stage. Chlorogenic acid carried only one Lipinski violation and was clean across every toxicity endpoint tested. 5-p-Coumaroylquinic acid was fully Lipinski-compliant and likewise clean on toxicity, docking more strongly than lisinopril (-7.7 kcal/mol, against lisinopril's own -7.3 kcal/mol reported in Section 4.6.3). Each of the four is compared against lisinopril individually in Section 4.7.

4.6 Reference Drug Selection and Screening

Lisinopril, a clinically established ACE inhibitor, was selected as the reference drug for this study. It was chosen specifically because it is the ligand co-crystallised

in ACE crystal structures reported in the literature [22] and is widely used as the benchmark inhibitor in comparable *In Silico* ACE-inhibitor screening studies. Lisinopril was subjected to the same screening pipeline applied to the candidate phytochemicals, described in Sections 4.2 through 4.4.

4.6.1 Identity and Drug-Likeness

Table 4.10 gives lisinopril's PubChem identity and two-dimensional structure, in the same format used for the candidate phytochemicals in Table 4.2.

TABLE 4.10: Lisinopril identity, PubChem CID, molecular formula, and 2D structure

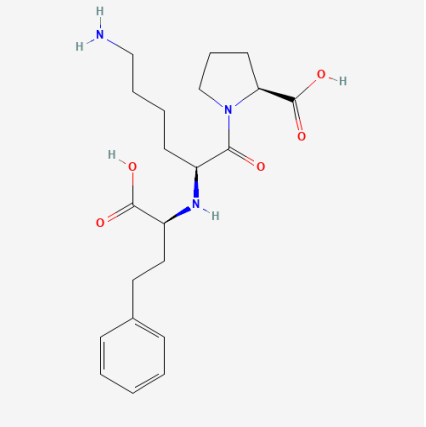
Ligand	**PubChem CID**	**Molecular Formula**	**2D Structure**
Lisinopril (reference drug)	5362119	C21H31N3O5	

TABLE 4.11: Lipinski parameters for lisinopril

Parameter	**Lisinopril (reference drug)**
MW (≤500 g/mol)	405.49
H-Bond Donors (≤5)	4
H-Bond Acceptors (≤10)	7
Consensus LogP (≤5)	-0.45
Rotatable Bonds	13

Continued on next page

TABLE 4.11: Lipinski parameters for lisinopril (continued)

Parameter	**Lisinopril (reference drug)**
Lipinski Violations	0

As Table 4.11 confirms, lisinopril passed Lipinski's Rule of Five [39] without exception, but its thirteen rotatable bonds failed Veber's rule [45], a related but separate bioavailability criterion that caps flexibility at ten rotatable bonds.

4.6.2 ADMET Profile

TABLE 4.12: Absorption parameters for lisinopril

Parameter	**Lisinopril (reference drug)**
Water Solubility (log mol/L)	-2.743
Caco-2 Permeability (log Papp, 10^{-6} cm/s)	0.107
Intestinal Absorption – Human (%)	13.022
Skin Permeability (log Kp)	-2.735
P-glycoprotein Substrate	No
P-glycoprotein I Inhibitor	No
P-glycoprotein II Inhibitor	No

TABLE 4.13: Distribution parameters for lisinopril

Ligand	**VDss Human (log L/kg)**	**Fraction Unbound Human (Fu)**	**BBB Permeability (log BB)**	**CNS Permeability (log PS)**
Lisinopril (reference drug)	-1.224	0.504	-1.15	-3.77

Table 4.14: Metabolism parameters for lisinopril

Parameter	**Lisinopril (reference drug)**
CYP2D6 Sub.	No
CYP3A4 Sub.	No
CYP1A2 Inh.	No
CYP2C19 Inh.	No
CYP2C9 Inh.	No
CYP2D6 Inh.	No
CYP3A4 Inh.	No

Table 4.15: Excretion parameters for lisinopril

Ligand	**Total Clearance (log mL/min/kg)**	**Renal OCT2 Substrate**
Lisinopril (reference drug)	0.476	No

Table 4.16: Toxicity parameters for lisinopril

Property	**Value**
Ligand	Lisinopril (reference drug)
AMES Toxicity	No
Max. Tolerated Dose (log mg/kg/day)	0.505
hERG I Inhibitor	No
hERG II Inhibitor	No
LD50 (mol/kg)	2.223
LOAEL (log mg/kg_bw/day)	2.227
Hepatotoxicity	Yes
Skin Sensitisation	No
T.Pyriformis Toxicity (log μg/L)	0.285
Minnow Toxicity (log mM)	5.759

Tables 4.12 through 4.16 report lisinopril's predicted pharmacokinetic and toxicity profile in the same format applied to the phytochemical panel. Its intestinal absorption was predicted at 13.0%, the lowest value returned for any ligand in this study (Table 4.12), with its volume of distribution and blood–brain barrier permeability set out in Table 4.13.

Lisinopril was not predicted to act as a substrate or inhibitor of any of the CYP450 isoforms screened (Table 4.14), and it returned a total clearance value of 0.476 log mL/min/kg with no predicted OCT2 liability (Table 4.15). Its toxicity profile was clean overall but for one flag, a positive hepatotoxicity prediction (Table 4.16), a distinction from all four lead phytochemicals discussed in Section 4.7 and returned to in Chapter 5.

4.6.3 Molecular Docking and Interaction Analysis

TABLE 4.17: Docking result for lisinopril

Ligand	Docking Score (kcal/mol)	Cavity Volume (Å³)	Docked Complex (Receptor + Lisinopril)
Lisinopril (reference drug)	-7.3	13,542	

Lisinopril settled into the same cavity, C1, used by all five ligands, at a score of -7.3 kcal/mol (Table 4.17); its interaction pattern is illustrated in Figure 4.10.

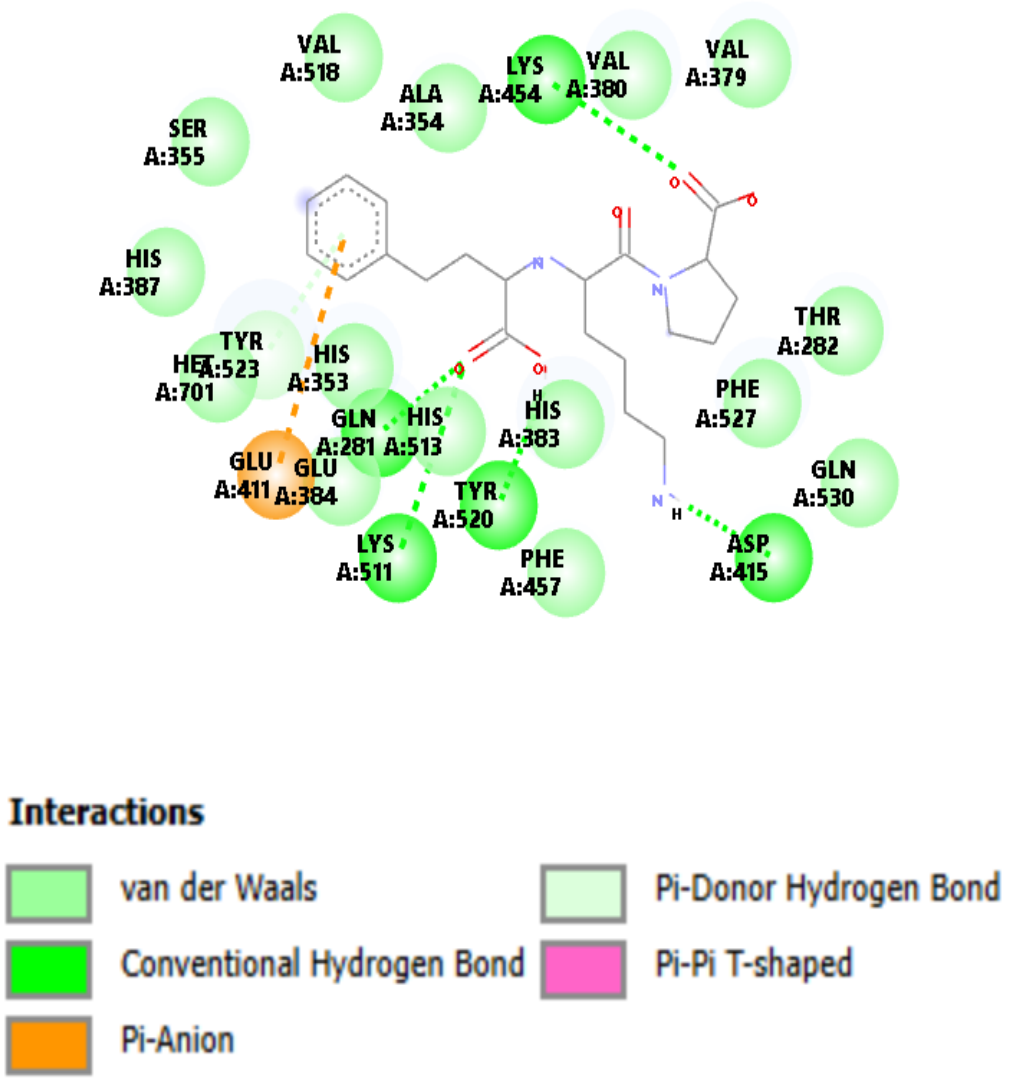


FIGURE 4.10: Molecular interaction analysis of lisinopril with ACE

4.7 Comparative Analysis of Lead Compounds with the Reference Drug

Each lead compound identified in Section 4.5 is compared directly against lisinopril, table for table, using the same identity, drug-likeness, ADMET, and docking format applied to the wider panel.

4.7.1 Chlorogenic Acid versus Lisinopril

TABLE 4.18: Identity of lisinopril and Chlorogenic acid, with PubChem CID, molecular formula, and 2D structure

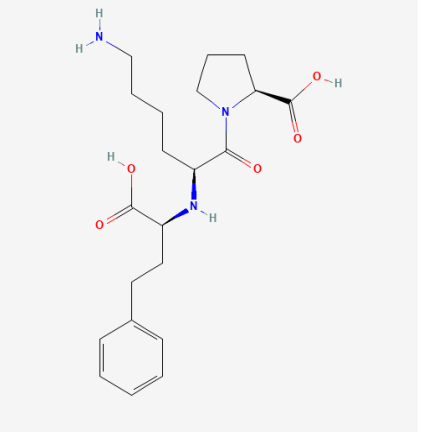
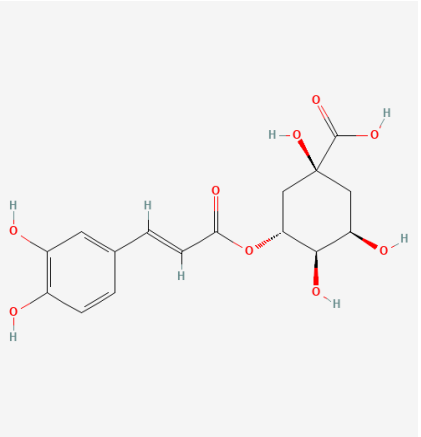
Sr. No.	Ligand	PubChem CID	Molecular Formula	2D Structure
1	Lisinopril (reference drug)	5362119	C21H31N3O5	
2	Chlorogenic acid	1794427	C16H18O9	

TABLE 4.19: Lipinski's Rule of Five parameters for lisinopril and Chlorogenic acid

Parameter	Lisinopril (reference drug)	Chlorogenic acid
MW (≤500 g/mol)	405.49	354.31
H-Bond Donors (≤5)	4	6
H-Bond Acceptors (≤10)	7	9

Continued on next page

Table 4.19: Lipinski's Rule of Five parameters for lisinopril and Chlorogenic acid (continued)

Parameter	**Lisinopril (reference drug)**	**Chlorogenic acid**
Consensus LogP (≤5)	-0.45	-0.71
Rotatable Bonds	13	5
Lipinski Violations	0	1: NHorOH>5

Table 4.20: Absorption parameters for lisinopril and Chlorogenic acid

Parameter	**Lisinopril (reference drug)**	**Chlorogenic acid**
Water Solubility (log mol/L)	-2.743	-2.449
Caco-2 Permeability (log Papp, 10^{-6} cm/s)	0.107	-0.84
Intestinal Absorption – Human (%)	13.022	36.377
Skin Permeability (log Kp)	-2.735	-2.735
P-glycoprotein Substrate	No	Yes
P-glycoprotein I Inhibitor	No	No
P-glycoprotein II Inhibitor	No	No

Table 4.21: Distribution parameters for lisinopril and Chlorogenic acid

Ligand	**VDss Human (log L/kg)**	**Fraction Unbound Human (Fu)**	**BBB Permeability (log BB)**	**CNS Permeability (log PS)**
Lisinopril (reference drug)	-1.224	0.504	-1.15	-3.77
Chlorogenic acid	0.581	0.658	-1.407	-3.856

Table 4.22: Metabolism (CYP450) parameters for lisinopril and Chlorogenic acid

Parameter	**Lisinopril (reference drug)**	**Chlorogenic acid**
CYP2D6 Sub.	No	No
CYP3A4 Sub.	No	No
CYP1A2 Inh.	No	No
CYP2C19 Inh.	No	No
CYP2C9 Inh.	No	No
CYP2D6 Inh.	No	No
CYP3A4 Inh.	No	No

Table 4.23: Excretion parameters for lisinopril and Chlorogenic acid

Ligand	**Total Clearance (log mL/min/kg)**	**Renal OCT2 Substrate**
Lisinopril (reference drug)	0.476	No
Chlorogenic acid	0.307	No

Table 4.24: Toxicity parameters for lisinopril and Chlorogenic acid

Toxicity Parameter	**Lisinopril**	**Chlorogenic acid**
AMES Toxicity	No	No
Max. Tolerated Dose (log mg/kg/day)	0.505	-0.134
hERG I Inhibitor	No	No
hERG II Inhibitor	No	No
Oral Rat Acute Toxicity LD50 (mol/kg)	2.223	1.973
Oral Rat Chronic Toxicity LOAEL (log mg/kg_bw/day)	2.227	2.982

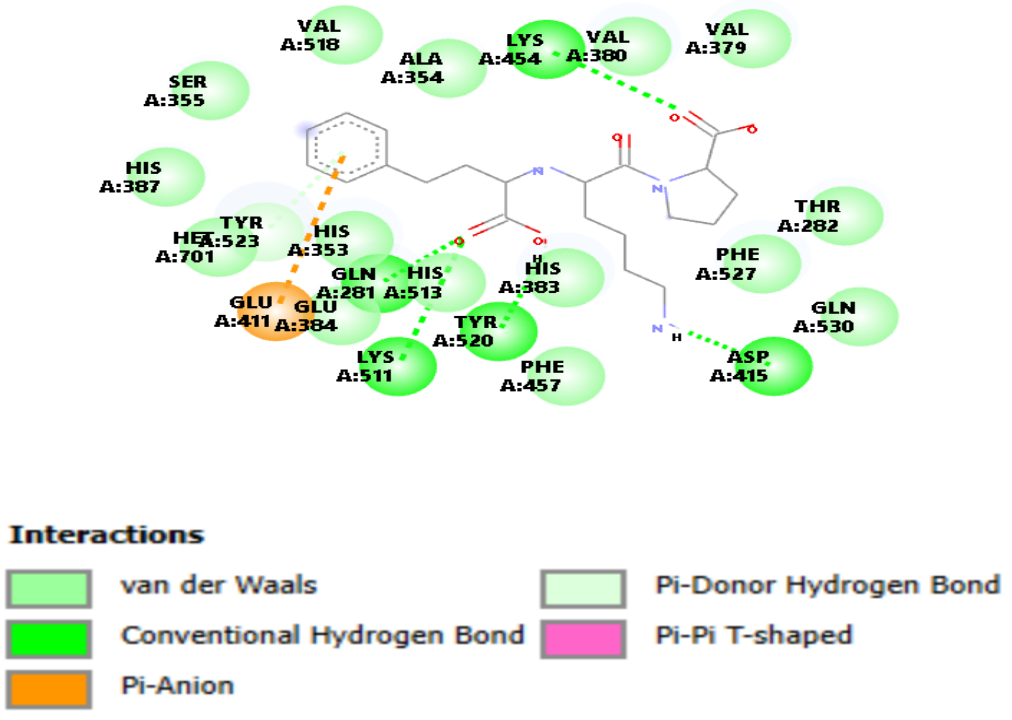
Continued on next page

TABLE 4.24: Toxicity parameters for lisinopril and Chlorogenic acid (continued)

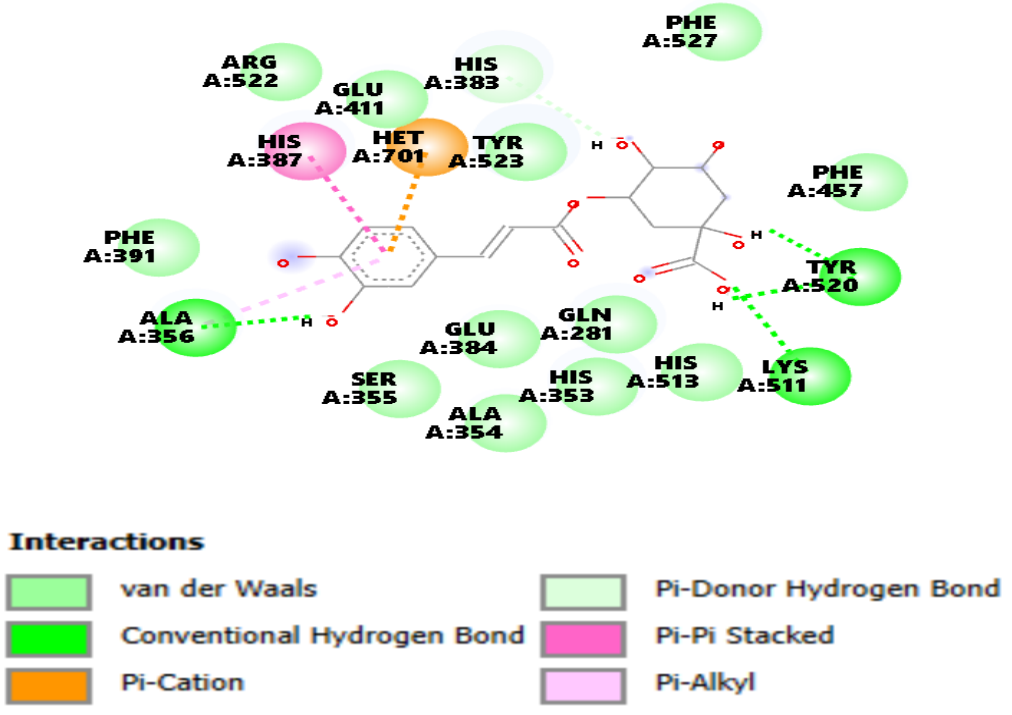
Toxicity Parameter	**Lisinopril**	**Chlorogenic acid**
Hepatotoxicity	Yes	No
Skin Sensitisation	No	No
T.Pyriformis Toxicity (log μg/L)	0.285	0.285
Minnow Toxicity (log mM)	5.759	5.741

TABLE 4.25: Docking scores and cavity volume for lisinopril and Chlorogenic acid, both occupying cavity C1, with their docked complexes

Ligand	**Docking Score (kcal/mol)**	**Cavity Volume (Å³)**	**Docked Complex (Receptor + Ligand)**
Lisinopril (reference drug)	-7.3	13,542	
Chlorogenic acid	-7.9	13,542	



Lisinopril



Chlorogenic acid

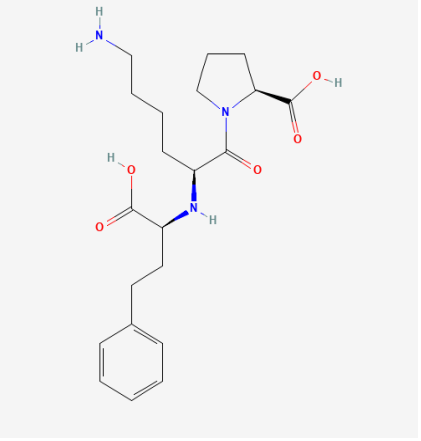
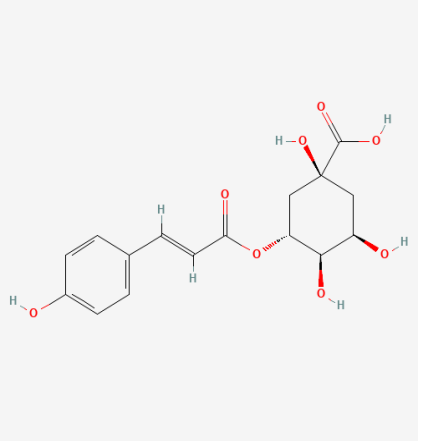
FIGURE 4.11: Molecular interaction analysis of lisinopril (top) and chlorogenic acid (bottom) with ACE

4.7.1.1 Interaction Comparison

Taken together, Tables 4.18–4.25 place chlorogenic acid alongside lisinopril across the full profile: matching identity data (Table 4.18), a single Lipinski violation against lisinopril's zero (Table 4.19), predicted intestinal absorption of 36.4% versus lisinopril's 13.0% (Table 4.20), a broadly comparable distribution profile (Table 4.21), and an identical, clean CYP450 metabolism result for both compounds (Table 4.22).

4.7.2 5-p-Coumaroylquinic Acid versus Lisinopril

TABLE 4.26: Identity of lisinopril and 5-p-Coumaroylquinic acid, with PubChem CID, molecular formula, and 2D structure

Sr. No.	Ligand	PubChem CID	Molecular Formula	2D Structure
1	Lisinopril (reference drug)	5362119	C21H31N3O5	
2	5-p-Coumaroylquinic acid	6441280	C16H18O8	

Its clearance was slightly lower than lisinopril's (Table 4.23), and it was clean across the entire toxicity panel, including the hepatotoxicity flag returned for lisinopril (Table 4.24). It also outdocked lisinopril, at -7.9 against -7.3 kcal/mol in the same C1 cavity (Table 4.25), with the corresponding poses compared in Figure 4.11.

TABLE 4.27: Lipinski's Rule of Five parameters for lisinopril and 5-p-Coumaroylquinic acid

Parameter	**Lisinopril (reference drug)**	**5-p-Coumaroylquinic acid**
MW (≤500 g/mol)	405.49	338.31
H-Bond Donors (≤5)	4	5
H-Bond Acceptors (≤10)	7	8
Consensus LogP (≤5)	-0.45	-0.31
Rotatable Bonds	13	5
Lipinski Violations	0	0

TABLE 4.28: Absorption parameters for lisinopril and 5-p-Coumaroylquinic acid

Parameter	**Lisinopril (reference drug)**	**5-p-Coumaroylquinic acid**
Water Solubility (log mol/L)	-2.743	-1.991
Caco-2 Permeability (log Papp, 10^{-6} cm/s)	0.107	-0.656
Intestinal Absorption – Human (%)	13.022	43.925
Skin Permeability (log Kp)	-2.735	-2.735
P-glycoprotein Substrate	No	Yes
P-glycoprotein I Inhibitor	No	No
P-glycoprotein II Inhibitor	No	No

Table 4.29: Distribution parameters for lisinopril and 5-p-Coumaroylquinic acid

Ligand	**VDss Human (log L/kg)**	**Fraction Unbound Human (Fu)**	**BBB Permeability (log BB)**	**CNS Permeability (log PS)**
Lisinopril (reference drug)	-1.224	0.504	-1.15	-3.77
5-p-Coumaroylquinic acid	0.034	0.612	-1.16	-3.693

Table 4.30: Metabolism (CYP450) parameters for lisinopril and 5-p-Coumaroylquinic acid

Parameter	**Lisinopril (reference drug)**	**5-p-Coumaroylquinic acid**
CYP2D6 Sub.	No	No
CYP3A4 Sub.	No	No
CYP1A2 Inh.	No	No
CYP2C19 Inh.	No	No
CYP2C9 Inh.	No	No
CYP2D6 Inh.	No	No
CYP3A4 Inh.	No	No

Table 4.31: Excretion parameters for lisinopril and 5-p-Coumaroylquinic acid

Ligand	**Total Clearance (log mL/min/kg)**	**Renal OCT2 Substrate**
Lisinopril (reference drug)	0.476	No
5-p-Coumaroylquinic acid	0.453	No

TABLE 4.32: Toxicity parameters for lisinopril and 5-p-Coumaroylquinic acid

Toxicity Parameter	**Lisinopril**	**5-p-Coumaroylquinic acid**
AMES Toxicity	No	No
Max. Tolerated Dose (log mg/kg/day)	0.505	-0.09
hERG I Inhibitor	No	No
hERG II Inhibitor	No	No
LD50 (mol/kg)	2.223	1.737
LOAEL (log mg/kg_bw/day)	2.227	2.508
Hepatotoxicity	Yes	No
Skin Sensitisation	No	No
T.Pyriformis Toxicity (log μg/L)	0.285	0.285
Minnow Toxicity (log mM)	5.759	4.611

TABLE 4.33: Docking scores and cavity volume for lisinopril and 5-p-Coumaroylquinic acid, both occupying cavity C1, with their docked complexes

Ligand	**Docking Score (kcal/mol)**	**Cavity Volume (Å³)**	**Docked Complex (Receptor + Ligand)**
Lisinopril (reference drug)	-7.3	13,542	

Continued on next page

TABLE 4.33: Docking scores and cavity volume for lisinopril and 5-p-Coumaroyl-quinic acid, both occupying cavity C1, with their docked complexes (continued)

Ligand	Docking Score (kcal/mol)	Cavity Volume (Å³)	Docked Complex (Receptor + Ligand)
5-p-Coumaroyl-quinic acid	-7.7	13,542	

4.7.2.1 Interaction Comparison

5-p-Coumaroylquinic acid followed the same identity and drug-likeness format (Table 4.26), returning zero Lipinski violations and matching lisinopril's own clean result (Table 4.27). Its predicted intestinal absorption reached 43.9%, more than three times lisinopril's 13.0% (Table 4.28), with a comparable distribution profile (Table 4.29) and no predicted interaction with any of the CYP450 isoforms screened, again mirroring lisinopril (Table 4.30).

Total clearance was marginally lower than the reference drug (Table 4.31), and the compound was clean on every toxicity endpoint, avoiding the hepatotoxicity prediction returned for lisinopril (Table 4.32). Docking placed it at -7.7 kcal/mol against lisinopril's -7.3 kcal/mol in cavity C1 (Table 4.33), with both binding poses compared in Figure 4.12.

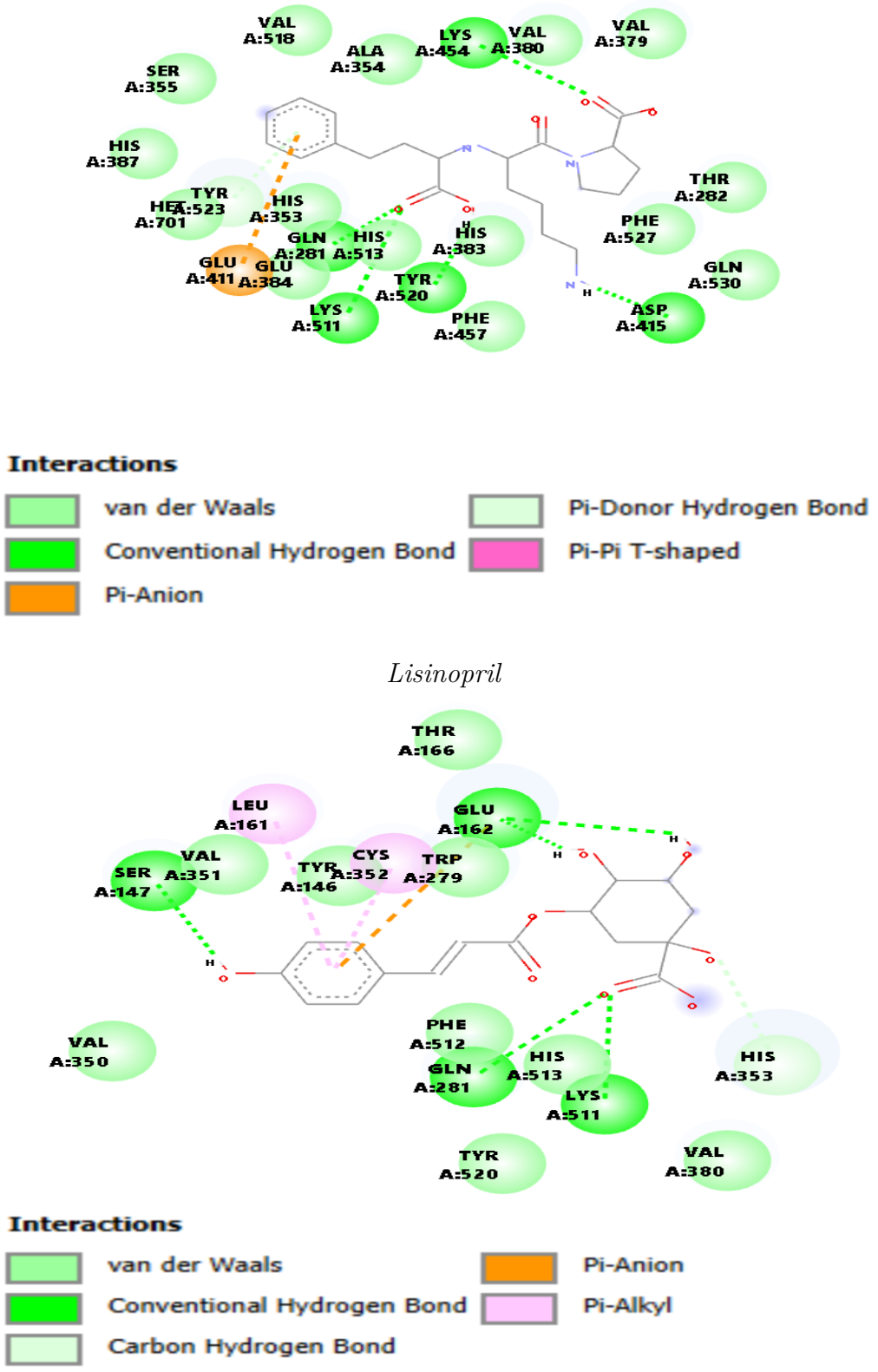


FIGURE 4.12: Molecular interaction analysis of lisinopril (top) and 5-p-coumaroylquinic acid (bottom) with ACE

4.7.3 Astragalin versus Lisinopril

TABLE 4.34: Identity of lisinopril and Astragalin, with PubChem CID, molecular formula, and 2D structure

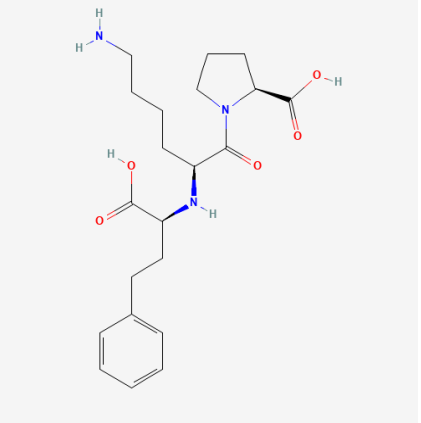
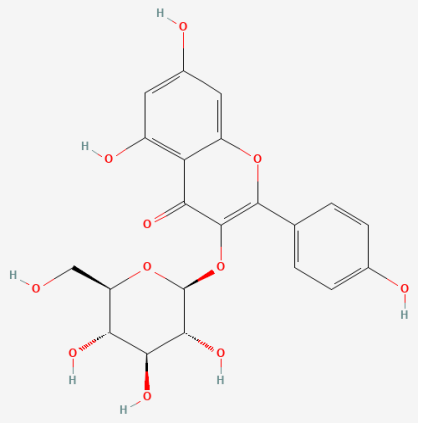
Sr. No.	Ligand	PubChem CID	Molecular Formula	2D Structure
1	Lisinopril (reference drug)	5362119	C21H31N3O5	
2	Astragalin	5282102	C21H20O11	

TABLE 4.35: Lipinski's Rule of Five parameters for lisinopril and Astragalin

Parameter	Lisinopril (reference drug)	Astragalin
MW (≤500 g/mol)	405.49	448.38
H-Bond Donors (≤5)	4	7
H-Bond Acceptors (≤10)	7	11
Consensus LogP (≤5)	-0.45	-0.94

Continued on next page

Table 4.35: Lipinski's Rule of Five parameters for lisinopril and Astragalin (continued)

Parameter	**Lisinopril (reference drug)**	**Astragalin**
Rotatable Bonds	13	4
Lipinski Violations	0	2: NorO>10, NHorOH>5

Table 4.36: Absorption parameters for lisinopril and Astragalin

Parameter	**Lisinopril (reference drug)**	**Astragalin**
Water Solubility (log mol/L)	-2.743	-2.863
Caco-2 Permeability (log Papp, 10^{-6} cm/s)	0.107	0.306
Intestinal Absorption – Human (%)	13.022	48.052
Skin Permeability (log Kp)	-2.735	-2.735
P-glycoprotein Substrate	No	Yes
P-glycoprotein I Inhibitor	No	No
P-glycoprotein II Inhibitor	No	No

Table 4.37: Distribution parameters for lisinopril and Astragalin

Ligand	**VDss Human (log L/kg)**	**Fraction Unbound Human (Fu)**	**BBB Permeability (log BB)**	**CNS Permeability (log PS)**
Lisinopril (reference drug)	-1.224	0.504	-1.15	-3.77
Astragalin	1.444	0.218	-1.514	-3.908

Table 4.38: Metabolism (CYP450) parameters for lisinopril and Astragalin

Parameter	**Lisinopril (reference drug)**	**Astragalin**
CYP2D6 Sub.	No	No
CYP3A4 Sub.	No	No
CYP1A2 Inh.	No	No
CYP2C19 Inh.	No	No
CYP2C9 Inh.	No	No
CYP2D6 Inh.	No	No
CYP3A4 Inh.	No	No

Table 4.39: Excretion parameters for lisinopril and Astragalin

Ligand	**Total Clearance (log mL/min/kg)**	**Renal OCT2 Substrate**
Lisinopril (reference drug)	0.476	No
Astragalin	0.462	No

Table 4.40: Toxicity parameters for lisinopril and Astragalin

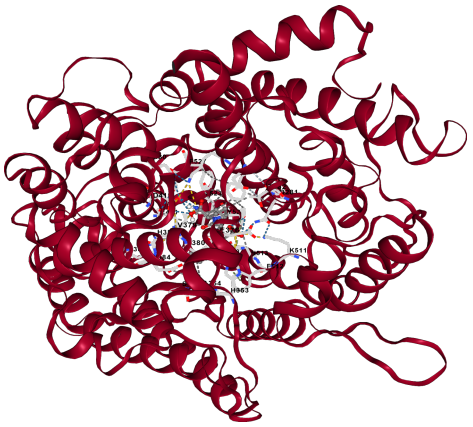
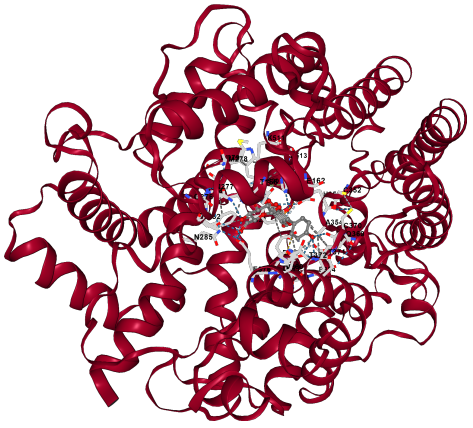
Toxicity Parameter	**Lisinopril**	**Astragalin**
AMES Toxicity	No	No
Max. Tolerated Dose (log mg/kg/day)	0.505	0.582
hERG I Inhibitor	No	No
hERG II Inhibitor	No	No
LD50 (mol/kg)	2.223	2.546
LOAEL (log mg/kg_bw/day)	2.227	4.53
Hepatotoxicity	Yes	No
Skin Sensitisation	No	No
T.Pyriformis Toxicity (log μg/L)	0.285	0.285

Continued on next page

TABLE 4.40: Toxicity parameters for lisinopril and Astragalin (continued)

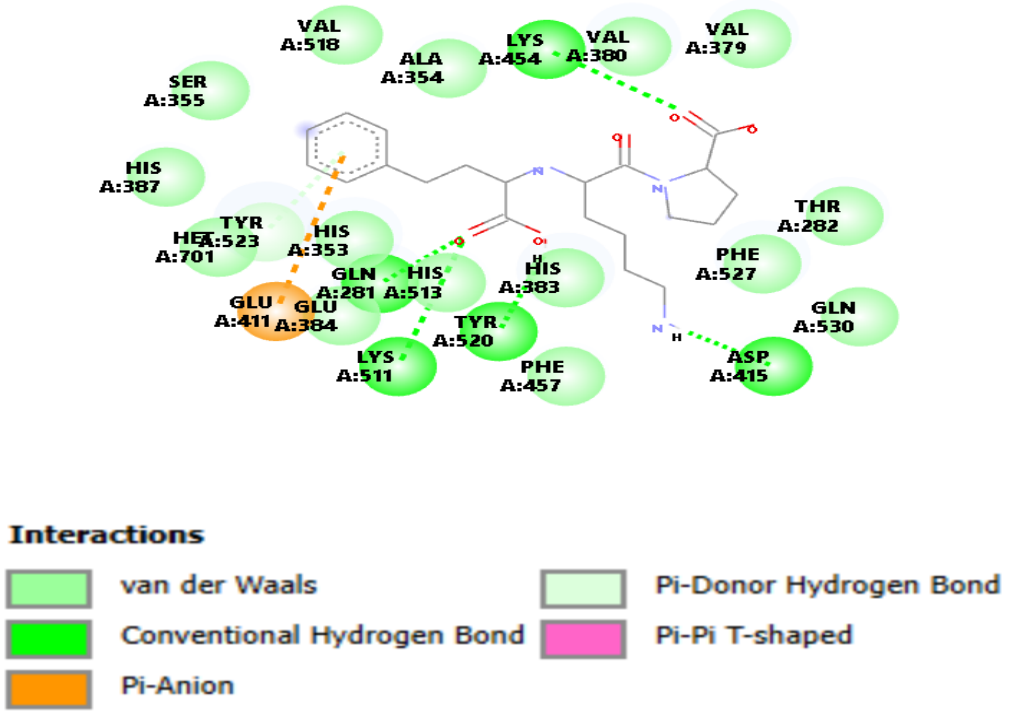
Toxicity Parameter	**Lisinopril**	**Astragalin**
Minnow Toxicity (log mM)	5.759	6.735

TABLE 4.41: Docking scores and cavity volume for lisinopril and Astragalin, both occupying cavity C1, with their docked complexes

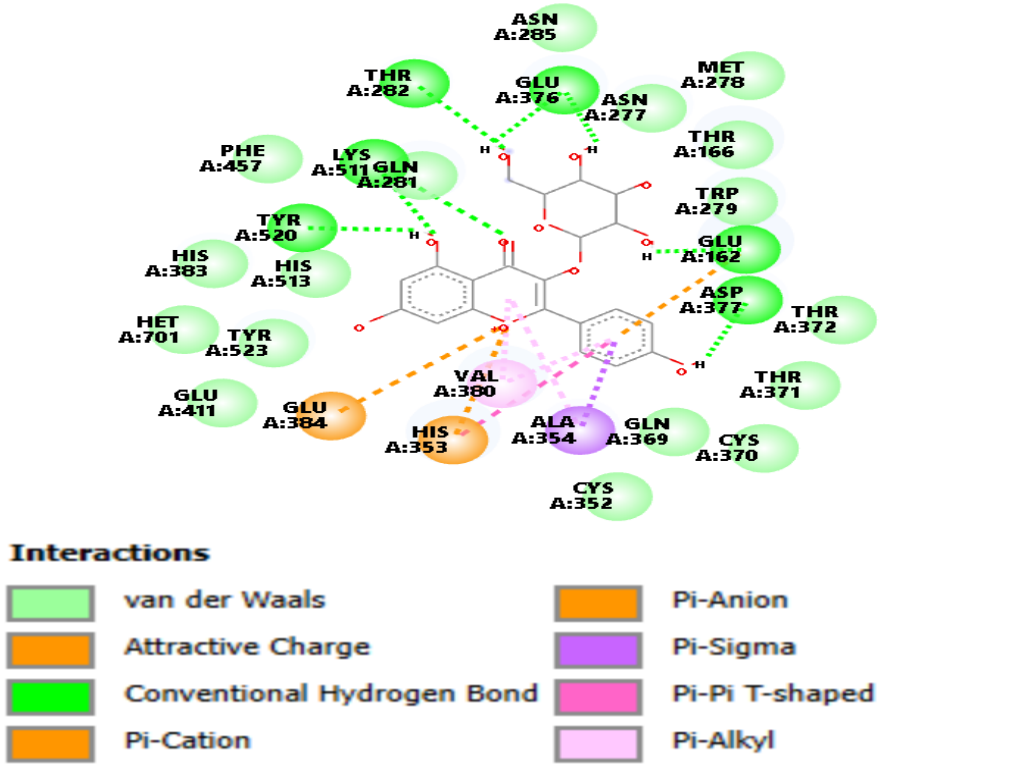
Ligand	**Docking Score (kcal/mol)**	**Cavity Volume (Å³)**	**Docked Complex (Receptor + Ligand)**
Lisinopril (reference drug)	-7.3	13,542	
Astragalin	-8.6	13,542	

4.7.3.1 Interaction Comparison

Astragalin's identity data appear in Table 4.34. Unlike the other leads, it failed Lipinski's Rule of Five outright, exceeding both the hydrogen-bond donor and acceptor limits against lisinopril's zero violations (Table 4.35)



Lisinopril



Astragalin

FIGURE 4.13: Molecular interaction analysis of lisinopril (top) and astragalin (bottom) with ACE

Its predicted intestinal absorption of 48.1%, while the lowest among the four leads, still exceeded lisinopril's 13.0% by a wide margin (Table 4.36). Its distribution (Table 4.37) and metabolism (Table 4.38) profiles were otherwise unremarkable relative to lisinopril, and its clearance was similarly close to the reference value (Table 4.39). Astragalin was clean across the toxicity panel, again avoiding lisinopril's hepatotoxicity flag (Table 4.40), and it returned the strongest docking score of the entire study, -8.6 kcal/mol against lisinopril's -7.3 kcal/mol (Table 4.41), the corresponding poses are compared in Figure 4.13.

4.7.4 Heliangine versus Lisinopril

TABLE 4.42: Identity of lisinopril and Heliangine, with PubChem CID, molecular formula, and 2D structure

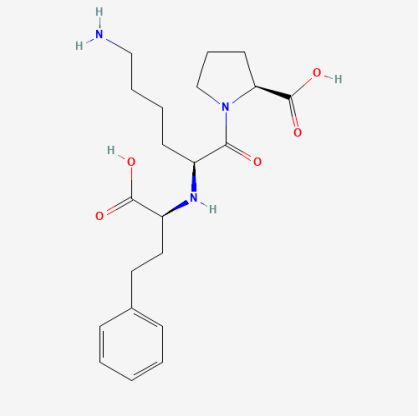
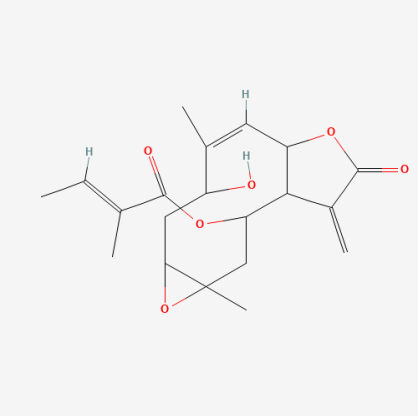
Sr. No.	Ligand	PubChem CID	Molecular Formula	2D Structure
1	Lisinopril (reference drug)	5362119	C21H31N3O5	
2	Heliangine	5838160	C20H26O6	

Table 4.43: Lipinski's Rule of Five parameters for lisinopril and Heliangine

Parameter	**Lisinopril (reference drug)**	**Heliangine**
MW (≤500 g/mol)	405.49	362.42
H-Bond Donors (≤5)	4	1
H-Bond Acceptors (≤10)	7	6
Consensus LogP (≤5)	-0.45	2.12
Rotatable Bonds	13	3
Lipinski Violations	0	0

Table 4.44: Absorption parameters for lisinopril and Heliangine

Parameter	**Lisinopril (reference drug)**	**Heliangine**
Water Solubility (log mol/L)	-2.743	-3.831
Caco-2 Permeability (log Papp, 10^{-6} cm/s)	0.107	1.178
Intestinal Absorption – Human (%)	13.022	97.894
Skin Permeability (log Kp)	-2.735	-3.306
P-glycoprotein Substrate	No	Yes
P-glycoprotein I Inhibitor	No	No
P-glycoprotein II Inhibitor	No	No

Table 4.45: Distribution parameters for lisinopril and Heliangine

Ligand	**VDss Human (log L/kg)**	**Fraction Unbound Human (Fu)**	**BBB Permeability (log BB)**	**CNS Permeability (log PS)**
Lisinopril (ref. drug)	-1.224	0.504	-1.15	-3.77
Heliangine	-0.086	0.363	-0.482	-2.95

Table 4.46: Metabolism (CYP450) parameters for lisinopril and Heliangine

Parameter	**Lisinopril (reference drug)**	**Heliangine**
CYP2D6 Sub.	No	No
CYP3A4 Sub.	No	Yes
CYP1A2 Inh.	No	No
CYP2C19 Inh.	No	No
CYP2C9 Inh.	No	No
CYP2D6 Inh.	No	No
CYP3A4 Inh.	No	No

Table 4.47: Excretion parameters for lisinopril and Heliangine

Ligand	**Total Clearance (log mL/min/kg)**	**Renal OCT2 Substrate**
Lisinopril (reference drug)	0.476	No
Heliangine	1.312	No

Table 4.48: Toxicity parameters for lisinopril and Heliangine

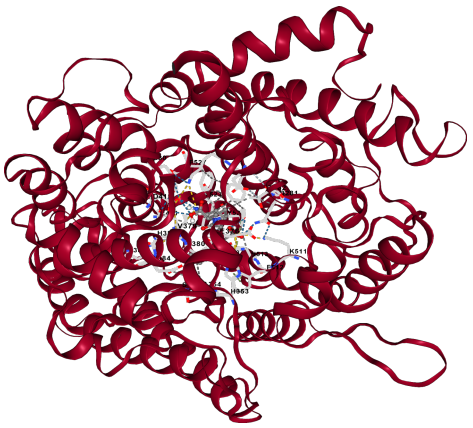
Toxicity Parameter	**Lisinopril**	**Heliangine**
AMES Toxicity	No	Yes
Max. Tolerated Dose (log mg/kg/day)	0.505	-0.202
hERG I Inhibitor	No	No
hERG II Inhibitor	No	No
LD50 (mol/kg)	2.223	2.997
LOAEL (log mg/kg_bw/day)	2.227	1.286
Hepatotoxicity	Yes	No
Skin Sensitisation	No	No
T.Pyriformis Toxicity (log μg/L)	0.285	0.401

Continued on next page

TABLE 4.48: Toxicity parameters for lisinopril and Heliangine (continued)

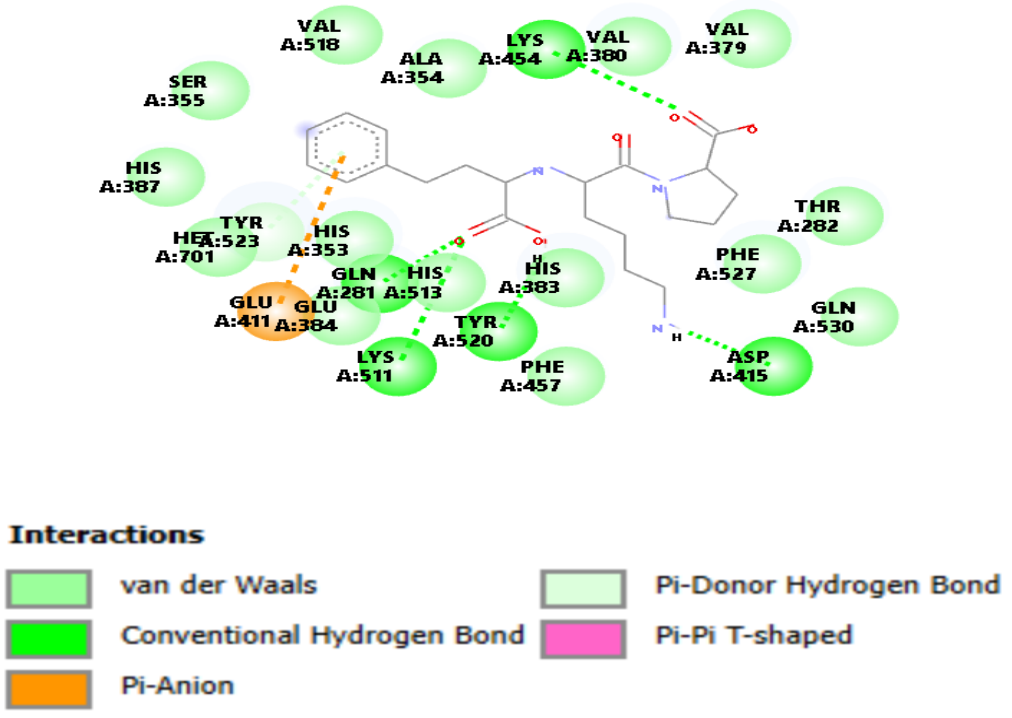
Toxicity Parameter	**Lisinopril**	**Heliangine**
Minnow Toxicity (log mM)	5.759	2.535

TABLE 4.49: Docking scores and cavity volume for lisinopril and Heliangine, both occupying cavity C1, with their docked complexes

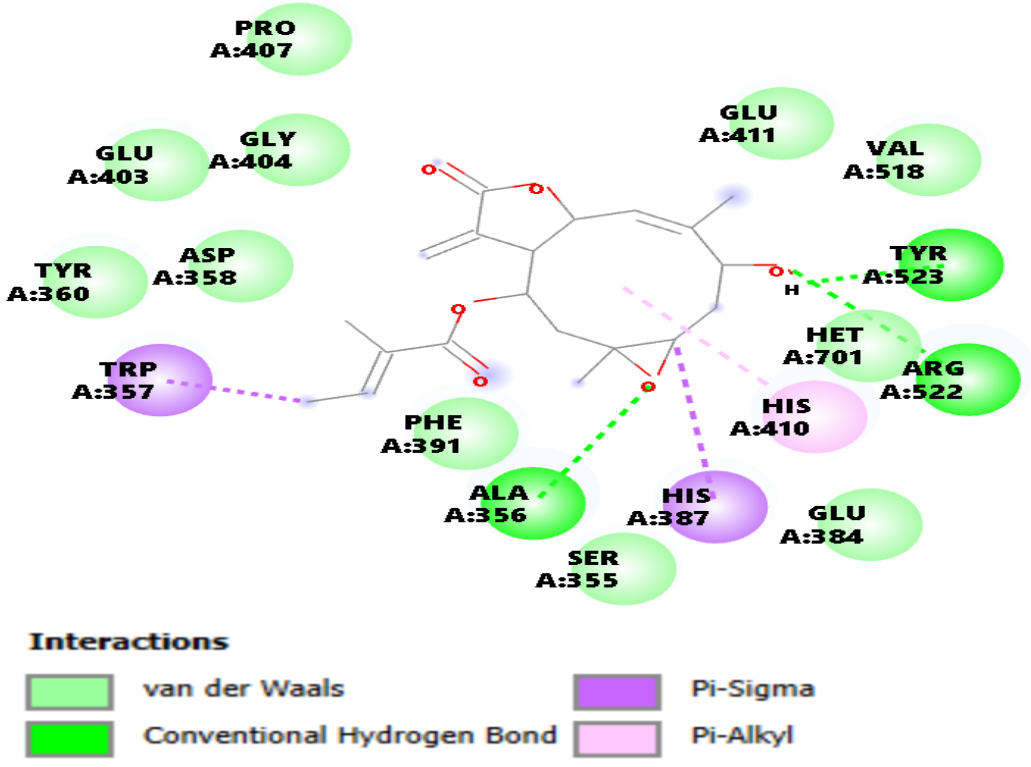
Ligand	**Docking Score (kcal/mol)**	**Cavity Volume (Å³)**	**Docked Complex (Receptor + Ligand)**
Lisinopril (reference drug)	-7.3	13,542	
Heliangine	-7.9	13,542	

4.7.4.1 Interaction Comparison

Heliangine's identity and structure are given in Table 4.42, and, like the other three leads, it satisfied Lipinski's Rule of Five without violation (Table 4.43).



Lisinopril



Heliangine

FIGURE 4.14: Molecular interaction analysis of lisinopril (top) and heliangine (bottom) with ACE

It returned the highest predicted intestinal absorption of the whole panel at 97.9%, well above lisinopril's 13.0% (Table 4.44), with its distribution profile shown in Table 4.45. It was the only lead predicted to act as a CYP3A4 substrate, though still without inhibiting any isoform tested (Table 4.46), and its clearance was the highest among the leads at 1.312 log mL/min/kg (Table 4.47). Its toxicity profile (Table 4.48) was clean of hepatotoxicity, unlike lisinopril, but returned the one AMES-positive mutagenicity result in the panel, a flag carried forward for experimental follow-up in Chapter 6. Heliangine tied chlorogenic acid for the second-strongest docking score at -7.9 kcal/mol against lisinopril's -7.3 kcal/mol (Table 4.49), with the interaction comparison shown in Figure 4.14.

Chapter 5

Discussion

This chapter provides an interpretation of the findings reported in Chapter 4., focusing on whether the four Jerusalem artichoke leaf phytochemicals identified as leads, chlorogenic acid, 5-p-coumaroylquinic acid, astragalin and heliangine, are computationally plausible, and in specific respects preferable, alternatives to lisinopril for ACE inhibition in chronic kidney disease (CKD). Each compound is discussed as a profile of trade-offs across binding affinity, drug-likeness, pharmacokinetics and toxicity, since this combined profile, rather than any single figure, determines whether a candidate suits a disease population that is often older, managed on multiple concurrent medications, and more vulnerable to added hepatic or renal drug-handling burden.

Confidence in the docking results interpreted throughout this chapter rests partly on the convergence of two independent lines of evidence on the same ACE cavity: the active site predicted independently by DoGSiteScorer in Section 4.2.2 coincided with cavity C1, the top-ranked pocket returned by CB-Dock2, and all six ligands docked in this study, the five candidate phytochemicals together with lisinopril, converged on this same cavity of identical volume (13,542 $Å^3$). Because every ligand is scored against the same pocket rather than settling into unrelated regions of the protein surface, the resulting docking scores are directly comparable, and their relative ranking can reasonably be read as chemically meaningful. Table 4.3 showed that four of the five screened phytochemicals passed Lipinski's Rule of

Five without exception, matching lisinopril's own clean profile on this specific filter. Where lisinopril and the phytochemicals diverge is on a criterion Lipinski's rule does not itself capture, namely molecular flexibility. Lisinopril's thirteen rotatable bonds exceed the ten-bond ceiling specified by Veber's rule [45], a related bioavailability heuristic that predicts poor oral absorption for excessively flexible molecules independently of Lipinski compliance. None of the four leads approaches this ceiling; their rotatable bond counts range from three, for heliangine, to five, for chlorogenic acid and 5-p-coumaroylquinic acid, a difference reflected directly in the absorption data discussed below. Astragalin is the only lead compound to itself fail a drug-likeness screen, exceeding both the hydrogen-bond acceptor and donor limits, consistent with its status as a glycosylated flavonoid rather than a free aglycone, a trade-off weighed later in this chapter against its docking performance.

The toxicity comparison in Section 4.8 identifies the most consistent point of differentiation between the lead compounds and lisinopril, and one with particular relevance to CKD specifically. pkCSM flagged lisinopril itself as hepatotoxic, whereas all four lead compounds returned a clean hepatotoxicity prediction, a distinction that carries added weight in a CKD population, where reduced renal clearance already shifts a greater share of drug elimination onto hepatic pathways and where polypharmacy for comorbid hypertension, diabetes and cardiovascular disease is the norm; a candidate that avoids adding predicted hepatic liability to this burden is an attractive profile to carry forward irrespective of its docking score. All five ligands, including lisinopril, were uniformly negative for hERG I and hERG II channel inhibition, and renal handling raised no additional flags either, with none of the compounds showing predicted affinity for the organic cation transporter OCT2 and clearance values across the panel staying within a comparatively tight range. The one toxicity flag that does distinguish within the lead panel itself is heliangine's positive AMES mutagenicity prediction, a signal that is not automatically disqualifying but does require this compound to be treated with more caution than the other three leads pending experimental confirmation.

Ranked from strongest to weakest, the docking scores obtained were astragalin (-8.6 kcal/mol), heliangine and chlorogenic acid tied at -7.9 kcal/mol, 5-p-coumaroylquinic

acid (-7.7 kcal/mol), lisinopril (-7.3 kcal/mol), and caffeic acid (-6.3 kcal/mol); every lead compound, without exception, returned a more negative predicted binding free energy than the reference drug itself, a pattern consistent with Islam et al.'s report that quercetin and rosmarinic acid from *Nypa fruticans* leaves likewise outdocked their enalapril reference against the same enzyme [11]. The interaction analysis in Section 4.5 points the same way: astragalin, heliangine and chlorogenic acid, the three tightest binders, each engaged a broader set of conventional hydrogen bonds inside cavity C1 than caffeic acid managed, in keeping with the extra hydroxyl and ester groups these larger molecules bring to the pocket relative to caffeic acid's comparatively simple scaffold. This also fits the structure-activity picture built up in Chapter 2, where hydroxyl-group count on the aromatic ring tracked closely with how strongly a phenolic compound inhibited ACE [9], suggesting the docking scores obtained here reflect a chemically sensible structural feature of the ligands rather than an artefact of the algorithm.

Of the four leads, chlorogenic acid offers the most balanced overall case for suitability in CKD. It outdocked lisinopril (-7.9 versus -7.3 kcal/mol), carried only a single, minor Lipinski violation against lisinopril's zero, and was clean across the entire toxicity panel, including the hepatotoxicity endpoint on which lisinopril itself was flagged. Its predicted intestinal absorption of 36.4% is modest, both relative to the other leads and in absolute terms, but this is offset by the strongest existing literature support in the panel: chlorogenic acid ranked highest in a nine-acid ACE-inhibition panel assayed independently [10], and separately shown to dock favourably against ACE in an unrelated inflammatory-disease context [33], evidence that converges from two independent directions on the same conclusion reached computationally in this study.

5-p-Coumaroylquinic acid is the only lead compound to combine a stronger docking score than lisinopril (-7.7 versus -7.3 kcal/mol) with a completely clean drug-likeness profile, zero Lipinski violations against lisinopril's own zero, and a fully clean toxicity panel. Its predicted intestinal absorption of 43.9% is the second-highest among the four leads. Unlike chlorogenic acid and astragalin, no direct ACE-inhibition assay for this specific compound was identified in the literature reviewed in Chapter 2, so

its case rests on plausible but indirect class-level evidence: the structurally related parent acid p-coumaric acid ranked second among phenolic acids tested for ACE inhibition [10], and domain-selective docking has separately placed its positional isomer, 4-O-caffeoylquinic acid, in preferential contact with the ACE C-domain, the domain chiefly responsible for converting angiotensin I in vivo [29]. On the present evidence, this makes 5-p-coumaroylquinic acid a computationally strong but experimentally unconfirmed candidate, and the strongest case in the panel for prioritised follow-up, precisely because so little direct evidence yet exists for it.

Astragalin returned the strongest binding affinity of the whole panel, at -8.6 kcal/mol, but is also the only lead compound to fail Lipinski's Rule of Five outright, exceeding both the hydrogen-bond donor and acceptor limits, and correspondingly returned the weakest predicted intestinal absorption among the four leads at 48.1%, although this still comfortably exceeds lisinopril's own 13.0%. This combination is chemically unsurprising: astragalin is the 3-O-glucoside of kaempferol, and glucosylation is known from the comparative ACE-inhibition literature to reduce, without eliminating, the ACE-inhibitory potency of the parent flavonoid aglycone [10]. Because kaempferol itself was independently ranked the third most potent of seven flavonoid aglycones tested for ACE inhibition [10], astragalin's strong docking score is consistent with, rather than contradicted by, prior structure-activity evidence, even though its absorption profile means it is the lead compound most likely to require targeted formulation strategies, for example glycoside hydrolysis prior to absorption or delivery-system optimisation, before its computational promise could translate into meaningful oral bioavailability in a CKD population.

Heliangine presents the most pronounced trade-off within the panel. It matched chlorogenic acid for the second-strongest docking score at -7.9 kcal/mol, passed Lipinski's Rule of Five without exception, and returned by a considerable margin the best predicted intestinal absorption of any compound tested, phytochemical or reference drug alike, at 97.9%. Set against this is its positive AMES mutagenicity prediction, the only such flag returned anywhere in the panel. This flag is treated here as a caveat calling for laboratory follow-up rather than automatic exclusion, not least because no published assay of heliangine's direct ACE-inhibitory activity

exists to weigh against it either way; the supporting evidence available for heliangine is instead indirect, drawn from its documented anti-inflammatory action in macrophage and vascular endothelial cell models, where it curbs excess nitric-oxide output and dials down adhesion-molecule signalling [19], mechanistically compatible with, but not itself confirmation of, ACE-inhibitory activity. Heliangine is accordingly the panel's most pharmacokinetically favourable candidate but also its least experimentally validated: excellent on every pharmacokinetic measure examined, but the one compound in this study for which an experimental mutagenicity assay, specifically an in vitro AMES test, is a prerequisite rather than an optional next step before any further development could reasonably proceed.

Caffeic acid's exclusion from the lead set is addressed here because it illustrates that the lead-selection process applied in this thesis did not simply accept every phytochemical tested. It returned the weakest docking score in the panel at -6.3 kcal/mol and was the only compound to score below lisinopril itself. This result is not an anomaly; Zielińska and colleagues assayed caffeic acid directly against ACE alongside eight other phenolic acids and found it came last of the nine, trailing chlorogenic acid, p-coumaric acid and every other compound in that comparison [10]. This exclusion is therefore corroborated by, rather than contradicted by, independent experimental evidence, which serves as a consistency check on the docking methodology used throughout this study rather than a limitation of it.

Read together, these profiles support a broader observation. Every lead compound in this study outdocked lisinopril, mirroring the pattern Islam et al. reported for structurally comparable *Nypa fruticans* phenolics screened against the same enzyme [11]. What this thesis adds is not a demonstration that plant phenolics can dock favourably against ACE, a point already reasonably well established, but a specific answer to a previously unaddressed question: whether this exact five-compound Jerusalem artichoke leaf panel behaves the same way. On the evidence generated here, it does, and with a toxicity differentiator, the absence of predicted hepatotoxicity across all four leads against its presence in lisinopril, that is more clinically salient for a CKD population than the docking scores themselves. The findings discussed above should be read against the boundaries of a purely computational

evaluation. All docking was performed using a single, static ACE structure and a single blind-docking algorithm, with no molecular dynamics simulation to test pose stability over time, a step that Yue et al. showed can meaningfully refine confidence in docking results for a comparable phenolic panel [28]. The ADMET and toxicity values reported throughout Chapter 4 are themselves model-derived estimates rather than laboratory measurements and should be read as hypothesis-generating rather than confirmatory, a caveat applying to every compound in this panel and not only the heliangine AMES flag. The evaluation also treated ACE as a single, undifferentiated target rather than distinguishing its N- and C-catalytic domains, a distinction that Darwish et al. linked to differences in side-effect burden between selective and non-selective inhibitors [29], and it compared pure, isolated compounds rather than the pharmacokinetics of these phytochemicals as they would actually be delivered, whether as a leaf extract, a purified fraction, or a formulated product. None of this undermines the internal consistency of the comparisons drawn here, but it does mean the findings are best read as a computational case for further, experimentally grounded investigation rather than a final verdict.

Considered together, the results discussed in this chapter support the conclusion that chlorogenic acid, 5-p-coumaroylquinic acid, astragalin and heliangine are each, in different ways, computationally plausible candidates for further development as ACE inhibitors relevant to chronic kidney disease, with the reference drug lisinopril generally serving to define a floor rather than a ceiling for the binding affinities observed. Chlorogenic acid and 5-p-coumaroylquinic acid offer the most balanced profiles overall; astragalin trades absorption for the strongest binding affinity in the panel; and heliangine, despite the best pharmacokinetic profile of any compound tested, carries a toxicity flag that must be resolved experimentally before its favourable computational profile can be pursued further. Caffeic acid's exclusion, corroborated independently by the wider literature, illustrates that this evaluation discriminated meaningfully between compounds rather than treating the whole panel uniformly favourably.

Overall, the findings of this chapter indicate that four structurally distinct Jerusalem artichoke leaf phytochemicals each present a case for further development as ACE

inhibitors relevant to chronic kidney disease, with each doing so on different, complementary grounds rather than by uniformly outperforming lisinopril on every measure considered. The following, final chapter draws these threads together, summarising what this thesis has established and setting out the specific experimental steps needed to test these computational findings directly.

Chapter 6

Conclusion and Future Work

6.1 Conclusion

This thesis evaluated five phytochemicals from Jerusalem artichoke (*Helianthus tuberosus* L.) leaves, chlorogenic acid, caffeic acid, 5-p-coumaroylquinic acid, astragalin and heliangine, as candidate ACE inhibitors for chronic kidney disease (CKD), using a structure-based virtual screening pipeline benchmarked against the reference drug lisinopril. Screening across target preparation, drug-likeness filtering, ADMET and toxicity profiling, molecular docking, and interaction analysis identified four of the five compounds, all but caffeic acid, as lead candidates. Each of these four leads returned a stronger predicted ACE-binding affinity than lisinopril and, unlike lisinopril, carried no predicted hepatotoxicity flag, a distinction relevant to a CKD population in which hepatic clearance and polypharmacy are often already compromised. These results are consistent with the hypothesis proposed in Chapter 1, that Jerusalem artichoke leaf phytochemicals would show ACE-inhibitory potential comparable to, or better than, an established reference drug on computational measures.

These results extend the literature on plant-derived ACE inhibitors reviewed in Chapter 2. To the extent of the literature surveyed for this thesis, this is the first structure-based virtual screening of Jerusalem artichoke leaf phytochemicals against

ACE conducted specifically in a CKD context, providing the first computational docking evidence for 5-p-coumaroylquinic acid and heliangine, compounds for which no prior direct ACE-inhibition assay was identified, and comparing four structurally distinct phytochemical classes against the same reference drug under one consistent protocol.

These findings are computational predictions rather than experimentally confirmed outcomes. As discussed in Chapter 5, the screening relied on a single static receptor structure, a single docking algorithm, and ADMET and toxicity values generated by predictive models rather than laboratory assays. These constraints define the scope of what this thesis can claim and directly motivate the future work outlined below.

6.2 Future Work

The limitations identified in this study, together with the findings on individual compounds presented in Chapter 5, highlight subsequent areas for further research. In vitro ACE-inhibition assays are needed for 5-p-coumaroylquinic acid and heliangine, the two lead compounds for which no direct enzymatic assay against ACE currently exists in the literature. Heliangine's positive AMES mutagenicity prediction likewise requires resolution through an in vitro AMES test or an equivalent genotoxicity assay before this compound is considered further, given its otherwise favourable predicted pharmacokinetic profile. Molecular dynamics simulation of the three strongest-binding complexes, astragalin, heliangine and chlorogenic acid, would test whether their docking poses remain stable over time, following the approach used for comparable phytochemical panels screened against ACE [28]. Astragalin's comparatively low predicted absorption also warrants direct investigation, for example through testing of deglycosylated derivatives, comparison against its aglycone kaempferol, or formulation approaches aimed at improving oral bioavailability without reducing its binding affinity. Finally, because this study modelled ACE as a single, undifferentiated target, extending the docking protocol

to distinguish binding at its N- and C-domains would clarify whether the leads identified here show the same domain selectivity that has been linked to reduced side-effect burden in prior work on ACE structure and inhibitor design [5, 29].

The most direct test of these findings would come from evaluating extracts or isolated fractions of Jerusalem artichoke leaf material, first in cell-based assays and subsequently in animal models of CKD or hypertension, to determine whether the ACE-inhibitory potential predicted here for individual compounds is retained when they are delivered as they would actually be administered. Such work would establish whether the computational profile reported in this thesis translates into a measurable biological effect, and represents the necessary next stage before these compounds could be considered for further pharmaceutical development.

Bibliography

[1] GBD 2023 Chronic Kidney Disease Collaborators, "Global, regional, and national burden of chronic kidney disease in adults, 1990–2023, and its attributable risk factors, a systematic analysis for the Global Burden of Disease Study 2023," *Lancet*, vol. 406, no. 10518, pp. 2461–2482, 2025.

[2] A. Ortiz, J. S. Lees, R. Torra, V. S. Stel, A. Kramer, and P. B. Mark, "The updated global burden of chronic kidney disease one death every 20 second," *Nephrol. Dial. Transplant.*, 2026, art. no. gfae040.

[3] G. Remuzzi, N. Perico, M. Macia, and P. Ruggenenti, "The role of renin-angiotensin-aldosterone system in the progression chronic kidney disease," *Kidney Int. Suppl.*, no. 99, pp. S57–S65, 2005.

[4] S. H. Ksiazek, L. Hu, S. Andò, M. Pirklbauer, M. D. Säemann, C. Ruotolo, G. Zaza, G. L. Manna, L. D. Nicola, G. Mayer, and M. Provenzano, "Renin-Angiotensin-Aldosterone System, From History to Practice of Secular Topic," *Int. J. Mol. Sci.*, vol. 25, no. 7, art. 4035, 2024.

[5] K. R. Acharya, E. D. Sturrock, J. F. Riordan, and M. R. W. Ehlers, "ACE revisited, a new target for structure-based drug design," *Nat. Rev. Drug Discov.*, vol. 2, pp. 891–902, 2003.

[6] D. W. Cushman and M. A. Ondetti, "History of the design of captopril and related inhibitors of angiotensin converting enzyme," *Hypertension*, vol. 17, no. 4, pp. 589–592, 1991.

[7] B. Singh, A. S. Cusick, A. Goyal, and P. Patel, "ACE Inhibitors," in *StatPearls*. StatPearls Publishing, 2026.

[8] A. Khaled, E. Ahmed, M. Mamdouh, H. Saad, A. Mohamed, M. Sobhy, D. Piatti, M. O. Sabry, M. A. Saad, O. M. Sabry, and G. Caprioli, "Natural angiotensin converting enzyme inhibitors, A safeguard against hypertension, respiratory distress syndrome, and chronic kidney diseases," *Phytother. Res.*, vol. 37, no. 12, pp. 5464–5472, 2023.

[9] N. A. Shukor, J. V. Camp, G. B. Gonzales, D. Staljanssens, K. Struijs, M. J. Zotti, K. Raes, and G. Smagghe, "Angiotensin-Converting Enzyme Inhibitory Effects by Plant Phenolic Compounds, A Study of Structure Activity Relationships," *J. Agric. Food Chem.*, vol. 61, no. 48, pp. 11 832–11 839, 2013.

[10] D. Zielińska, M. Starowicz, M. Wronkowska, and H. Zieliński, "Angiotensin-Converting Enzyme Inhibitory Activity of Selected Phenolic Acids, Flavonoids, Their O-Glucosides, and Low-Molecular-Weight Phenolic Metabolites in Relation to Their Oxidation Potentials," *Metabolites*, vol. 15, no. 7,art. 443, 2025.

[11] F. Islam, M. N. H. Zilani, T. A. Arian, F. I. Rodru, S. S. Khandker, M. R. Rahman, and S. Yesmine, "Computational Evaluation of *Nypa fruticans* Phytochemicals as ACE Inhibitors Against Hypertension and Chronic Kidney Disease," *ChemistrySelect*, vol. 11, no. 5, art. e04031, 2026.

[12] F. Islam, M. Kamal, S. Ahmad, M. Shahriar, F. I. Rodru, M. N. Hasan, M. N. H. Zilani, M. A. Rahman, S. S. Khandker, and S. Yesmine, "Unveiling the renal therapeutic potential of *Nypa fruticans* leaves, An integrated experimental and *In Silico* approach," *Comput. Biol. Med.*, vol. 203, 2026, art. no. 111482.

[13] D.-H. Kim, W. Lee, Y. Pyo, and D.-K. Choi, "Phytochemical Composition and Mechanistic Pharmacology of Jerusalem Artichoke (*Helianthus tuberosus* L.), Implications for Functional and Therapeutic Applications," *Curr. Issues Mol. Biol.*, vol. 48, no. 2, art. 180, 2026.

[14] A. M. Corlatti, H. Bach, I. J. Agudelo, O. G. Elso, R. Ricco, L. C. Laurella, and V. P. Sülsen, "Phytochemical Insights and Biological Potential of the Helianthus Genus," *Plants*, vol. 15, no. 3, art. 401, 2026.

[15] GBIF Secretariat, "*Helianthus tuberosus* L. GBIF Backbone Taxonomy," 2024. [Online]. Available: https://www.gbif.org/species/3119175

[16] M. M. Showkat, A. B. Falck-Ytter, and K. O. S. tkvern, "Phenolic Acids in Jerusalem Artichoke (*Helianthus tuberosus* L.), Plant Organ Dependent Antioxidant Activity and Optimized Extraction from Leaves," *Molecules*, vol. 24, no. 18, art. 3296, 2019.

[17] L. Kaszás, T. Alshaal, H. El-Ramady, Z. Kovács, J. Koroknai, N. Elhawat, E. Nagy, Z. Cziáky, M. Fári, and E. Domokos-Szabolcsy, "Identification of Bioactive Phytochemicals in Leaf Protein Concentrate of Jerusalem Artichoke (*Helianthus tuberosus* L.)," *Plants*, vol. 9, no. 7, art. 889, 2020.

[18] X. Yuan, M. Cheng, M. Gao, R. Zhuo, L. Zhang, and H. Xiao, "Cytotoxic constituents from the leaves of Jerusalem artichoke (*Helianthus tuberosus* L.) and their structure-activity relationships," *Phytochem. Lett.*, vol. 6, no. 1, pp. 21–25, 2013.

[19] P. Saiki, M. Yoshihara, Y. Kawano, H. Miyazaki, and K. Miyazaki, "Anti-Inflammatory Effects of Heliangin from Jerusalem Artichoke (*Helianthus tuberosus* L.) Leaves Might Prevent Atherosclerosis," *Biomolecules*, vol. 12, no. 1, art. 91, 2022.

[20] M. A. Alsalloum, M. A. Albekery, and I. S. Alhomoud, "Management of hypertension in chronic kidney disease, current perspectives and therapeutic strategies," *Front. Med.*, vol. 12, 2025, art. no. 1630160.

[21] S. Alshahrani, "Renin-angiotensin-aldosterone pathway modulators in chronic kidney disease, a comparative review," *Front. Pharmacol.*, vol. 14, 2023, art. no. 1101068.

[22] E. Ku *et al.*, "Angiotensin-Converting Enzyme Inhibitors or Angiotensin-Receptor Blockers for Advanced Chronic Kidney Disease, A Systematic Review and Retrospective Individual Participant-Level Meta-analysis of Clinical Trial," *Ann. Intern. Med.*, vol. 177, no. 7, pp. 953–963, 2024.

[23] S. Spencer *et al.*, "Optimizing renin-angiotensin-aldosterone inhibition in advanced chronic kidney disease, balancing benefits and risks," *Curr. Opin. Nephrol. Hypertens.*, vol. 34, no. 6, pp. 469–476, 2025.

[24] R. Natesh, S. L. U. Schwager, E. D. Sturrock, and K. R. Acharya, "Crystal structure of the human angiotensin-converting enzyme lisinopril complex," *Nature*, vol. 421, no. 6922, pp. 551–554, 2003.

[25] I.-W. Chen, Y.-H. Lin, V.-C. Wu, J.-Y. Chen, and M.-H. Wu, "Discontinuation versus continuation of renin-angiotensin system inhibitors in chronic kidney disease stage 3–5 patients, a systematic review and meta-analysis," *Front. Pharmacol.*, vol. 16, 2025, art. no. 1646969.

[26] H. M. Berman, J. Westbrook, Z. Feng, G. Gilliland, T. N. Bhat, H. Weisig, I. N. Shindylov, and P. E. Bourne, "The Protein Data Bank," *Nucleic Acids Res.*, vol. 28, no. 1, pp. 235–242, 2000. [Online]. Available: https://www.rcsb.org

[27] L. Guerrero, J. Castillo, M. Q. nones, S. Garcia-Vallve, L. Arola, G. Pujadas, and B. Muguerza, "Inhibition of angiotensin-converting enzyme activity by flavonoids, structure-activity relationship studies," *PLoS One*, vol. 7, no. 11, art. e49493, 2012.

[28] G. Yue, H. Gu, K. Zhang, Y. Song, and Y. Hao, "ACE inhibitors from *Suaeda salsa*, 3D-QSAR modeling, metabolomics, molecular docking and molecular dynamics simulations," *In Silico Pharmacol.*, vol. 12, 2024, art. no. 59.

[29] M. M. Darwish, R. S. Ibrahim, A. M. Metwally, and R. S. R. Mahrous, "In-Depth *In Silico* and In Vitro Screening of Selected Edible Plants for Identification of Selective C-domain ACE-1 Inhibitor and Its Synergistic Effect With Captopril," *Food Biosci.*, vol. 59, 2024, art. no. 104115.

[30] D. F. Veber, S. R. Johnson, H.-Y. Cheng, B. R. Smith, K. W. Ward, and K. D. Kopple, "Molecular properties that influence the oral bioavailability of drug candidates," *J. Med. Chem.*, vol. 45, no. 12, pp. 2615–2623, 2002.

[31] A. Ramlal, I. Bhat, A. Nautiyal, P. Baweja, S. Mehta, V. Kumar, S. Tripathi, R. K. Mahto, M. Saini, B. P. Mallikarjuna, S. Saluja, S. K. Lal, S. Subramaniam, I. M. Fawzy, and A. Rajendran, "*In Silico* analysis of angiotensin-converting enzyme inhibitory compounds obtained from soybean [*Glycine max* (L.) Merr.]," *Front. Physiol.*, vol. 14, 2023, art. no. 1172684.

[32] Z. Shahzadi, Z. Yousaf, I. Anjum, M. Bilal, H. Yasin, A. Aftab, A. Booker, R. Ullah, and A. Bari, "Network pharmacology and molecular docking, combined computational approaches to explore the antihypertensive potential of Fabaceae species," *Bioresour. Bioprocess.*, vol. 11, 2024, art. no. 53.

[33] S. Fang, H. Su, J. Liu, K. Zhai, Y. Gao, Y. Xiang, H. Li, R. Sun, and H. Cheng, "Network pharmacology and molecular docking to explore the potential mechanism of chlorogenic acid in septic acute liver injury and experimental validation of TLR4/NF-κB pathway in vivo," *Naunyn Schmiedebergs Arch. Pharmacol.*, vol. 398, no. 6, pp. 7331–7342, 2025.

[34] H. Chen, B. Pan, S. Zhang, X. Li, Y. Zhang, K. Gao, D. Chen, L. Wang, T. Jiang, C. Luo, and C. Huang, "Recent Advances in Biosynthesis and Bioactivity of Plant Caffeoylquinic Acids," *Curr. Issues Mol. Biol.*, vol. 47, no. 11, art. 942, 2025.

[35] S. Kim, J. Chen, T. Cheng, A. Gindulyte, J. He, S. He, Q. Li, B. A. Shoemaker, P. A. Thiessen, B. Yu, L. Zaslavsky, J. Zhang, and E. E. Bolton, "PubChem 2023 update," *Nucleic Acids Res.*, vol. 51, no. D1, pp. D1373–D1380, 2023. [Online]. Available: https://pubchem.ncbi.nlm.nih.gov

[36] A. Volkamer, D. Kuhn, F. Rippmann, and M. Rarey, "DoGSiteScorer, a web server for automatic binding site prediction, analysis and druggability assessment," *Bioinformatics*, vol. 28, no. 15, pp. 2074–2075, 2012. [Online]. Available: https://proteins.plus

[37] A. Daina, O. Michielin, and V. Zoete, "SwissADME, a free web tool to evaluate pharmacokinetics, drug-likeness and medicinal chemistry friendliness of small molecules," *Sci. Rep.*, vol. 7, 2017, art. no. 42717.

[38] Y. Liu, X. Yang, J. Gan, S. Chen, Z.-X. Xiao, and Y. Cao, "CB-Dock2, improved protein-ligand blind docking by integrating cavity detection, docking and homologous template fitting," *Nucleic Acids Res.*, vol. 50, no. W1, pp. W159–W164, 2022. [Online]. Available: https://cadd.labshare.cn/cb-dock2/

[39] C. A. Lipinski, F. Lombardo, B. W. Dominy, and P. J. Feeney, "Experimental and computational approaches to estimate solubility and permeability in drug discovery and development settings," *Adv. Drug Deliv. Rev.*, vol. 23, no. 1–3, pp. 3–25, 1997.

[40] D. E. V. Pires, T. L. Blundell, and D. B. Ascher, "pkCSM, predicting small-molecule pharmacokinetic and toxicity properties using graph-based signatures," *J. Med. Chem.*, vol. 58, no. 9, pp. 4066–4072, 2015. [Online]. Available: http://structure.bioc.cam.ac.uk/pkcsm

[41] E. Gasteiger, C. Hoogland, A. Gattiker, S. Duvaud, M. R. Wilkins, R. D. Appel, and A. Bairoch, "Protein identification and analysis tools on the ExPASy server," in *The Proteomics Protocols Handbook*, J. M. Walker, Ed. Totowa, NJ: Humana Press, 2005, pp. 571–607. [Online]. Available: https://web.expasy.org/protparam/

[42] T. Paysan-Lafosse *et al.*, "InterPro in 2022," *Nucleic Acids Res.*, vol. 51, no. D1, pp. D418–D427, 2023. [Online]. Available: https://www.ebi.ac.uk/interpro/

[43] Schrödinger, LLC, "The PyMOL Molecular Graphics System, Version 2.6.2 (Incentive Product)," New York, 2024. [Online]. Available: https://pymol.org

[44] Dassault Systèmes BIOVIA, "Discovery Studio Visualizer, Version 2025 (Academic Licence)," San Diego, 2025. [Online]. Available: https://www.3ds.com/products/biovia/discovery-studio

[45] A. R. Rasjava, N. H. Akbar, A. R. Arfan, D. A. P. Wardani, A. M. P. Putra, K. Muslimawati, P. H. J. Buih, and T. M. Fakih, "Molecular Docking and *In Silico* Evaluation of Beluntas (*Pluchea indica*) Phytochemicals as Potential Angiotensin-Converting Enzyme Inhibitors for Hypertension Treatment," *Borneo J. Pharm.*, vol. 9, no. 1, pp. 88–100, 2026.